EXPERIMENTAL STUDY OF RESERVOIR TURBIDITY CURRENTS VENTING

BY
MARIELYS RAMOS-VILLANUEVA

THESIS

Submitted in partial fulfillment of the requirements
for the degree of Master of Science in Civil Engineering
in the Graduate College of the
University of Illinois at Urbana-Champaign, 2016

Urbana, Illinois

Adviser:

Professor Marcelo H. García

ABSTRACT

Reservoirs are one of the most important components of our hydraulic systems around the world, and the effectiveness of their performance is threatened by sediment deposition within the impoundment. To achieve long-term sustainable performance of reservoirs, and to reach effective sediment management techniques, it is necessary to understand the characteristics of sediment and how it behaves before, during and after the turbid inflow plunges and flows along the bottom of the storage pool.

For this study, a series of experiments were conducted on a laboratory flume to analyze the behavior of turbidity currents while using the pass-through sediment management technique of venting. The main focus was to explore and develop a better understanding of the streamwise flow velocity and suspended sediment concentration vertical profiles, and the deposition patterns while the turbidity currents are vented. For this, two sediment management conditions or scenarios were recreated: the Turbidity Currents Venting scenario, where sediment-laden underflow was intended to be released through the low-level outlets of the scaled dam; and the Normal Reservoir Operation scenario, where the bottom outlets were closed and the discharge flowed over the dam. This was considered the control scenario.

The efficiency of the turbidity currents venting technique varies for each case depending on the geometry, and sedimentological and hydrological characteristics. Those characteristics were set constant for all the experimental runs performed on this study. The flow velocities of the turbidity currents generated by the experimental design did not have the capacity to maintain all the inflowing sediment in suspension. Therefore, significant deposition occurred along the bed, reducing the suspended sediment concentration of the turbidity currents reaching the dam. Even though venting did not eliminate the sediment deposition completely, the results show that the useful life of the storage pool was extended when applying the turbidity currents venting technique. This supports the theory where the application of this technique is expected to reduce the sediment deposition inside the storage pool.

Para los pilares de mi vida: mi mamá María, mi tía Crucita, mis hermanos Orlando, Carlos y Leonela, mi compañero de vida Javier, y las futuras generaciones que comienzan con mi querida Amalia.

"Air, I want air, and sunshine, and blue sky, the feeling of the breeze upon my face, the feeling off the turf beneath my feet, and no walls but the far-off mountain tops. Then I am free and strong, once more myself." Beltran Cruzado (The Spanish Student by Henry Wadsworth Longfellow, 1843)

ACKNOWLEDGEMENTS

This project would not have been possible without the support of many people. I would like to express my gratitude to my advisor Marcelo H. García for providing me the opportunity of conducting this research study, his guidance during my journey in graduate school, and his patience and expertise. I would also like to thank Matt Czapiga for all the support and help to perform the experiments; it was a two-man job. And finally, thanks to Javier, my friends and family who kept me sane during this long process, always offering support.

TABLE OF CONTENTS

CHAPTER 1: INTRODUCTION

"*If water is life, rivers are its arteries. Dams regulate or divert the flow through these arteries, affecting the life-blood of humanity*." - World Commission on Dams, 2000 (p. 3)

Water covers about 70% of planet Earth, so it would be easy to think that it is and will be plenty for our supply and use. However, only 2.53% of the world's water is fresh water, and only 0.31% is available for us in the form of lakes (0.26%), rivers (0.01%), and in the atmosphere as possible precipitation (0.04%), (Shiklomanov, 1993). Even though groundwater constitutes 30.11%, the lack of accessibility makes it significantly less important than surface water supplies. According to the World Wildlife Fund (WWF), about 1.1 billion people in the world have limited to non-existent access to water, and around 2.7 billion people experience water scarcity for at least one month every year. In the last decades, the human population on the planet has rapidly increased resulting in increasing the water supply demand for agriculture, daily supply, and industrial supply for the production of energy and commodities. While the water demand quickly increases, the water circulating through the hydrologic cycle is a fixed amount. Recognition of a limited worldwide water reserve is leading to the search for efficient water management, distribution, and use.

Since modern society is mostly dependent on surface water, it is necessary to secure the availability of this resource. Most surface water hydraulic systems withdraw water from streams that have periods of very low flow during dry seasons. Reservoirs provide the commodity of a regulated water supply which secures a convenient and accessible system. However, the construction of a dam impacts the transport capacity of both water and sediment in a river. Placing a dam on a river increases the cross section available for the inflow, which leads to a decrease of flow velocity and sediment transport capacity, resulting in sediment deposition within the reservoir. The coarser sediment particles tend to settle faster at the entrance of the reservoir where the transport capacity decreases, forming what is known as the *delta* (Figure 1), while the finer particles travel further downstream. For high enough sediment concentrations, the sediment-laden inflow could become *turbidity current*.

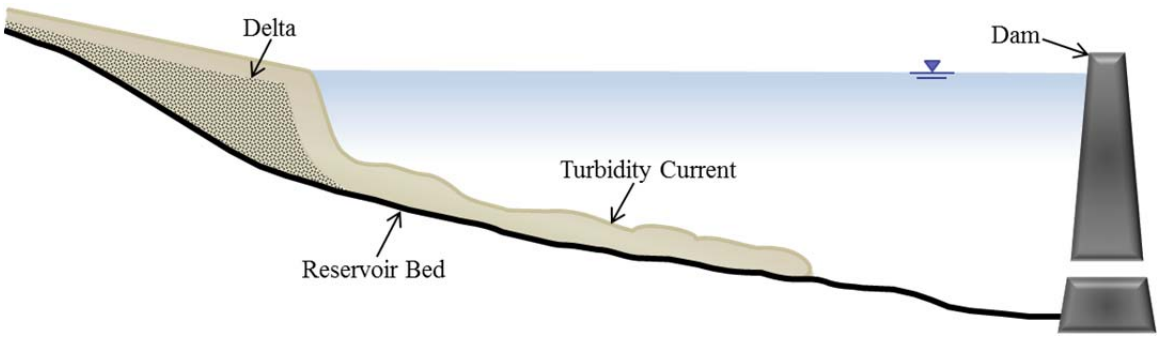

Figure 1. Turbidity current entering a reservoir.

Turbidity currents are flows driven by density differences caused by the suspended sediment load it carries. Depending on the combination of climatic conditions, reservoir geometry, and the geomorphology of the watershed, turbidity currents could dissipate or continue flowing and reach the deepest part of the reservoir near the dam. Either way, if the sediment carried by turbidity currents settles and deposits in the reservoir, it contributes to storage capacity losses. Annandale (2006), Morris and Fan (1998), and Mahmood (1987), have summarized how reservoir sedimentation impacts recreational and commercial navigation, water supply, irrigation, flood management, power generation, the environment, infrastructure, and even the economy. If the turbidity currents extend to the area near the dam, it could also lead to sediment reaching and clogging intakes and low-level outlets, and damaging gates and other hydraulic machinery (Boillat and Delley, 1992; Morris and Fan, 1998).

In 2011, the World Register of Dams, published by the International Commission of Large Dams (ICOLD), included 58,266 large dams where all have a structural dam height above foundation not less than 15 meters. About 0.5% to 1.0% of the world reservoir storage capacity is lost annually because of sedimentation problems (Mahmood, 1987). The estimated loss rate on the 48 conterminous states in the United States is about 0.22% per year (Crowder, 1987); and according to Dendy et al. (1973), the storage loss rates in the United States tends to be higher on smaller reservoirs than in larger ones.

Turbidity currents play an important role on the sediment problems affecting reservoirs around the world, and the effects they have on reservoirs should be considered during the early design stage in order to obtain sustainable sediment management solutions. Knowing about the

behavoir, properties, and characteristics of these density currents is key for the planning and design of sustainable sediment management techniques.

Water scarcity is starting to be experienced already around the world, and it will become more severe with increased water demand in the coming years. More attention is being paid to improve water management and develop sustainable alternatives to ease the water shortage to come. Reservoirs are a key component of the hydraulic system of modern society, and turbidity currents are a significant hazard that severely affects their performance. To achieve long-term sustainable performance and operation of reservoirs, it is necessary to be prepared to manage sediments. This study is intended to explore the behavior of turbidity currents under different management techniques to obtain a better understanding of their properties and characteristics.

For this study, a physical model was built to recreate a scaled reservoir. Turbidity currents were generated to analyze the sediment management technique of *turbidity current venting*. With this technique, the sediment-laden underflow reaches the dam and is passed-through the low-level outlets. Another scenario was recreated where turbidity currents were generated and the bottom outlets were closed, the *normal reservoir operation* scenario. This was considered the control scenario. Properties including the streamwise flow velocity, suspended sediment concentration, and sediment deposition were measured for both scenarios. In the next chapter, Chapter 2, a summary of the basic concepts that serve as foundation for study are presented, previous works related to the topic are discussed, and the motivation and scope for this study are stated. Chapter 3 presents and discusses the equations for a turbid inflow plunging on a reservoir, the development and motion of sediment-laden underflows, and the optimal characteristics of the low-level outlets of a dam for turbidity current venting. In Chapter 4, the experimental setup and procedures are discussed. The experimental results are presented on Chapter 5, and the summary and conclusions on Chapter 6.

CHAPTER 2: LITERATURE REVIEW

Most reaches of natural streams have a balanced sediment transport process; there is equilibrium between the sediment inflow and outflow. When a stream enters the still water of a lake or reservoir, both the flow velocity and the sediment transport capacity decrease, and the coarser sediment (e.g. sand and gravel) deposits creating the delta. The finer (fine sand, silt, and clay) sediment has lower settling velocities and is carried in suspension further into the impoundment as a surface plume, interflow, or underflow. If the muddy flow is sufficiently dense, it plunges and flows along the bottom (Morris and Fan, 1998; García, 2008, Chapter 2).

2.1 Turbidity Currents in Lakes and Reservoirs

Density currents are stratified flows caused by density differences between the inflow and the still water. The inflow could be moving under, through, or over the reservoir water depending on the density of each. The stratification is caused by differences in temperature, the presence of dissolved materials, or the presence of suspended solids. If the presence of suspended sediment in the inflowing water is the main or only cause of stratification, the density current is known as *turbidity current*. When turbidity currents enter a reservoir, they plunge beneath the fresh water traveling down the slope. If the turbidity current reaches the dam, it may be vented through the low-level outlets, thus preventing the deposition of sediment in the reservoir.

2.1.1 Turbidity Current Structure

Turbidity currents are characterized by a distinctively defined front, or *head of the current*, followed by a thinner layer known as the *body of the current* (Figures 2 and 3). The flow in the head is very unstable, as it has to overcome resistance forces. The body of the current is relatively stable and develops along the bed in a steady non-uniform condition (Tokyay and García, 2014). To be continuous, turbidity currents have to generate enough turbulence to maintain sediment in suspension. When a current is not able to hold the suspended sediment, it rapidly deposits all the sediment and dies.

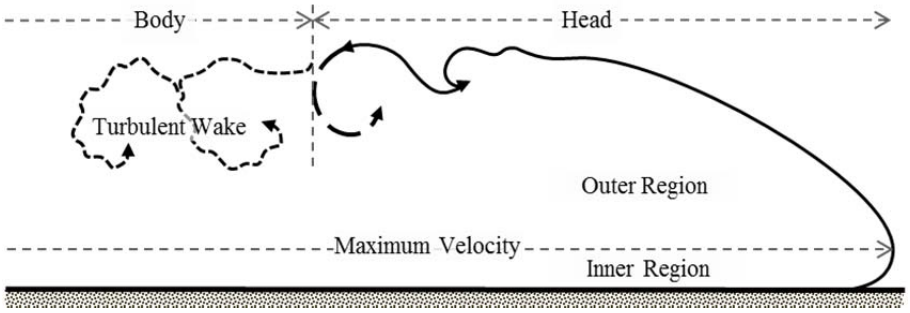

Figure 2. Structure of the head and body of turbidity currents (modified from Middleton, 1993).

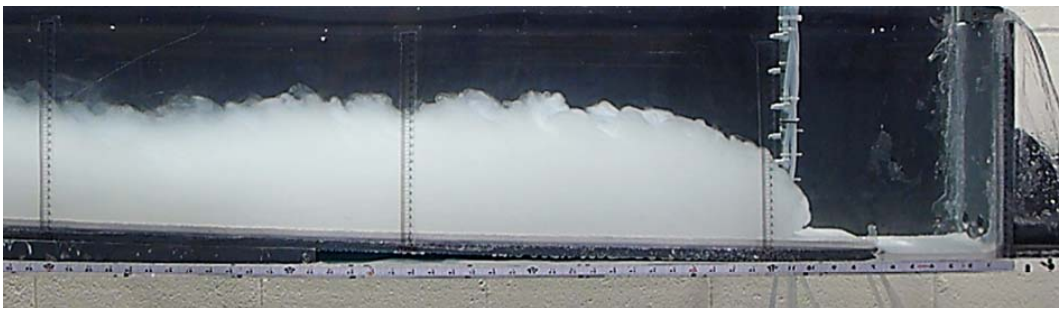

Figure 3. Turbidity current flowing downslope on a laboratory reservoir (from the experiments for this study).

2.1.2 Field Observations of Turbidity Currents

Many studies in the past have indicated that the occurrence of turbidity currents in lakes and reservoirs is a common process. The first documented case of observed dense sediment-laden flows entering a lake was reported by Forel (1885) who suggested that cold, muddy glacial meltwater inflow from the Rhone River produced underflows on Lake Geneva creating subaqueous channels and levees. Grover and Howard (1938) reported that turbid water flows were observed traveling through Lake Mead since the first year of reservoir operation in 1935. Early studies of turbidity currents on lakes and reservoirs include Norris Reservoir, Norris, Tennessee (Wiebe, 1939), Tennessee Valley Authority reservoirs (Fry et al., 1953; Churchill, 1957), Bighorn Lake, Montana (Soltero et al., 1974), Lake Superior, Minnesota (Normark and Dickson, 1976), Lake Kootenay, British Columbia (Hamblin and Carmack, 1978), Kamloops Lake, British Columbia (Carmack, 1979), Lake Constance (Lambert, 1982), Te-Chi Reservoir,

Taiwan (Young and Lin, 1991), and the Sanmenxia, Guanting, Shanyiujiang and Liujiaxia reservoirs in China (Fan and Morris, 1992), among others.

Chikita (1980, 1989, 1990) conducted an extensive and continuous program of field measurements of turbidity currents in Katsurazawa Reservoir, Hokkiado, Japan, collecting and providing detailed information about the structure and composition of turbidity current. Water temperature, velocity and suspended sediment concentration were measured at different locations. Suspended and bottom sediment samples were also collected to obtain grain size distributions.

2.1.3 Previous Turbidity Currents Experimental Studies

Motivated by the hypothesis of Daly (1936) and the observations of Grover and Howard (1938), Bell (1942) conducted physical experiments from which he concluded that density currents are among the most common phenomena in nature and play an important role in sediment transport. He suggested that special attention should be given to the mechanism that drives these currents in order to resolve sedimentation problems. Since then, several theoretical and experimental investigations have been conducted focusing on this topic. Some of them are discussed here.

Middleton (1967) conducted experiments using plastic beads to create discontinuous currents and study the deposition and formation of turbidites. The experiments showed that the initial suspension has a significant effect on the structure of the deposits. Tesaker (1969) also collaborated on the depositional currents field by using clay to create continuous turbidity currents. Different amounts of sand were added to the current to analyze the sand transport capacity. Luthi (1981) conducted experiments on non-channelized turbidity currents modeling the formation of deltas at the entrance of a lake. In this case the experiments showed that without channelization, flow creates a wide angle deposition pattern, the turbidity currents spread and dilute faster, and mean sediment grain size of the deposition decreases with distance.

García (1985) also found that the coarsest portion of the sediment was rapidly deposited near the inflow area. The experiments were conducted using quartz flour for continuous turbidity currents on slopes from 0 to 0.0056 with an erodible bed. The intentions were to allow

the currents entrain sediment from the bed to generate self-acceleration on a 20 meters long channel, which was not clearly accomplished. According to García (1989), numerical models (Parker, 1982; Fukushima et al., 1985; Akiyama and Stefan, 1986) estimate that it would take hundreds of meters long under the experimental setup of García (1985) to allow the currents to accelerate and entrain sediment from the bed. Recently, Sequeiros et al. (2009) were able to observe self-acceleration in the laboratory.

Parker et al. (1987) conducted a series of experiments of continuous supercritical turbidity currents using non-cohesive silt on an erodible bed. Measurements of velocity and concentration profiles of the current's body were used to develop approximate similarity relations, and to estimate shape factors for the vertically-integrated equations of motion. These factors included the coefficients of water entrainment from above, sediment entrainment from the bed, and bed resistance.

The experiments conducted by Altinakar et al. (1990) were focused on analyzing the behavior of the head of the turbidity currents along beds of small slopes. The turbidity currents were continuous, and sediment exchange with the bed was allowed. The shape of the turbidity current head, rather than having a universal profile, is influenced by the ratio of the head height to the total ambient fluid, by the Reynolds number of the head, and by secondary flows present in the ambient fluid.

The behavior of turbidity currents transitioning from supercritical to subcritical, where a hydraulic jump forms, was studied by García (1993). During the study, different materials and sediment grain size distributions were used to reproduce the turbidity currents. The velocity and concentration profiles were proven to depend on the flow regime, and the amount of water entrained by the flow at the hydraulic jump area was small. It was also found that the deposition patterns between the two regions (supercritical and subcritical) change depending on the initial sediment mean grain size.

More recently, de Villiers et al. (2010) constructed a circular basin to study the morphodynamics and sediment formations on a wide basin. The study was divided in two parts: the basin was filled during the first part, and emptied during the second part simulating a dam removal or basin rim breaching. According to the results, delta deposits can be predicted depending on the formation time and the characteristics of the upstream channel and sediment.

On this wide basin, lateral channel migration was the principal cause of delta formation. During the simulation of dam removal, the delta formations were partially destroyed, but a large part of the delta deposits tended to remain deposited.

Other experimental studies focused on turbidity currents include Stow and Bowen (1980), Hauenstein and Dracos (1984), Altinakar et al. (1996), Lee and Yu (1997), and De Cesare and Schleiss (1999). More recent laboratory experiments include Yu et al. (2000), Gladstone et al. (2004), Hosseini et al. (2006), Kantoush et al. (2007), De Cesare et al. (2008), Takahara and Matsumura (2008), and Sequeiros et al. (2010).

2.1.4 Previous Turbidity Currents Analytical Studies

Numerous simplified predictive models have been proposed intending to delineate the equations of motions to predict the characteristics of turbidity currents. Early proposed models provided detailed analytical treatments, but were based on conservative density currents. Ellison and Turner (1959) proposed a conservative model which allowed entrainment from the ambient fluid and assumed it was related to the current velocity and its Richardson number. After that, other models (including Hinze, 1960; Plapp and Mitchell, 1960; and Chu et al., 1979), presented a one-dimensional numerical model based on the hydrodynamics of steady-state turbidity currents, still not considering sediment exchange between the stratified layer and the bed.

Pantin (1979) proposed a model based on a phase-plane analysis, providing a description of currents that allow sediment erosion or deposition. Parker (1982) formulated a model that revealed that an equilibrium state could be reached on turbidity currents. He stated that flows with velocities below equilibrium would die out, and flows above it would "ignite" and entrain sediment from the bed to the stratified layer. In 1986, Parker et al. derived a set of equations using a layer-averaged approach to describe the mechanics of steady, spatially developing underflows, also taking into consideration sediment entrainment from the bed. The assumptions and shape factors from this model (Parker et al., 1986) were evaluated and validated with laboratory experiments conducted by García (1994).

In more recent years, several researchers have taken advantage of computational advances and new technologies to develop new numerical systems, including three-dimensional

models, to predict turbidity current behavior and to analyze the vertical structure of turbulence. Necker et al. (2002) conducted high-resolution, three-dimensional direct numerical simulations (DNS) of turbidity currents to predict the current structure, the spreading of the front, and the maximum spreading distance. They simulated sediment-laden flows in a small lock-exchange and, even though the model did not account for erosion and resuspension, it revealed that the formation of Kelvin-Helmholtz vortices at the bottom wall could initiate large shear stresses. A few years later, Necker et al. (2005) conducted a follow-up study to obtain a better understanding the differences of the energy budget and the mixing behavior between shallow and deep-water flows.

Huang et al. (2005) developed a three-dimensional model of turbidity currents based on the Reynolds averaged Navier-Stokes (RANS) equations. The model was developed to predict the vertical structure of the velocity, concentration and change in bed level due to erosion and deposition of suspended sediment. The deformable bottom grid adjusts during each time step in response the sediment deposition and entrainment during the computations. On follow-up studies, the model was applied to simulate experiments on poorly sorted turbidity currents on slope and horizontal channels (Huang et al., 2007); and to simulate turbidity currents at the field scale to study the influence of different initiation mechanisms and different bed slopes (Huang et al., 2008).

Using the commercial computational fluid dynamics (CFD) code FLUENT, Georgoulas et al. (2010) presented a three-dimensional model simulating the dynamics and flow structure of turbidity currents through a multiphase flow approach, to predict the influence of temporal and spatial evolution of the simulated currents on the suspended sediment mixture composition, the development of hydraulic jumps, and the sediment exchange between the current and the bed.

Sequeiros et al. (2009) used the 4-equation model of Parker et al. (1986) in combination with laboratory experiments and real collected data to conduct a calibrated numerical model to study the management of sediment in reservoirs currently being built in Chicago to reduce flooding and combined-sewer-overflows. According to the sediment management technique presented in the study, fine bed sediment would be eroded by jet discharges and then transported in suspension as turbidity current.

2.2 Depositional Zones

There are three basic longitudinal deposition zones: *topset*, *foreset*, and *bottomset* (Figure 4). The topset corresponds to the aggrading beds formed by the coarse sediment rapidly depositing at the inflow zone. This part of the delta rises as the sediment is deposited over it, maintaining an essentially parallel bed profile, with a slightly concave curve in some cases. The downstream limit of the topset is usually located where the stream carrying the sediment meets the still water. There is an abrupt change in slope and the deposits begin avalanching. This inclined face of the delta is the foreset. The difference in the sediment grain size between the deposits from the topset and the foreset is significant, where the coarser sediment particles are found on the topset bed (Fan and Morris, 1992a). The delta is formed by the topset and foreset, and as the sediment is deposited, it grows in the downstream direction. The vertical and upstream could also have significant growth in some cases.

According to Morris and Fan (1998), the bottomsets are formed by the finer sediment and suspended materials deposited beyond the delta, along the reservoir bed. Theses deposits are carried by density currents or non-stratified flows. While the delta grows in the downstream direction as sediment is fed into the impoundment, the topset and foreset deposit layers of coarse sediment over previously deposited bottomset beds of finer sediments. For the cases where turbidity currents reach the dam, the current rises up against the dam and falls back forming a submerged *muddy lake*. There usually is a sharp interface, with horizontal profile that extends upstream of the dam, between the muddy lake and the overlying clear water.

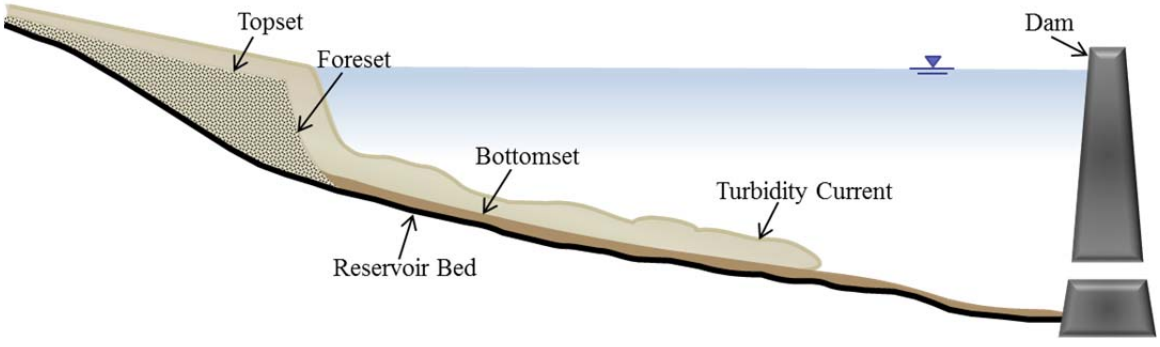

Figure 4. Basic longitudinal depositional zones on a reservoir.

2.3 Plunging Point

After the coarse sediment is deposited in the delta zone, the remaining muddy water continues flowing downstream. If the muddy inflow is denser than the still water, the inflow dips beneath the clear water and continues as a stratified underflow. The location on the water surface where the inflow plunges is called the *plunging point* or *plunging line*. Its location depends on several factors, including morphological factors and the resisting shear forces. The plunging process creates a reverse current in the ambient water just downstream of the plunge line, where the surface ambient water moves in the upstream direction and also plunges at the plunging point zone as presented on Figure 5. The two currents move in the downstream direction near the bottom of the reservoir. This plunging point zone, or plunging line, can be visibly identified because the floating debris tends to accumulate at the line where the currents flowing downstream (muddy inflow) and upstream (ambient water) converge.

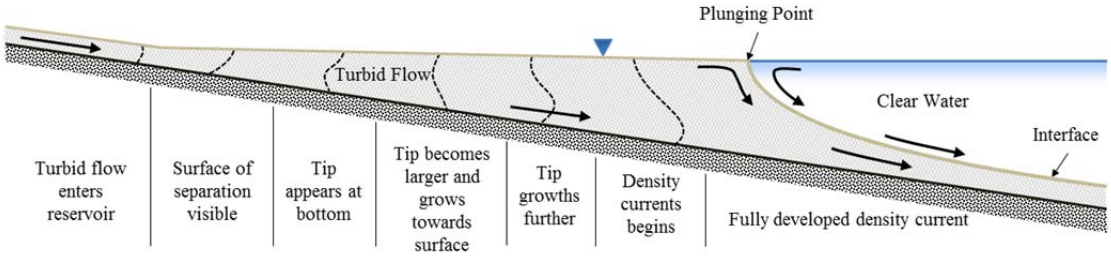

Figure 5. Muddy inflow transitioning from unstratified, free-surface flow to stratified flow at the plunging point (modified from Singh and Shan, 1971).

The first reported case of identified density current plunging appears to be that of Bell (1942). On May 3, 1940, he observed an accumulation of floating debris in Lake Mead, which was so extensive that it created a floating barrier. On the other hand, Fan (1960) conducted the first quantitative work about the plunging point positing. He examined plunging flow using a two-layer flow analysis. Several other researchers have studied the plunging criterion of the turbidity currents, including Bata (1957), Singh and Shah (1971), Savage and Brimberg (1975), Akiyama and Stefan (1984), Farrell and Stefan (1986, 1988), Kostic and Parker (2003a, 2003b), and Dai and García (2009).

Bata (1957) also used the two-layer flow analysis to compute the interface profile of a cold-water inflow plunging in a cooling water intake channel. Singh and Shah (1971) recreated a scaled ambient water reservoir, and had a dyed saline water solution plunging beneath the ambient water to observe the progress of the dense flow along the reservoir. Savage and Brimberg (1975) presented numerical models of the plunging phenomenon in reservoirs, and the predictions about plunge depth agree reasonably with the measurements from Singh and Shah (1971). Akiyama and Stefan (1984) used the momentum equation to analyze the balance of forces taking into account mixing in the plunging zone, and developed new equations for the plunge depth. Farrell and Stefan (1988) developed two dimensions numerical models of a dense inflow plunging into a reservoir, generating values to predict plunge depths and initial entrainment values at plunging. Kostic and Parker (2003a, 2003b) conducted numerical and experimental models studying the progradation and evolution of sand-mud deltas on reservoirs and lakes. The experiments revealed the interaction between the three depositional zones of the delta. The numerical model also captured the same interaction results, which were also compared against observed data from the delta in Colorado River, USA at the confluence with Lake Mead.

2.4 Management of Reservoir Sedimentation

Reservoir sedimentation is the principal problem that affects the effective performance of reservoirs and their useful life. Turbidity currents are to blame for much of the sediment deposition in reservoirs (De Cesare et al., 2001; Fan, 1986; Fan and Morris, 1992a). These currents can transport substantial amounts of sediment inside the reservoirs, even reaching the dam, and causing problems like increased flood levels, clogging of low-level outlets, entry of sediment into hydropower turbines and storage capacity losses, among others. Ackerman et al. (2009) presented an updated version of the Reservoir Sedimentation Survey Information System (RESIS) database, which offers a compilation of survey data from 1,823 reservoirs on United States and Puerto Rico, with the purpose of documenting changes in sedimentation through time. The database includes information about reservoir location, physical attributes of the reservoir and dam, surface area of the reservoir during each survey, percentage of sediment in each of the specified reservoir depth ranges, and drainage area.

It is essential to understand the behavior, mechanisms and characteristics of these currents, and the patterns and rates of its deposits, to develop efficient sediment management techniques that are sustainable. It could require major changes in the way reservoirs are designed and operated. The design of reservoirs should be focused on efficient management of water and sediment, rather than a limited useful life. According to Morris and Fan (1998), there are basic strategies to reach sustainability in reservoir sediment management, including:

1. *Reduce sediment inflow* by applying techniques like basin erosion control and upstream sediment trapping.
2. *Route sediment* hydraulically beyond the storage pool to reduce or eliminate sediment deposition, with techniques such as off-stream reservoirs, drawdown during sediment-laden floods, sediment bypass, and turbidity currents venting.
3. *Remove sediment deposits* by hydraulic flushing, hydraulic dredging, dry excavation, or flushing.
4. *Provide large storage volume* that exceeds the volume of the sediment supplied by the tributary watershed. It could be included inside the storage pool or as more upstream impoundments.
5. *Sediment placement* during deposition should be focused to areas that facilitate its removal, minimizing interference with reservoir operation.

2.4.1 Pass-Through Sediment Routing

Sediment routing refers to techniques where the sediment is passed through or around the storage or intake to maintain the sediment in suspension and minimize deposition by preserving the initial inflow sediment transport characteristics. Morris and Fan (1998) explained that the greatest amount of the inflowing sediment in a reservoir is contained in a fraction of the inflowing water. They also explain that the purpose of routing techniques is to identify the sediment-laden portion of the inflow, so it can be managed differently than clear water inflow to prevent, reduce, or focus the sediment deposition.

Sediment management techniques classified as sediment routing are divided in two categories, sediment by-pass and sediment pass-through techniques. The sediment by-pass category includes on-channel storage, off-channel storage, and subsurface storage; while the

techniques on the pass-through category include seasonal drawdown, flood drawdown by hydrograph prediction, flood drawdown by rule curve, and venting turbid density currents. Focusing on the pass-through techniques, venting turbidity currents is the only one that does not require drawdown. It releases the turbid flow through the low-level outlets maintaining the storage pool levels by trying to match the outflow volume at the low-level outlets with the turbid inflowing volume.

2.4.2 Turbidity Currents Venting

After plunging, turbidity currents flow downslope along the bottom of the reservoir seeking the lowest part of the cross section (Morris et al., 2008, Chapter 12 in ASCE Sedimentation Engineering Manual No. 110). In reservoirs where a channel is maintained by sediment routing or flushing, the turbidity currents and its deposits are concentrated along the channel facilitating their removal during later free-flow events. On the contrary, if the submerged channels are filled with sediment, the turbidity current will tend to spread across the flat bottom of the reservoir, which would reduce its velocity and sediment transport capacity, resulting in dissipation of the current and deposition of the sediment load.

According to Morris and Fan (1998), if a dam has low-level openings, turbidity currents that flow downslope all the way to the dam could be vented out, reducing the sediment accumulation in the impoundment without the need to release major amounts of clear water. Certain conditions are necessary to form turbidity currents and maintain them in suspension long enough to reach the dam, which include reservoir geometry, temperature distributions within the reservoir, sedimentological and hydrological characteristics, and topographic variations in the reservoir. Once the turbidity currents reach the dam, the efficiency of venting depends on the presence and proper location of low-level outlets, inlet structure and discharge capacity of the outlets, matching the outflow rate with the turbid flow rate that reaches the dam, and timing and duration of the turbidity current release through venting.

The sediment management technique of turbidity current venting has been considered since turbidity currents started being identified and observed (Lewis, 1936; Grover and Howard, 1938; Bell, 1942; Johnson, 1942; Brown, 1944; Ellison and Turner, 1959; Oberle et al., 1967). In China and Algeria, it is a common practice to vent turbidity currents through low-level outlets

to manage the high concentration of inflowing sediment load in reservoirs and reduce the high sedimentation problems affecting the storage capacity (Fan, 1985). In the Iril Emda Reservoir in Algeria, density currents carry very high sediment concentration loads during floods, and it was reported (Duquennois, 1959) that about 45% to 60% of the annual inflowing sediment was vented out between 1953 and 1958. The venting system in the Nebeur Reservoir in Tunisia (Abid, 1980) had an efficiency range from 59% to 64% during the period of 1954 to 1980, where the total amount of sediment discharge was about 91 million tons. According to Bruk (1985), the topography of the Fengjiashan Reservoir in China, along with sediment characteristics, and the hydraulic structures for sluicing created a system favorable for flushing and venting of turbidity currents where the released efficiency was between 23% and 65%. At Heisonglin Reservoir in China, venting turbidity currents was combined with seasonal drawdown and flushing. The release efficiency is relatively high, from 50% to 60%, combining the different techniques with the short length of the reservoir, steep slope, well-defined submerged channel maintained by flushing, and high inflow concentration of fine sediments. The practice of venting has been documented on Guanting Reservoir (Fan, 1982), Fengjiashan, Sanmexia and Guanting Reservoirs in China (Fan, 1986), and Xiaolangdi Reservoir in China (Yellow River Conservancy Commission, 2006), among others.

Venting turbidity currents on reservoirs has also been dealt with in America, Europe, and Africa. The Hydraulic Laboratory Report by Lane (1954) reviews the use of turbidity currents venting on Lake Arthur Reservoir in South Africa, where the sediment concentration of the inflow varied on a range from 1.5% to 25%. To reduce the waste of clean water, the outlets remained closed accumulating the sediment load on the muddy lake, until the concentration of the inflow near was near the maximum. Another case of turbidity currents venting discussed by Lane (1954) was Elephant Butte Reservoir in New Mexico. The event of record was on July 1919, with inflow suspended sediment concentration of 72 grams per liter, and turbid outflow release through the low-level outlets with concentration of 41 grams per liter.

In the Cachí Reservoir in Costa Rica, the combination of flushing and venting was implemented (Sundborg and Jansson, 1992). About 18% of the inflow sediment load flowed downslope along the flushing channel, reached the dam and passed through the turbines. About 54% of the total inflowing sediment load was deposited before reaching the hydropower inlet.

According to Muller and De Cesare (2009), a number of turbidity measurement sensors were placed in different locations in the Mapragg Reservoir in Switzerland during the spring of 2005, to measure the activity of sediment load inflow. The purpose of the study was to find feasible sediment management techniques to prevent sedimentation, and, as part of it, a turbidity currents venting concept was developed. Results show that large sediment loads were carried to the dam by turbidity currents during flood events, and a relevant portion of that load could be discharged if the low-level outlets were open during those events. The pertinent authorities have given permission since 2007 to vent turbidity currents when sediment load at the low-level outlets reaches a concentration level higher than 2 grams per liter (g/L).

As mentioned earlier, the effectiveness of venting turbidity currents depends, in part, on the location or position of the low-level outlets. At the moment of venting, water is aspired from above and below the outlet level, and there is potential to entrain clear water from above or turbid water from the muddy lake (Morris and Fan, 1998). Researchers (Craya, 1946; Gariel, 1946, 1949; Fan, 1960) conducted theoretical analyses to estimate the limits of *height of entrainment*. Craya (1946) conducted laboratory experiments in flumes using slots or orifices. The equations developed on the study provide a two-dimensional flow field for the slots, and a three-dimensional field for the orifices. Gariel (1946, 1949) based his analyses on experiments with dissolved solids density currents (saline water), and also developed equations for a slot and an orifice. The experiments conducted by Fan (1960) were performed with turbidity currents describing the mixing pattern near the orifice and the slot. In this case, the equations for the entrainment height from below the slot and orifice are different from the equations for above the slot or orifice. The entrainment height limit equations developed by Fan (1960) are discussed in this report, on Section 3.6

Other experimental and analytical studies related to turbidity current venting have been conducted through the years (Harleman et al., 1959; Wood, 1978; Lawrence and Imberger, 1979; Bryant and Wood, 1976; Forbes and Hocking, 1990; Forbes et al., 1996). Smrcek (1929) conducted qualitative laboratory experiments studying the possibility of venting turbidity currents on lakes and reservoirs reported by Forel (1885). Jirka and Katalova (1979) conducted an experimental study to analyze the characteristics of supercritical withdrawal using a round horizontal axis intake located on a vertical wall. The experiments were conducted on a two-layered fluid system with a diffuse interface. They were intended to evaluate the effect of the

intake dimensions and the thickness of the diffuse interface on the withdrawal conditions, and the behavior of the selective withdrawal when both layers of the system were part of the discharged flow.

The analysis conducted by Fan (1986) was based on measured and observed data in reservoirs and laboratory flumes, focusing on the physical features of the turbidity currents. Fan proposed a schematic model of the movement of density currents in reservoirs and a method to estimate the vented turbidity currents discharge flow, which were in accordance with measured data from Guanting Reservoir and Lake Mead.

A three-dimensional model was developed by Lee et al. (2014) to study outflow concentration and venting efficiency through reservoir bottom outlets. A new formula was developed, based on theoretical analysis and the experimental data, to estimate outflow concentration and venting efficiency.

2.5 Present Work

2.5.1 Motivation

Reservoirs bring the unique commodity of a regulated water supply, which becomes more valuable over time as the water demand increases along with increasing population. In many places, reservoirs are the principal water supply over any other accessible surface or groundwater supply system. However, even though reservoirs play an important role on the modern hydraulic systems, "uncontrolled sediment accumulation makes storage reservoirs the key non-sustainable component of modern water supply systems" (Morris and Fan, 1998). Detailed analyses, focused on reservoir sedimentation and its management, are required to develop progress to reach sustainable reservoir performance and secure the availability of functional water supply systems (Morris et al., 2008).

2.5.2 Scope and Objectives

The objectives of this study are to conduct an experimental analysis to examine the hydraulics, deposition patterns, and general behavior of turbidity currents while applying different reservoir operation scenarios at the dam on a scaled reservoir. The scope is to obtain a

better understanding about the dynamics of turbidity currents in reservoirs and the efficiency of turbidity currents venting.

CHAPTER 3: THEORETICAL BACKGROUND

3.1 Plunging Flow into the Reservoir

Following the concepts discussed by Parker and Toniolo (2007) consider a stationary body of ambient water with a uniform density ρ_a, no ambient stratification formed. A turbid inflow discharge per unit width q_o is reaching the impoundment with initial depth h_o, streamwise velocity U_o and suspended sediment concentration C_o. The initial density, ρ_o, is higher than the ambient water density, where the suspended sediment carried by the inflow discharge is the only cause for the difference in density, $\Delta\rho_o$,

$$\rho_o = \rho_a + \Delta\rho_o \qquad \text{Equation 1}$$

Once the turbid inflow reaches the area, h_p, U_p, and C_p correspond to the plunging depth, flow velocity and suspended sediment concentration just upstream of the plunging point, respectively, as presented on Figure 6.

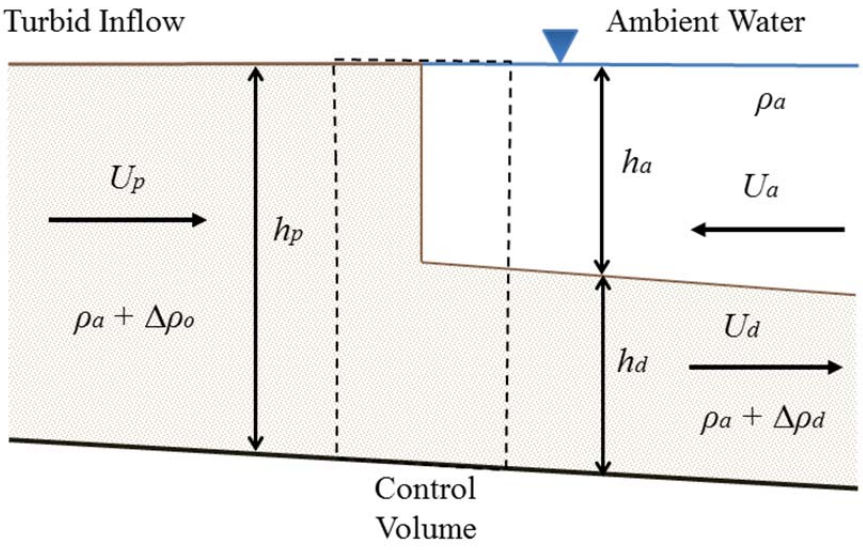

Figure 6. Definition of parameters near the plunging point.

The layer thickness, velocity, and concentration that correspond to the underflow formed just downstream of the plunging point are given by h_d, U_d, and C_d. Applying the law of mass

conservation on the control volume from Figure 6, yields

$$q_o = U_o h_o = U_p h_p = U_d h_d - U_a h_a \qquad \text{Equation 2}$$

where U_a denotes the velocity at which the countercurrent of ambient water enters the underflow in the plunging point vicinity; h_a denotes its thickness.

The entering ambient flow discharge can be obtained assuming that it is directly related to the inflow discharge, q_o, multiplied by a mixing coefficient, γ,

$$q_a = U_a h_a = \gamma q_o \qquad \text{Equation 3}$$

from which the coefficient of mixing of the ambient water into the underflow can be redefined as

$$\gamma = \frac{U_a(h_p - h_d)}{U_p h_p} \qquad \text{Equation 4}$$

and the flow discharge per unit width just downstream the plunging point could then be obtained as follows,

$$q_d = U_d h_d = U_p h_p + U_a h_a \gamma = q_o(1 + \gamma) \qquad \text{Equation 5}$$

In order to produce a plunging point with entrainment of ambient fluid, the mixing coefficient is required to have a value higher than zero ($\gamma > 1$). The density of the underflow is assumed to change due to the ambient countercurrent mixing. Applying the law of mass conservation on the control volume from Figure 6, gives

$$\Delta\rho_o = (1 + \gamma)\Delta\rho_d \qquad \text{Equation 6}$$

The densimetric Froude numbers of the inflow, plunging point, and underflow are defined respectively as

$$F_o^2 = \frac{q_o^2}{\left(\Delta\rho_o / \rho_a\right) g h_o^3} \qquad \text{Equation 7}$$

$$F_p^2 = \frac{q_p^2}{\left(\Delta\rho_o / \rho_a\right) g h_p^3} \qquad \text{Equation 8}$$

$$F_d^2 = \frac{q_d^2}{\left(\Delta\rho_d/\rho_a\right) g h_d^3} \qquad \text{Equation 9}$$

Defining the ratio between the flow depth at the plunging point and the depth (i.e. thickness) of the flow downstream of the plunging point as $K = h_p/h_d$ which can be expressed as

$$K = \frac{1}{2(1+\gamma)}\left[\frac{2+\gamma}{2} + F_d^2 + \sqrt{\left(\frac{2+\gamma}{2} + F_d^2\right)^2 - \frac{4F_d^2}{(1+\gamma)}}\right] \qquad \text{Equation 10}$$

The plunge point densimetric Froude number can then be expressed as

$$F_p^2 = \frac{F_d^2}{(1+\gamma)^3 K^3} \qquad \text{Equation 11}$$

and combining it with Equations 7, 8 and 9, the dimensionless plunge point depth is defined as

$$\frac{h_p}{h_o} = \left(\frac{F_o}{F_p}\right)^{2/3} = K(1+\gamma)\left(\frac{F_o}{F_d}\right)^{2/3} \qquad \text{Equation 12}$$

The analysis of the plunging phenomenon and underflows presented above takes into consideration a steady turbid inflow discharge of constant concentration and depth, plunging into a reservoir or lake of clear water.

3.2 Morphodynamics of Turbidity Currents

The scenario presented in Figure 7 follows the models proposed by Akiyama and Stefan (1985), Parker et al. (1986) and García (1989). It presents a stationary body of clean water with uniform density ρ and indefinitely depth. The bottom is flat with a small constant slope *S*, where *x* denotes the downstream direction and *z* denotes the upward normal direction. The bed is covered with sediment and has a constant roughness. The cross section is rectangular and wide enough that the effects of the lateral walls or variations in the lateral direction can be neglected. A two-dimensional, steady turbidity current is flowing downslope under a layer of clear water. The turbidity current density has a density ρ_s, significantly higher than the clean water density ρ, which makes the turbid flow plunge to the bottom.

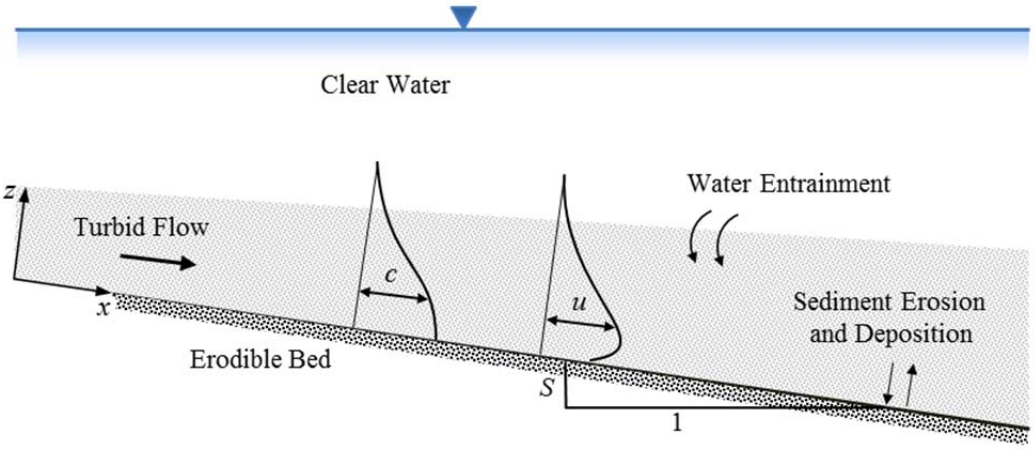

Figure 7. Turbidity current flowing downslope through a stationary body of clear water.

The so-called Boussinesq approximation is invoked in this scenario. The difference in density between the two fluids is taken into account for the driving force, but the impact of the density difference on the convective accelerations (i.e. inertia effects) is neglected. With this, the submerged weight (W_s) of the particles from the suspended sediment is given by the actual weight of the particle minus the buoyancy force applied to the particle. For a particle of volume V_p, and using the symbol g for the earth acceleration, that is

$$W_s = (\rho_s - \rho) g V_p = \rho R g V_p \qquad \text{Equation 13}$$

where

$$R = \left(\frac{\rho_s}{\rho} - 1\right) \qquad \text{Equation 14}$$

represents the submerged specific gravity of the sediment.

The volumetric sediment concentration for each i grain size range is denoted by c_i, averaged over turbulence; and the total volumetric concentration of suspended sediment for a given location is given by

$$c = \sum c_i \qquad \text{Equation 15}$$

It is assumed that the values of c and Rc are significantly less than 1, denoted by

$$c \ll 1 \quad and \quad Rc \ll 1 \qquad \text{Equation 16}$$

everywhere within the flow, which justifies the assumption of a kinetic viscosity v equal to the value for clear water.

The local mean components of the downstream flow velocity are u for the x direction, and w for the z direction and are averaged over turbulence. Since turbidity currents are underflows, the streamwise flow velocity u and the sediment concentration c are assumed to tend to zero, as z grows far above the turbidity current. The fluctuating components of the flow velocity are u' and w', and the fluctuating volumetric concentration of sediment is c', given by the difference between the instantaneous value minus the turbulence averaged value. Following the slender-body approximation, it is assumed that

$$u \gg w \quad and \quad \frac{\partial}{\partial z} \gg \frac{\partial}{\partial x} \qquad \text{Equation 17}$$

Under these assumptions, the equations governing the morphodynamics of turbidity currents are defined as:

- Mean mass balance

$$\frac{\partial u}{\partial x} + \frac{\partial w}{\partial z} = 0 \qquad \text{Equation 18}$$

- Mean sediment mass balance

$$\frac{\partial uc}{\partial x} + \frac{\partial wc}{\partial z} = -\frac{\partial\left(\overline{c'w'} - v_s c\right)}{\partial z} \qquad \text{Equation 19}$$

- Momentum balance in the z direction

$$0 = -\frac{1}{\rho}\frac{\partial p}{\partial z} - gRc \qquad \text{Equation 20}$$

- Momentum balance in the x direction

$$\frac{\partial u^2}{\partial x} + \frac{\partial wu}{\partial z} = -\frac{1}{\rho}\frac{\partial p}{\partial x} + gSRc + \frac{1}{\rho}\frac{\partial \tau}{\partial z} \qquad \text{Equation 21}$$

where v_s is the fall velocity of the sediment, τ is the Reynolds stress defined as $-\rho\overline{u'w'}$, and p is the hydrostatic pressure due to sediment weight. The terms gS and $-g$ from the momentum

balance equations (Equations 20 and 21) are the gravitational acceleration components in the *x* and *z* direction, respectively. The term *gSRc* represents the downslope driving force per unit mass, due to gravity acting on the excess fractional density of the underflow.

3.3 Vertical Integration of Governing Equations

The same scenario and assumptions established for Section 3.2 are applied for the following analysis, where the equations of balance and momentum are integrated in the *z* direction. Recalling that, as part of the established assumptions, the streamwise flow velocity *u* and the sediment concentration *c* tend to zero, as *z* tends to infinite.

- Integration of the mean mass balance, from Equation 18.

$$\frac{d}{dx}\int_0^\infty u\,dz + w_\infty = 0 \qquad \text{Equation 22}$$

where w_∞ is a velocity resulting from the boundary layer velocity approximation that, for the diagram presented on Figure 7, is defined as

$$w_\infty = \frac{\partial h}{\partial t} - w_e \qquad \text{Equation 23}$$

The term $\frac{\partial h}{\partial t}$ is the rate of growth over time of the layer thickness *h* and, since a steady turbidity current is being considered, is equal to zero; and w_e represents the entrainment velocity. Then, Equation 22 is reduced to

$$\frac{d}{dx}\int_0^\infty u\,dz = w_e \qquad \text{Equation 24}$$

- Integration of the mean sediment mass balance, from Equation 19.

$$\frac{d}{dx}\int_0^\infty uc\,dz = \left(\overline{c'w'}\right)_b - v_s c_b \qquad \text{Equation 25}$$

where *b* is a value of *z* near the bed (near zero), but high enough to avoid boundary layer viscous effects; and c_b is the suspended sediment concentration near the bed. The term $\left(\overline{c'w'}\right)_b$ is the volumetric upward normal Reynolds flux of sediment near the bed, which can be expressed as the entrainment rate of sediment from bed into

suspension due to turbulence. This expression takes the form of Equation 26, in terms of the dimensionless entrainment rate E_s (García and Parker, 1991)

$$\left(\overline{c'w'}\right)_b = v_s E_s \qquad \text{Equation 26}$$

Then, the integrated equation of sediment mass balance in the *z* direction is defined as

$$\frac{d}{dx}\int_0^\infty uc\, dz = v_s(E_s - c_b) \qquad \text{Equation 27}$$

where $v_s(E_s - c_b)$ represents the difference between the sediment entrainment rate, $v_s E_s$, and the sediment deposition rate, $v_s c_b$. For cases where E_s is higher than c_b, erosion of deposited sediment will occur. On the contrary, if c_b is higher than E_s, deposition of suspended sediment will occur. There should be neither erosion, nor deposition of sediment on a system where a steady uniform suspension has been achieved ($E_s = c_b$).

- Integration of the momentum balance in the z direction, from Equation 20.

Integrating Equation 20 and clearing for the first term of the right side, the following equation is obtained

$$p = \rho g R \int_z^\infty c\, dz \qquad \text{Equation 28}$$

which represents the hydrostatic pressure caused by the suspended sediment in the turbidity current.

- Integration of the momentum balance in the x direction, from Equation 21.

Merging Equation 28 into Equation 21, the mean momentum balance expands to

$$\frac{\partial u^2}{\partial x} + \frac{\partial wu}{\partial z} = -gR\frac{\partial}{\partial x}\int_z^\infty c\, dz + gSRc + \frac{1}{\rho}\frac{\partial \tau}{\partial z} \qquad \text{Equation 29}$$

The integration in the z direction is

$$\frac{d}{dx}u^2 dz = -gR\frac{d}{dx}\int_0^\infty \int_z^\infty c\, dz' dz + gRS\int_0^\infty c\, dz + u_*^2 \qquad \text{Equation 30}$$

where u_*^2 represents an approximation of the kinematic bed shear stress, at $z=b$ near the bed, defined as τ_b/ρ. The terms u_* and τ_b are the shear velocity and shear stress at the bed, respectively.

3.4 Simplified Approximation

Assuming that the vertical shears across the turbidity current layer are much smaller than the average shear between turbidity current and the entrainment zone layer, the underflow can be simplified to obtain a more tractable model. The turbidity current is considered to be moving like a slab, and both the streamwise velocity u and the suspended sediment concentration c are assumed to maintain approximately uniform profiles along the vertical direction. The terms U and C denote the layer averaged streamwise velocity and volume concentration of suspended sediment, respectively, for a layer of thickness h, where

$$\frac{u(x,z)}{U(x)} = \xi_u(\eta) \quad and \quad \frac{c(x,z)}{C(x)} = \xi_c(\eta) \qquad \text{Equation 31}$$

where

$$\eta = \frac{z}{h} \qquad \text{Equation 32}$$

Ellison and Turner (1959) and Parker et al. (1987) defined U, C and h through the following set of moments:

$$Uh = \int_0^\infty u\, dz \qquad \left[\int_0^\infty \xi_u\, d\eta = 1\right] \qquad \text{Equation 33}$$

$$U^2 h = \int_0^\infty u^2\, dz \qquad \left[\int_0^\infty \xi_u^2\, d\eta = 1\right] \qquad \text{Equation 34}$$

$$UCh = \int_0^\infty uc\, dz \qquad \left[\int_0^\infty \xi_u \xi_c\, d\eta = 1\right] \qquad \text{Equation 35}$$

Combined with these definitions for U, C and h (Equations 33 to 35), the integrals from section 3.3 are reduced to

- Mass balance

$$\frac{dUh}{dx} = w_e \qquad \text{Equation 36}$$

- Sediment mass balance

$$\frac{dUCh}{dx} = v_s(E_s - c_b) \qquad \text{Equation 37}$$

- Momentum balance

$$\frac{dU^2h}{dx} = gRChS - \frac{1}{2}gR\frac{dCh^2}{dx} - u_*^2 \qquad \text{Equation 38}$$

Equations 36 to 38 form a three-equation model capable of describing the development of turbidity currents as underflows in an impoundment. The equations are valid for steady state analysis of two-dimensional, continuous turbidity currents.

3.5 Closure Relations for Theoretical Model

Before being able to use the governing equations, some basic properties of the turbidity currents need to be defined algebraically. The water entrainment velocity, w_e; bed shear velocity, u_*; bed shear stress due to friction, τ_b; dimensionless rate of sediment entrainment, E_s; and dimensionless rate of sediment deposition, c_b, must be solved in terms of U, C, and h. The entrainment of ambient water from above is defined as

$$w_e = e_w U \qquad \text{Equation 39}$$

where e_w is a water entrainment coefficient that, based on the experimental data from Parker et al. (1987), is defined as

$$e_w = \frac{0.075}{\sqrt{1 + 718R_i^{2.4}}} \qquad \text{Equation 40}$$

The term R_i is the bulk Richardson number, given by

$$R_i = \frac{RgCh}{U^2} \qquad \text{Equation 41}$$

According to Equation 40, e_w approaches a value of 0.075 as R_i approaches zero, which is appropriate for a non-stratified flow (García, 1989); and decreases rapidly as R_i increases.

The bed shear velocity is given by the following expression (Turner, 1973):

$$u_* = C_D U^2 \qquad \text{Equation 42}$$

where C_D is a coefficient of bed friction. This coefficient can be expected to be a function of boundary layer parameters, and can be taken as constant. According to García (1985), the value of C_D ranges between 0.002 and 0.05.

Different equations have been developed to estimate sediment entrainment under equilibrium conditions, including Akiyama and Fukushima (1986), and Parker et al. (1987). The following relation of the sediment entrainment coefficient was developed by García and Parker (1991):

$$E_s = \frac{AZ_u^5}{\left(1 + \frac{A}{0.3}Z_u^5\right)} \qquad \text{Equation 43}$$

where A is equal to 1.3×10^{-7} and

$$Z_u = \frac{u_*}{\mathrm{v_s}} R_{ep}^{0.6} \;\; ; \;\; u_* = \sqrt{ghS} \;\; ; \;\; R_{ep} = \frac{\sqrt{RgD}D}{\nu} \qquad \text{Equation 44}$$

The term R_{ep} represents the particle Reynolds number, and D is the geometric mean sediment diameter.

A series of equations have been proposed to estimate the near-bed sediment concentration under equilibrium conditions; Einstein (1950), Engelund and Fredsoe (1976; 1982), Smith and McLean (1977), Itakura and Kishi (1980), Rijn (1984), Celik and Rodi (1984). Parker (1982), with the help of the Rouse-Vanoni-Ippen sediment distribution (García, 2008), proposed that the near-bed sediment concentration c_b is related to the layer-averaged concentration C and a concentration ratio factor r_o, as follows

$$c_b = r_o C \quad \text{Equation 45}$$

where

$$r_o = 1 + 31.5\mu^{-1.46} \quad \text{Equation 46}$$

where μ represents the dimensionless shear velocity $\frac{u_*}{v_s}$, which has been tested and validated with different physical experiments. García (1985) established that the formula is acceptable for a range of $5 < \frac{u_*}{v_s} < 50$, and that a constant value of 1.6 would also be a good approximation for the case of turbidity currents. Parker et al. (1987) also found it to be acceptable as a constant, equal to about 2.0, for a wide range of $\frac{u_*}{v_s}$.

Combined with Equations 39, 42 and 45, Equations 36, 37 and 38 are reduced to

- Mass balance

$$\frac{dUh}{dx} = e_w U \quad \text{Equation 47}$$

- Sediment mass balance

$$\frac{dUCh}{dx} = v_s(E_s - r_o C) \quad \text{Equation 48}$$

- Momentum balance

$$\frac{dU^2 h}{dx} = gRChS - \frac{1}{2} gR \frac{dCh^2}{dx} - C_D U^2 \quad \text{Equation 49}$$

3.6 Turbidity Currents Venting Through Low-Level Outlets of a Dam

When the low-level outlets of a dam are opened and turbidity currents reach the dam, the turbidity current can be vented. During this process, water from both above and below the outlet level is entrained. Even when the outlets are located above the muddy lake, part of the muddy lake could be entrained from below the outlet level, as presented on Figure 8. At the same time, it is possible that unnecessary release of clean water could happen if clean water is aspired from above the turbidity current (Figure 9). Section 14.7.5 of Morris and Fan (1998) presents

different equations that have been developed to define the limiting height of entrainment for turbid water (h_L) from above and below the venting outlets, including those by Craya (1946), Gariel (1946 and 1949), and Fan (1960).

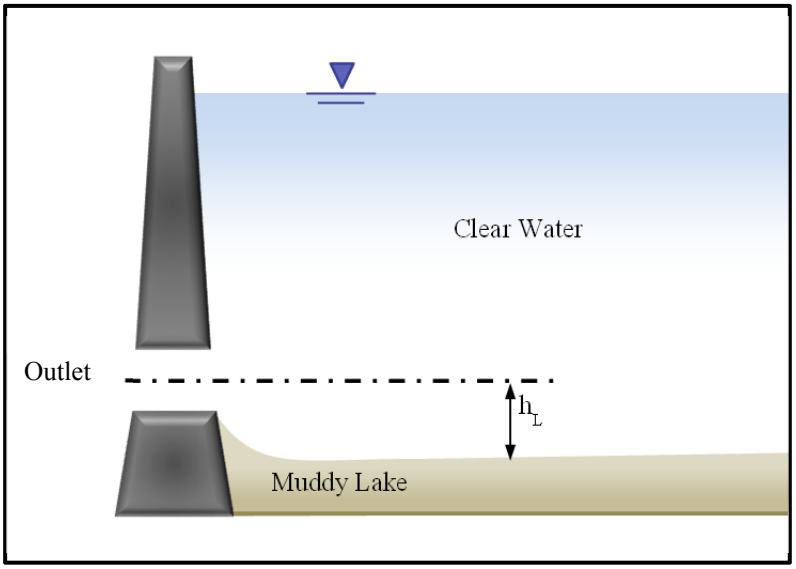

Figure 8. Entrainment height limit before releasing turbid water from muddy lake.

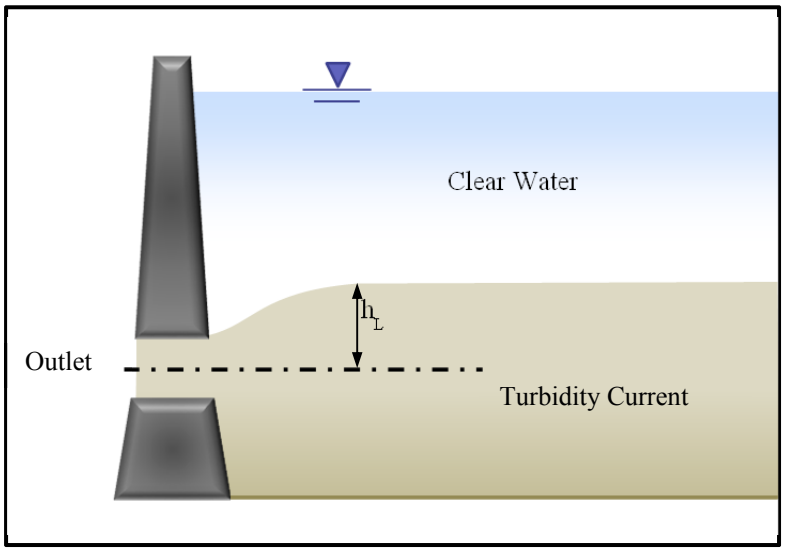

Figure 9. Aspiration height limit before releasing clean water while venting turbidity currents.

Based on theoretical analysis of the limiting height of aspiration of a density current, Craya (1946) developed the following expression:

$$\frac{\Delta\rho}{\rho}\frac{g{h_L}^3}{q^2} = \frac{27}{8\pi^2} = 0.34 \qquad \text{Equation 50}$$

where h_L is the height of aspiration and $\Delta\rho$ is the difference in density due to suspended sediment and q is the discharge per unit width of slotted outlet.

Gariel (1946 and 1949) conducted experiments in laboratory flumes to determine the limiting height of aspiration, using saline water density currents. The experiments were conducted using slots, which produce a two-dimensional flow field, and orifices, which produce three-dimensional flow fields. The condition for the limiting height of aspiration for a slot was defined as

$$\frac{\Delta\rho}{\rho}\frac{g{h_L}^3}{q^2} = 0.43 \qquad \text{Equation 51}$$

where q is discharge per unit width of slotted outlet. The relationship for the limiting height of aspiration for an orifice was defined as

$$\frac{\Delta\rho}{\rho}\frac{g{h_L}^5}{Q^2} = 0.154 \qquad \text{Equation 52}$$

where Q is the total discharge through orifice.

According to Fan (1960), the limits of aspiration for turbid water can also be defined in terms of the densimetric Froude number. Fan performed flume tests for turbidity currents, using slots and orifices. For turbid water, the limiting depth for aspiration from below the slot axis is given by

$$F_2 = \left[\frac{\Delta\rho}{\rho}\frac{g\left(h_{L_b}\right)^3}{q^2}\right]^{1/3} = 0.75 \qquad \text{Equation 53}$$

and the aspiration height limit from above the slot is defined as

$$F_2 = \left[\frac{\Delta\rho}{\rho}\frac{g\left(h_{L_a}\right)^5}{q^2}\right]^{1/3} = 0.75 \qquad \text{Equation 54}$$

where the terms h_{Lb} and h_{La} are the height of aspiration limit from below and from above, respectively; and F_2 is the two-dimensional densimetric Froude number. It was also established that the limiting depth for aspiration of turbid water below an orifice axis is given by

$$F_3 = \left[\frac{\Delta\rho}{\rho}\frac{g\left(h_{L_b}\right)^5}{Q^2}\right]^{1/5} = 0.8 \qquad \text{Equation 55}$$

and the limiting height at which clear water from above potentially begins to be released through an orifice is obtained from

$$F_3 = \left[\frac{\Delta\rho}{\rho}\frac{g\left(h_{L_a}\right)^5}{Q^2}\right]^{1/5} = 1.2 \qquad \text{Equation 56}$$

where F_3 is the three-dimensional densimetric Froude number. Equations 55 and 56 are then cleared for h_{La} and h_{Lb}, respectively, to obtain

$$h_{L_a} = \left[\frac{\rho}{\Delta\rho}\frac{Q^2(1.2)^5}{g}\right]^{1/5} \qquad \text{Equation 57}$$

and

$$h_{L_b} = \left[\frac{\rho}{\Delta\rho}\frac{Q^2(0.8)^5}{g}\right]^{1/5} \qquad \text{Equation 58}$$

Adding the result of both Equations 57 and 58, plus the diameter of the low-level outlets, provides an approximation of the vertical range of aspiration available.

CHAPTER 4: EXPERIMENTAL SETUP & PROCEDURE

4.1 Approach & Methodology

In order to perform the intended reservoir sedimentation analysis, a scaled reservoir physical model was built in a rectangular flume to recreate the typical conditions of stream inflow and turbidity currents in a reservoir. The experiment was divided into two sets of runs under different scenarios of sediment management to analyze and compare the sediment deposition, concentration distribution and velocity profiles. The first group of runs was set to analyze the behavior of turbidity currents under *normal* dam operation, in which the low-level outlets are closed and the discharge flows over the dam. For the second sediment management scenario, the low-level outlets were open to recreate the process of turbidity current venting. In this case, the outlets remained closed until the turbidity current was about 3 feet from the dam, then opened at that moment to ensure the turbidity current flow was maintained.

The experimental study was carried out at the Ven Te Chow Hydrosystems Laboratory, Department of Civil and Environmental Engineering, of the University of Illinois at Urbana-Champaign.

4.2 The Flume

The experiments were conducted on a flume represented by Figure 10. It was 7.3 meters long, 15 centimeters wide, and 40 centimeters deep. An artificial initial delta and sloping bed were built from PVC plastic to represent typical conditions at which turbidity currents are usually produced in lakes and reservoirs. The upstream inclined bed of the initial delta, the topset, had a slope of 0.011 and a length of 2.3 meters. The topset was followed by the foreset with a slope of 0.631 and a length of 29 centimeters. The drastic change in slope from the topset to the foreset, combined with the density difference between the fresh stored water and the turbid inflow, help with the development of turbidity currents. Finally, the bottomset, which went from the downstream end of the foreset to the dam with a length of 3.81 meters, had a slope of 0.026.

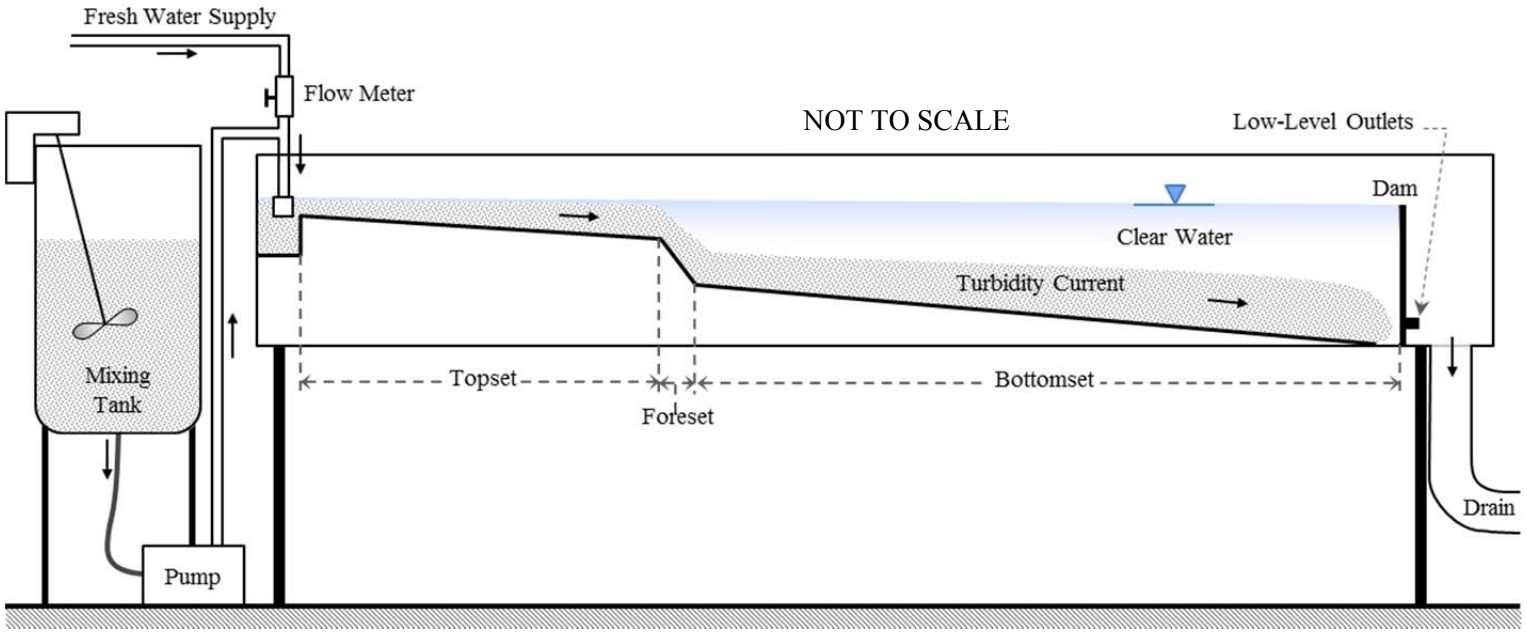

Figure 10. Schematic of the experimental setup.

The dam was also made from PVC plastic and had three low-level outlets. It was 30 centimeters tall and 15 centimeters wide.

Three PVC plastic pipes were used to simulate scaled low-level outlets on the dam. The pipes had an inner diameter of 1.25 centimeters and were about 12.5 centimeters long. According to Equations 57 and 58, the aspiration limits of the low level outlets are h_{Lb} = 5.11 centimeters and h_{La} = 7.67 centimeters. The centerline of the outlet pipes was placed 3.5 centimeters from the bed, providing a total range of 11.8 centimeters of vertical aspiration.

4.3 Inflow Characteristics

The analysis includes the generation of turbidity currents by using sediment-laden inflow. The turbid inflows were produced in a mixing tank with a capacity of 159 liters (5.6 cubic feet) where sediment and water were mixed. The mixing tank has a height of 70 centimeters and a diameter of 55 centimeters. As presented on Figure 10, the inflow was pumped from the mixing tank into the flume through a pipe placed at the upstream end of the scaled reservoir where a diffuser assures even flow and sediment concentration distribution along the cross section. A damping tank was placed at the downstream side of the dam to collect the outflowing mixture of water and sediment.

Each sediment management technique performed on this project had a set of seven experimental runs. Each set had a combined total time of about 240 minutes (4 hours) of turbidity currents flowing along the flume. After filling the experimental flume with fresh water before each run, an overconcentrated turbid mixture of water and suspended sediment was fed from the mixing tank at a rate of 2 liters per minute. At the same time, 41.7 liters per minute of clear water were fed into the inflow pipe and combined with the turbid-water mixed at the upstream diffuser. The resulting inflow rate was 43.7 liters per minute, with an initial concentration of 0.0045 by volume, and 1,006.45 kilograms per cubic meters of density. The density difference between the inflow and the fresh impounded water, 998.21 kilograms per cubic meters at temperature of 20 degrees Celsius (°C), acted as the force that made the current flow as a stratified layer near the reservoir bed. The development and maintenance of these turbidity currents made it possible to measure the flow characteristics in detail.

4.4 Sediment Materials

The solid material used for the sediment-laden inflow was silica flour Sil-Co-Sil® 106. This material comes from quartz, the most common sediment type encountered in riverine and coastal environments. The specific gravity (S.G.) for quartz and silica flour is 2.65.

Table 1 and Figure 11 present the sediment grain size distribution (GSD) according to sediment size distribution analyses carried on at the laboratory, combining sieve analysis for sediment coarser than 75 micrometer and hydrometer analysis for sediment finer than the same grain size, as outlined in the ASTM D422 Standard Test Method. The mean grain diameter (D_{50}) size of the sediment material is 31.04 micrometers. Additional sediment characteristics are summarized in Table 2, including the sediment grain sizes for which 84% (D_{84}) and 16% (D_{16}) of the sample by weight consists of finer grains.

Table 1. Sediment grain size distribution before conducting the experiments.

Finer Percent (%)	Grain Size (μm)
100.0	210.00
100.0	177.00
99.9	149.00
99.6	125.00
97.8	105.00
93.3	88.00
88.0	75.00
76.7	66.22
74.5	63.54
66.5	45.52
60.4	38.48
54.4	32.78
48.3	29.31
45.3	26.90
42.3	24.55
33.2	19.23
30.2	16.67
27.2	14.41
24.2	12.86
21.1	11.12
18.1	8.84
15.1	6.97
12.1	4.73
0.0	1.01

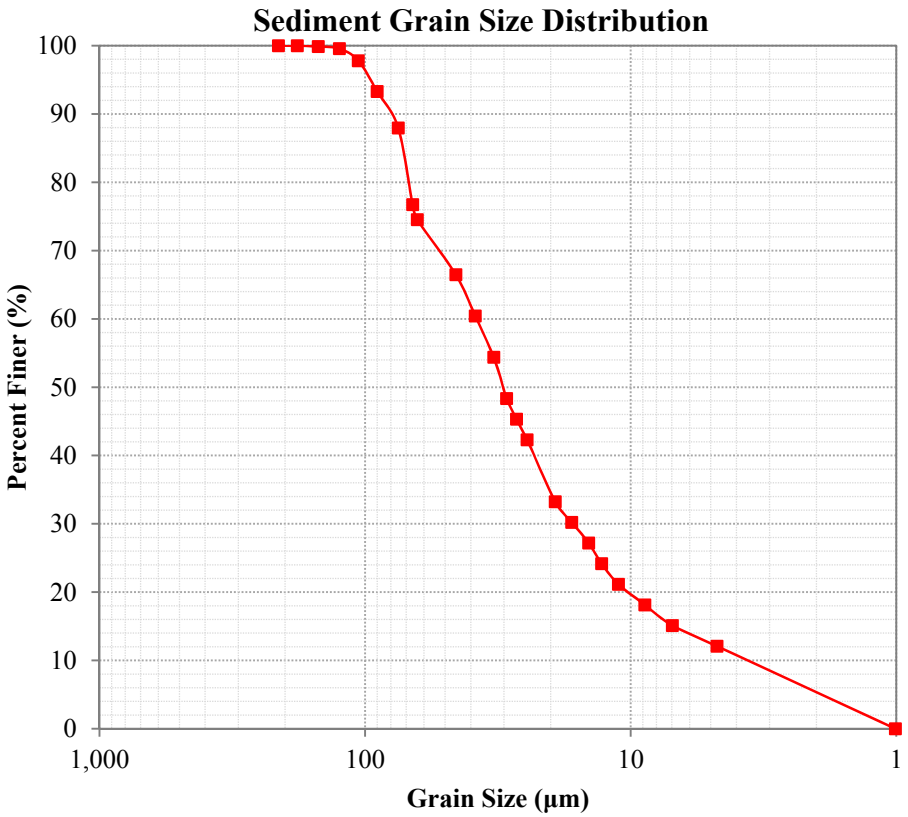

Figure 11. Sediment grain size distribution before conducting the experiments.

Table 2. Other sediment grain size characteristics.

Parameter	Value
D_{50} (µm)	30.27
Dg (µm)	23.71
D_{84} (µm)	71.91
D_{16} (µm)	7.52
Φ_m	5.40
σ_g	3.14

The sedimentological scale Φ provides a sediment classification system according to the grain size. It is defined as

$$D = 2^{-\Phi} \quad \text{Equation 59}$$

The mean grain size (Φ_m) is given by

$$\Phi_m = \sum_{i=1}^{n} \overline{\Phi_i} p_i = \sum_{i=1}^{n} -\left[\frac{\ln(\overline{D_i})}{\ln(2)}\right] p_i \quad \text{Equation 60}$$

where $\overline{\Phi_i}$ is the sedimentological size for each fraction p_i of material in the sediment sample being analyzed, which corresponds to the grain size in terms of equivalent diameter given as $\overline{D_i}$. In this case, Φ_m = 5.40 which indicates that the material that dominates is classified as medium silt. This value is used to calculate the geometric mean size (D_g) and the geometric standard deviation (σ_g). The corresponding equations are

$$D_m = 2^{-\Phi_m} \quad \text{Equation 61}$$

and

$$\sigma_g = 2^{\sigma} \quad \text{Equation 62}$$

where

$$\sigma^2 = \sum_{i=1}^{n} (\overline{\Phi_i} - \Phi_m)^2 p_i \quad \text{Equation 63}$$

The D_g value represents the analytical most frequent particle size in the sediment sample, based on mass. The analyzed sample resulted in a σ_g = 3.09, higher than 1.6, which means the sediment material is considered poorly-sorted.

4.5 Measuring Instruments

4.5.1 Inflow Control

The two reservoir operation scenarios simulated in this study, normal operation and turbidity currents venting, were designed to run with turbid water inflow. The turbidity inflow was generated at the mixing tank described in Section 3.4, and was controlled by a semi-

automatic peristaltic pump filling system with a maximum capacity of 3.4 liters per minute. Fresh water flow was controlled with a flow meter with a maximum capacity of 75 liters per minute.

4.5.2 Flow Velocity Measurements

One-dimensional velocity profiles were measured at different locations along the longitudinal axis of the scaled reservoir using an Ultrasound Doppler Velocity Profiler (UVP). The UVP is designed to measure velocity in liquid flows as function of both space and time in a non-intrusive way. The equipment consists of a set of transducers that emit pulsations of ultrasound signals, the measuring unit that collects and processes the acoustic signal, and the user interface for data analysis and storage. Three transducers of 4 MHz of frequency were used for this project, with an external diameter of 8 millimeters and a divergence half-angle of 2.2 degrees (γ in Figure 12).

The transducers were placed at an angle of 30 degrees form the vertical (θ in Figure 12), looking upstream and remained on the same position and place for every experimental run. The velocity measurements were taken through all the running time, and were taken only inside the impoundment, downstream of the plunging point. The first transducer was placed at the dam, the second at 183 centimeters upstream from the dam, and the last one at 366 centimeters upstream from the dam.

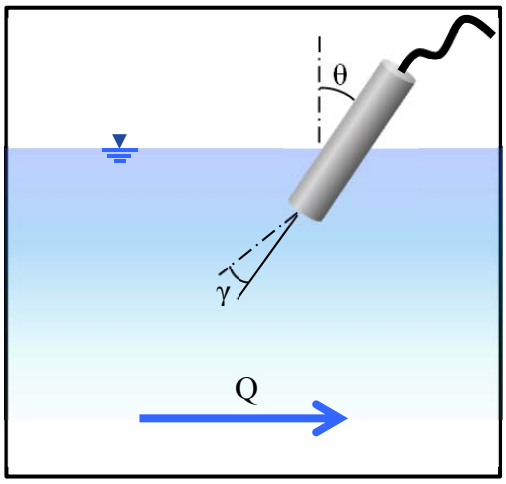

Figure 12. Positioning of transducers used to measure flow velocity on the experiments.

4.5.3 Suspended Sediment Concentration Measurements

To measure concentration of suspended sediment, three sets of siphons were located at different positions along the channel to obtain concentration samples at different elevations. The elevations of the siphons for Set A were 1.25, 3.20, 5.70, 9.55, 13.65, and 18.40 centimeters above the bed. The set was located at 358 centimeters upstream from the dam, 46 centimeters downstream from the plunging point. Set B is located at 186 centimeters upstream from the dam and the siphons were located 1.25, 3.20, 6.00, 9.20, 13.00, 16.85, and 21.90 centimeters above the bed. The last set, Set C (1.25, 3.20, 5.70, 8.90, 12.40, 16.85, 21.60, and 24.45 centimeters from the bed), was located at 23 centimeters upstream from the dam. Before each run, all the siphons sets were raised until the lowest siphon was 1.25 centimeters from the new bed elevation with the sediment deposited after the previous run.

On the experimental runs assigned for collection of sediment concentration samples, the samples were collected at three different times to obtain a better understanding of the evolution of the vertical concentration distribution with the given constant characteristics. The first sample was taken when the turbidity current reached the location of each siphon set, with a reference time of $t = 0$. The second and third samples were taken 10 and 20 minutes, respectively, from the first sample.

4.5.4 Sediment Deposition Measurements

Adhesive measure scales were placed along the sidewall of the flume to measure sediment deposition. The first scale was placed 1 foot upstream from the dam, followed by scales placed every 46 centimeters (1.5 feet) along the bottomset and topset. The deposition was measured 24 hours of each run to provide time for the suspended sediment to settle.

The scales were also used to measure the height of the turbidity currents while the experiment was running, as presented on Figure 13.

Figure 13. Scale used to measure turbidity current height during the experiments and sediment deposition after each experimental run.

4.5.5 Other Measurements

A thermometer was used measure the temperature of the stored water before running inflow and the temperature of the inflow. In addition, two digital photographic cameras and dye colorant (red, blue and green) were used to obtain visual measurements. Figure 14 shows the turbidity current dyed with red colorant making possible to identify it.

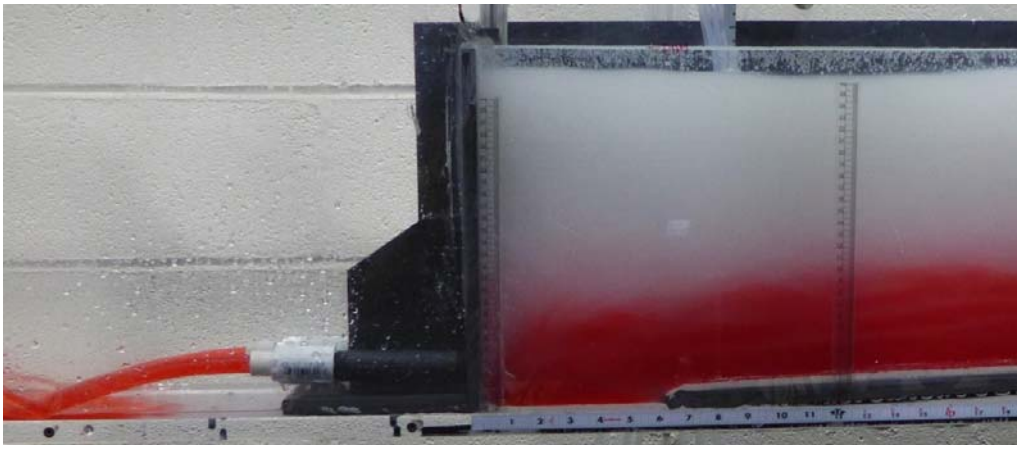

Figure 14. Red dye used to visualize the turbidity current.

The cameras were placed to capture the area of the plunging point and the area near the dam. The dye was added on the upstream part during the experimental runs to highlight the turbidity currents along the flume.

4.6 Experimental Procedure

Each section of Chapter 4 explains the role played by each component of the experimental setup during the experimental runs. Section 4.6 summarizes experimental procedure for a more clear understanding of the process.

Before each run, the impounded water was slowly decontaminated by feeding the flume with a very slow flow to make sure that the sediment bed deposited from the previous runs was not altered. After the impoundment was filled with fresh water, the siphons sets were placed at 1.25 centimeters of elevation from the bed, the UVP system was set and prepared to start collecting data, and the dense fluid was prepared in the mixing tank. At that point the experiment was ready to be run, so the cameras were put in place and set to take video or pictures, and the stored water temperature was measured.

4.6.1 The Experimental Run

All experimental runs started by delivering the turbid fluid at the upstream end of the scaled reservoir. The overconcentrated fluid in the mixing tank was pumped using the peristaltic pump, and the uncontamined water was fed from a hose and controlled by a flow meter. Both fluids were combined in a pipe that ended on a diffuser to assure a homogeneous mix. The turbidity current was then allowed to flow and stabilize until reaching the plunging point. Sediment concentration samples were taken immediately once the current reached the locations of the siphons sets. The low-level outlets at the dam remained closed during the Normal Reservoir Operation scenario runs and the overflow inside the storage pool spilled over the dam as presented on Figure 15. For the Turbidity Current Venting runs (Figure 16), the low-level outlets were opened when the current reached a distance of about 61 centimeters (2 feet) upstream from the dam. After that, two more concentration samples were taken after 10 and 20 minutes, respectively. In the meantime, pictures and videos were taken, dye was used to visually

highlight the turbidity currents (Appendix A), the inflow temperature and current height were measured, the UVP data collection was monitored, and concentration samples of the outflow were taken. When the run was done, the velocity data was saved, the concentration samples processed to obtain the concentration data, and the deposition was measured after 24 hours.

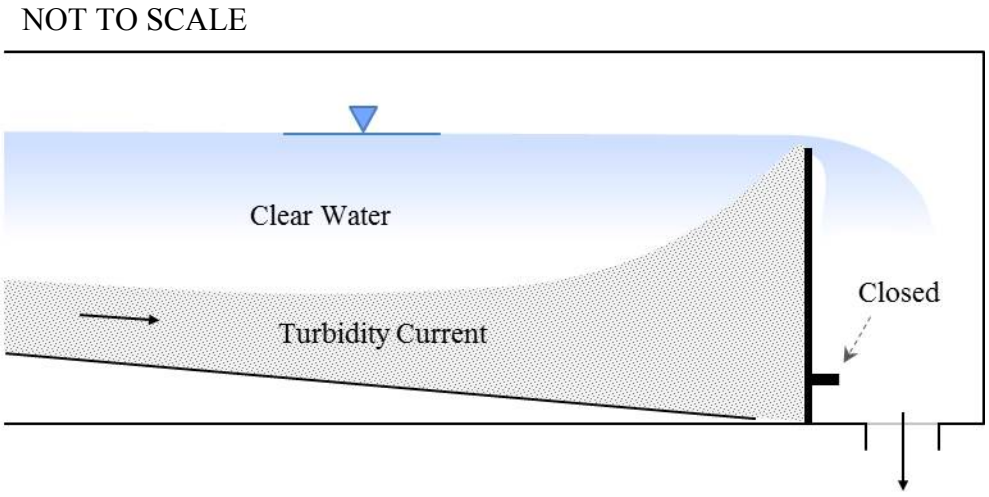

Figure 15. Schematic of the Normal Reservoir Operation sediment management technique, used as the control conditions in this study.

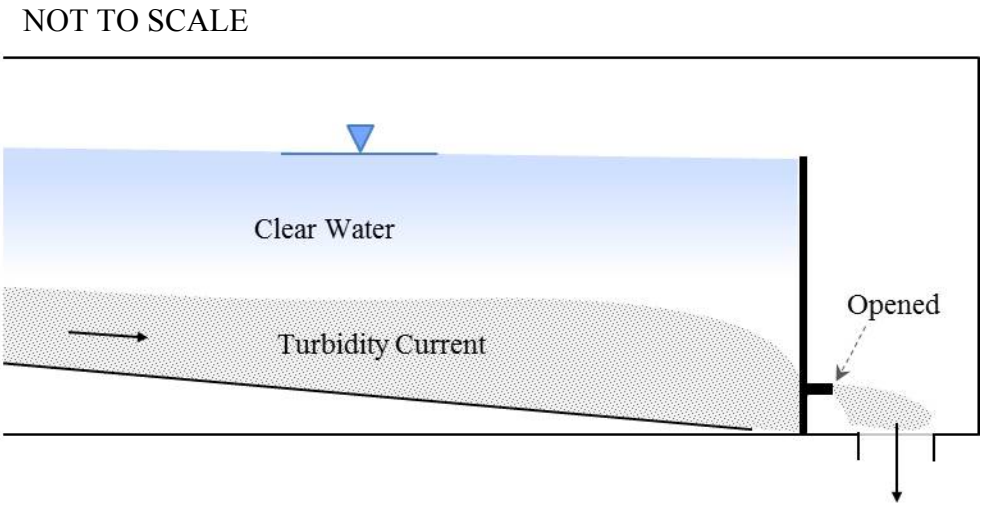

Figure 16. Schematic of the Turbidity Current Venting sediment management technique studied in these experiments.

CHAPTER 5: EXPERIMENTAL RESULTS & DISCUSION

5.1 Purpose of the Experiments

These experiments were conducted to obtain a better understanding of the dynamics of turbidity currents under the sediment management technique of venting through low-level outlets. The main focus was to explore the difference in the vertical composition of velocity and concentration, and the deposition patterns while the turbidity currents were vented compared with reservoir normal operation (overflow).

5.2 Overview of the Experiments

For this experimental study, two scenarios were recreated to test turbidity currents under different sediment management techniques on reservoirs. The first scenario was considered as Normal Reservoir Operation (NRO), where the flow control is overflow at the dam. This scenario was used as the control condition in order to identify and analyze the effects of venting the turbidity currents. The second scenario was Turbidity Current Venting (TCV) through low-level outlets at the dam. About twenty-five experimental runs were conducted for each scenario as preliminary tests to adjust the experimental facilities and measuring techniques. After that, seven experimental runs were conducted for each scenario. The inlet flow rate per unit width (q_o) and inlet suspended sediment concentration (C_o) were set constant at 47.8 cm^2/s and 0.0045 by volume, respectively for all experimental runs. The inlet layer-averaged velocity (U_o) and inlet height (h_o) varied due to the sediment deposition that was accumulated after each experimental run of each scenario. The values of U_o, h_o, and Ri_o ranged as presented in Table 3.

Table 3. Range of values of the inlet layer-average velocity, height and Richardson number.

Inlet Parameter	Lowest Value	Highest Value
Layer-Averaged Velocity, U_o (cm/s)	8.7	15.4
Height, h_o (cm)	3.1	5.5
Richardson Number, Ri_o	0.095	0.531

As sediment was being deposited during the experimental runs, the initial eight h_o became smaller, and this resulted in higher velocities for U_o. The Richardson number was significantly smaller than one, resulting in supercritical flow development, which changed once the flow reached the storage pool. The inlet conditions for the NRO and TCV experiments are summarized on Tables 4 and 5, respectively. On these tables, T_f represents the temperature of the clear water inside the flume, and T_i represents the temperature of the turbid inflow. The sediment fall velocity was calculated based on the inflow temperature T_i and the geometric mean grain size, D_g = 23.75 μm, obtained from Section 4.4 of this report. The inlet Reynolds number was greater than 2,700 indicating that the flow was turbulent.

Table 4. Inlet conditions and other characteristics of the Normal Reservoir Operation experimental runs (NRO).

Run	Time (min)	Accum Time (min)	q_o (cm^2/s)	h_o (cm)	U_o (cm/s)	C_o x10^3	Ri_o	T_f (^oC)	T_i (^oC)	w_s (cm/s)	Re_o
N1	20	20	47.8	5.5	8.7	4.50	0.531	23.0	14.5	0.043	4,091.6
N2	20	40	47.8	5.5	8.7	4.50	0.531	20.5	15.0	0.044	4,144.8
N3	20	60	47.8	5.3	9.0	4.50	0.475	24.0	15.0	0.044	4,144.8
N4	20	80	47.8	5.1	9.4	4.50	0.423	17.0	15.0	0.044	4,144.8
N5	20	100	47.8	4.7	10.2	4.50	0.331	20.0	15.0	0.045	4,252.1
N6	60	160	47.8	3.7	12.9	4.50	0.162	17.5	15.0	0.045	4,252.1
N7	80	240	47.8	3.1	15.4	4.50	0.095	18.0	15.0	0.045	4,198.3

Table 5. Inlet conditions and other characteristics of the Turbidity Current Venting experimental runs (TCV).

Run	Time (min)	Accum Time (min)	q_o (cm^2/s)	h_o (cm)	U_o (cm/s)	C_o x10^3	Ri_o	T_f (^oC)	T_i (^oC)	w_s (cm/s)	Re_o
V1	20	20	47.8	4.7	10.2	4.50	0.331	17.0	16.0	0.045	4,252.1
V2	20	40	47.8	4.5	10.6	4.50	0.291	16.5	16.0	0.045	4,252.1
V3	20	60	47.8	4.3	11.1	4.50	0.254	23.0	16.0	0.045	4,252.1
V4	20	80	47.8	4.1	11.7	4.50	0.220	20.0	16.0	0.045	4,252.1
V5	20	100	47.8	3.9	12.3	4.50	0.189	19.0	15.5	0.045	4,198.3
V6	60	160	47.8	3.8	12.6	4.50	0.175	20.0	16.5	0.046	4,306.2
V7	80	240	47.8	3.5	13.7	4.50	0.137	20.5	16.5	0.046	4,306.2

5.3 Experimental Measurements

The flume was full of clear water up to the top of the dam before each experimental run, decontaminated of suspended sediment from previous runs by slowly feeding it with a very slow flow to make sure the previous sediment deposition was not altered. Before beginning an experimental run, water temperature of the flume was taken, siphons sets were placed at 1.25 cm from the bed, and the UVP system was set to start collecting data. A turbid flow of 43.7 L/min (728.3 cm^3/s) was delivered from the inlet, and once the flow reached the storage pool, the difference in density compared to the clean water made it plunge to the bottom and continue flowing downslope as turbidity current. The turbidity current would then flow downslope until it reached the dam where it produced overflow at the top of the dam for the NRO scenario. For the TCV scenario, the low-level outlets were opened with the intention of maintaining the sediment of the current in suspension while releasing the flow.

Several vertical profiles of the local downstream velocity u were measured continuously during all experiments, from beginning to end. Sediment concentration c was measured three times at three different locations, focusing mainly on the current body. Accumulated sediment deposition was measured after each run at fourteen locations along the bed. After the last experimental run of each scenario, samples of the deposited sediment were taken from eight locations along the bed to conduct a grain size distribution analysis. Measurements procedures and techniques were consistent during all runs for both scenarios.

As presented in Tables 4 and 5, the duration of the experimental runs varied from 20 to 80 minutes. Runs 1 to 5 from both scenarios had duration of 20 minutes, while Runs 6 and 7 lasted 60 and 80 minutes, respectively. From Run 1 to Run 4, the accumulated time of turbidity currents flowing along the reservoir was 80 minutes. Runs 5 and 6 combined provide 80 more minutes of turbidity current activity on the flume; and Run 7 provides the last 80 minutes period. Runs 4, 6 and 7 from both scenarios were chosen to present and discuss results in a consistent way, creating three time intervals of experimental runs of 80 minutes. Table 6 provides the runs that correspond to each 80 minutes time interval group denoted as 1^{st}, 2^{nd} and 3^{rd} Time Interval.

Table 6. Distribution of experimental runs per Time Interval.

Time Interval	NRO Runs	TCV Runs	Time (min)	Accumulated Time (min)
1st	N1	V1	20	80
	N2	V2	20	
	N3	V3	20	
	N4	V4	20	
2nd	N5	V5	20	80
	N6	V6	60	
3rd	N7	V7	80	80

5.4 Vertical Composition of the Turbidity Currents

Measurements of the vertical composition of the streamwise flow velocity and suspended sediment concentration, sediment deposition, and others were conducted in two scenarios, NRO and TCV, to compare and analyze the effect of turbidity currents venting on reservoirs.

5.4.1 Streamwise Flow Velocity

Velocity profiles were taken at measuring stations A, B, and C inside the storage pool, moving from upstream near the plunging point to downstream near the dam, as presented on Figure 17. Station A was at 366 cm (12 ft) from the dam, at about 15 cm from the downstream end of the foreset. Station B was at 183 cm (6 ft) from the dam, at about the middle of the storage pool; and Station C is at the top of the dam where the low-level outlets were closed for the NRO scenario, and opened for the TCV scenario. The velocity was measured from beginning to end in all experimental runs, and an average was calculated after each run. Figures 18 to 20 present the typical mean velocity u profiles at Stations A, B and C; for the 1st, 2nd, and 3rd Time Intervals, represented by Runs 4, 6 and 7, respectively. In Figure 18, the velocity profiles near the plunging point (Station A) are compared between the NRO and TCV management techniques. Figures 19 and 20 present the velocity profiles for Stations B and C. These velocity profiles were used to obtain the current thickness h and the layer-averaged mean velocity U at each measuring location, based on Equations 64 and 65.

NOT TO SCALE

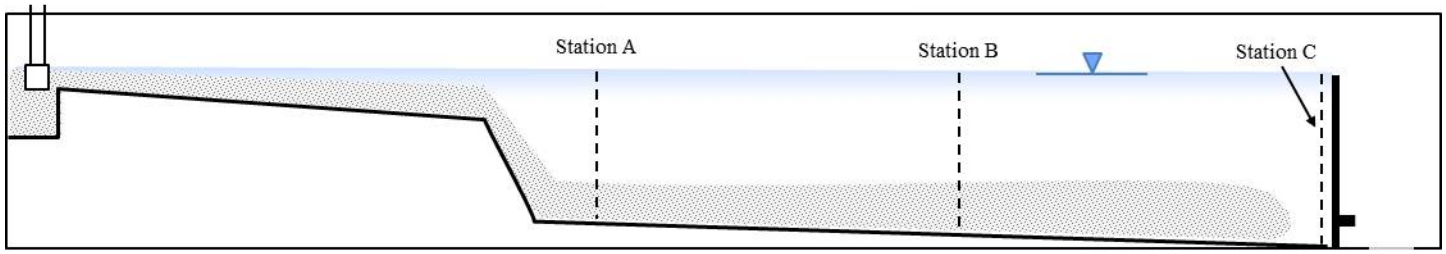

Figure 17. Schematic of the flume showing the location of the measuring Station A at 366 cm upstream from the dam, Station B at 183 cm upstream from the dam, and Station C at the dam.

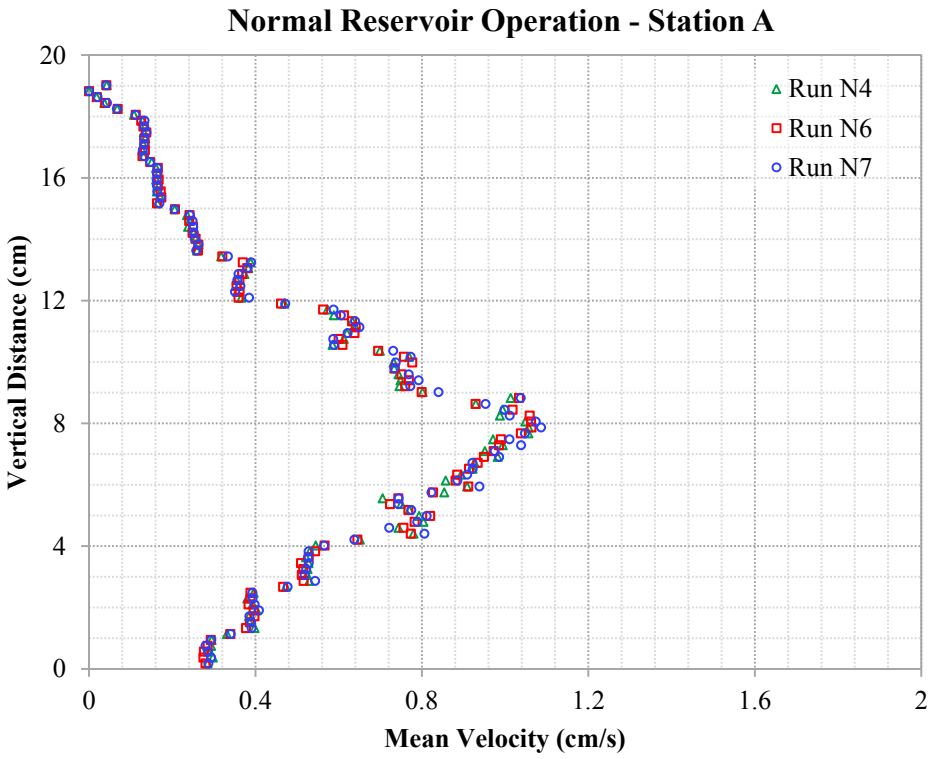

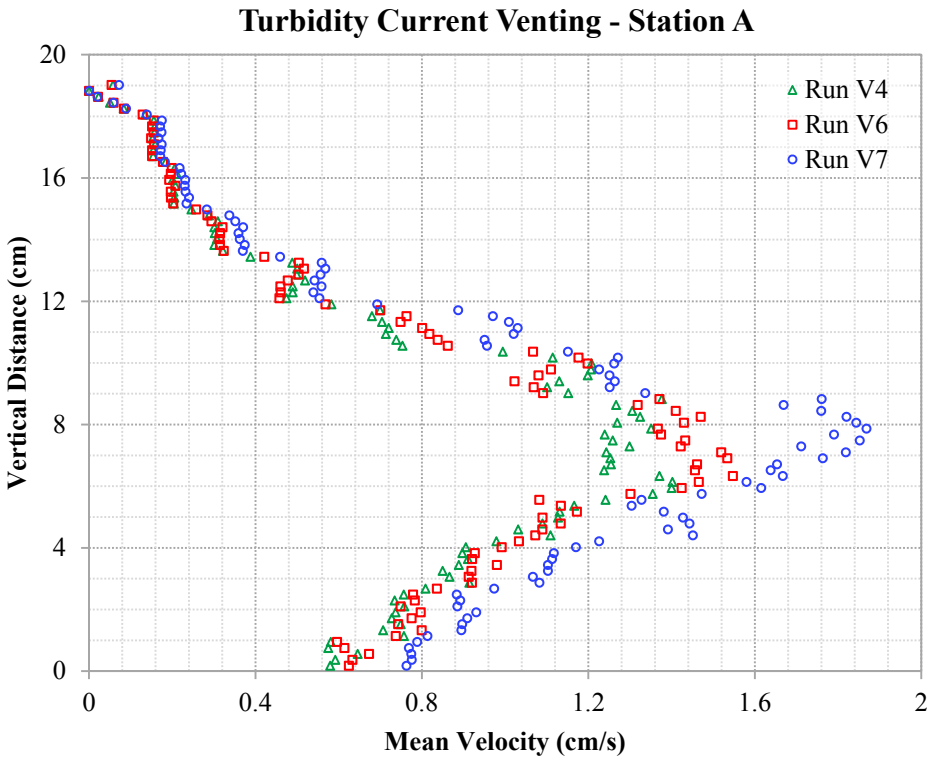

Figure 18. Mean velocity profiles at Station A - 366 cm from the dam.

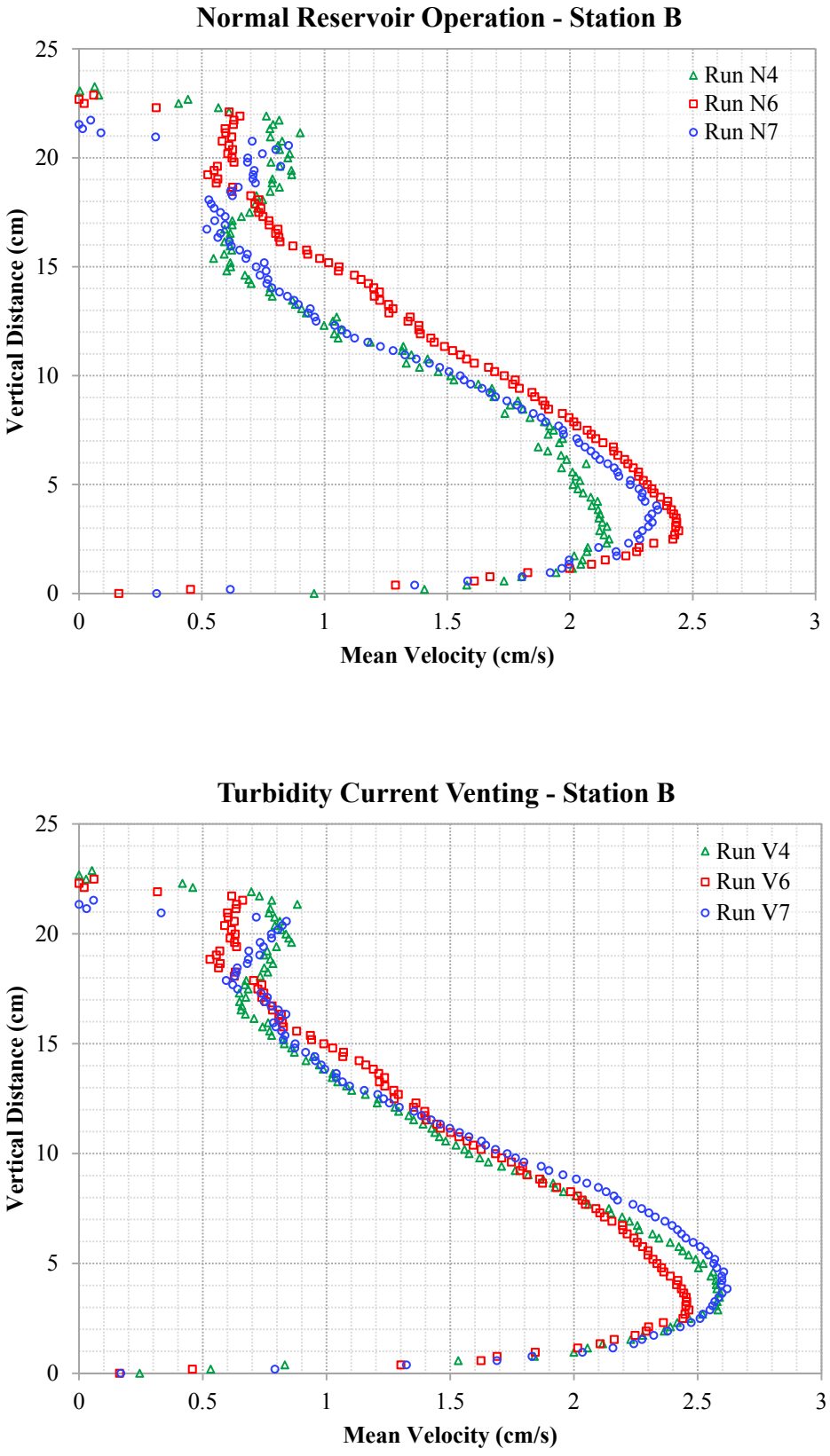

Figure 19. Mean velocity profiles at Station B - 183 cm from the dam.

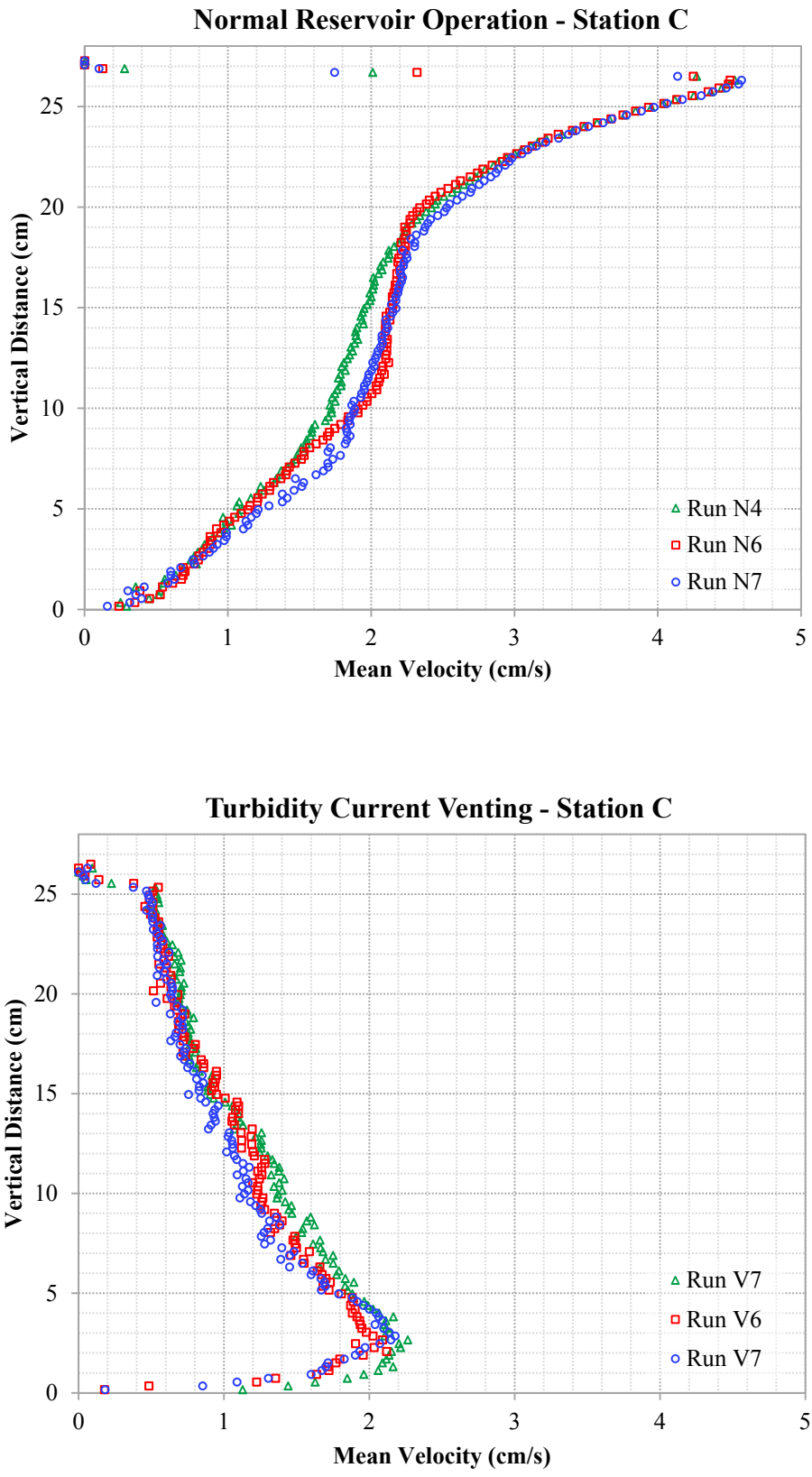

Figure 20. Mean velocity profiles at Station C – near the dam.

$$h = \frac{\left[\int_0^\infty u \ dz\right]^2}{\int_0^\infty u^2 \ dz} \qquad \text{Equation 64}$$

$$U = \frac{\int_0^\infty u^2 \ dz}{\int_0^\infty u \ dz} \qquad \text{Equation 65}$$

At Station A near the plunging point, the typical velocity profile obtained had a sharp shape with the highest streamwise velocity *u* value at around 8 cm from the bed, for both scenarios. This location is close to the plunging point and to the hydraulic jump that is generated when the underflow goes from supercritical, at the foreset, to subcritical at the bottomset. This velocity profile could indicate that the turbid current had not had time to stabilize yet. At Station B, the observed typical velocity profiles were very similar for both scenarios, with the highest velocity values near the bottom and a *nose* shape. This *nose* shape seems to be more elongated for the TCV scenario, with higher velocities than the NRO scenario. Even though the velocity profiles were very similar at Stations A and B, when the turbid flow reached the dam and Station C, the velocity in the water column adapted according to the sediment management technique that was applied at the moment.

The typical velocity profile produced near the dam for the NRO management technique has the highest *u* value at the top of the dam. That way, cleaner water is released because it usually is over the turbid water due to the density difference. For the TCV scenario, the highest velocity vertically at Station A was near the bottom due to the aspiration from the low-level outlets. This helps to maintain the velocity of the underflow, and to maintain the sediment in suspension.

The normalized velocity profiles were determined for the same runs using their corresponding current thickness *h* and layer-averaged velocity *U*. Tables 7 and 8 present the values of *h*, *U* and the maximum normalized local velocity *u/U*, and Figures 21 to 23 provide the normalized velocity profiles. These currents reached a normal state on which the velocity *U* became constant in time, and the current thickness *h* was growing linearly due to water entrainment from above (Ellison and Turner, 1959). The values of *u*, z, z/*h*, and *u/U* are available in Appendix B.

Table 7. Current thickness and layer-averaged velocity for the Normal Reservoir Operation scenario (NRO).

Location	Run	Max *u* (cm/s)	*U* (cm/s)	*h* (cm)	Max *u/U*
Station A	N4	1.056	0.675	14.010	1.564
	N6	1.063	0.680	13.959	1.564
	N7	1.086	0.686	13.957	1.583
Station B	N4	2.159	1.573	19.019	1.372
	N6	2.443	1.765	18.540	1.384
	N7	2.357	1.695	17.170	1.391
Station C	N4	4.537	2.454	21.639	1.849
	N6	4.505	2.494	22.106	1.806
	N7	4.584	2.538	22.215	1.806

Table 8. Current thickness and layer-averaged velocity for the Turbidity Currents Venting scenario (TCV).

Location	Run	Max *u* (cm/s)	*U* (cm/s)	*h* (cm)	Max *u/U*
Station A	V4	1.402	0.966	14.189	1.452
	V6	1.547	1.020	13.993	1.517
	V7	1.868	1.227	13.842	1.523
Station B	V4	2.592	1.814	18.152	1.429
	V6	2.465	1.778	18.157	1.387
	V7	2.619	1.916	17.296	1.367
Station C	V4	2.265	1.468	21.473	1.543
	V6	2.119	1.334	21.602	1.589
	V7	2.177	1.312	20.999	1.660

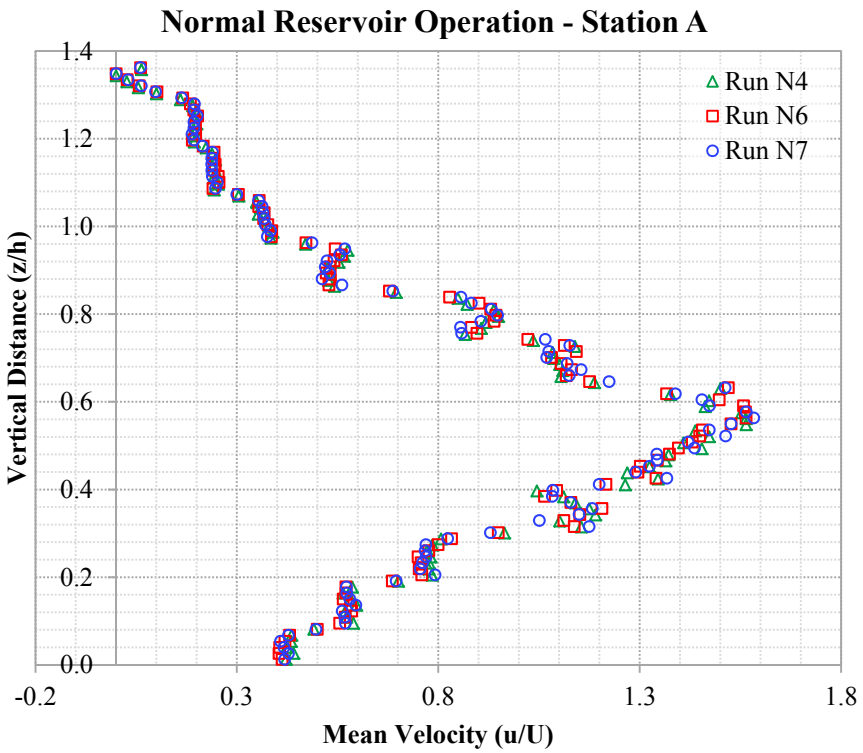

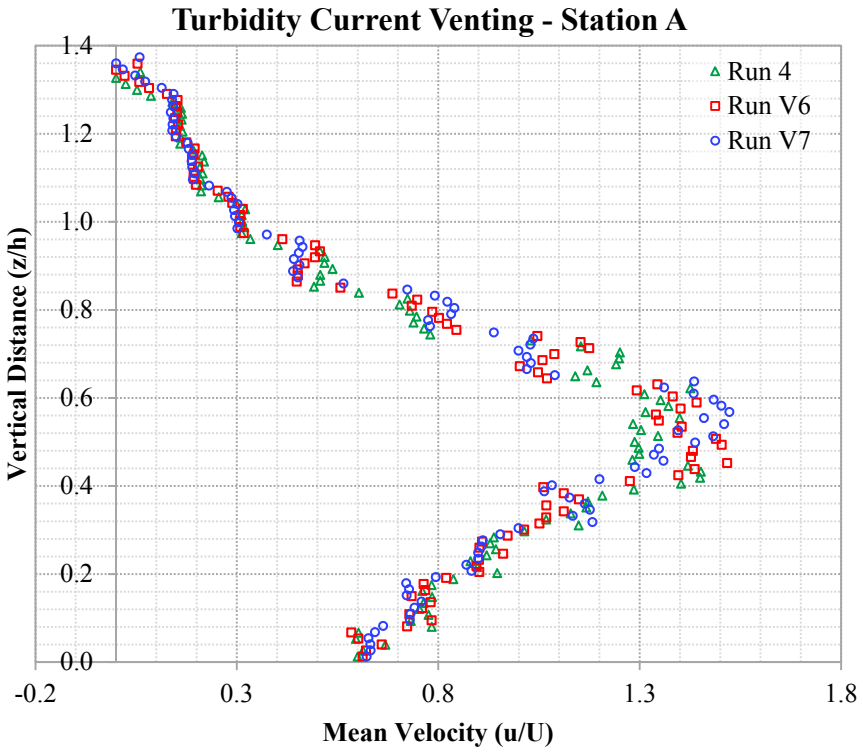

Figure 21. Normalized velocity profiles at Station A – 366 cm from the dam.

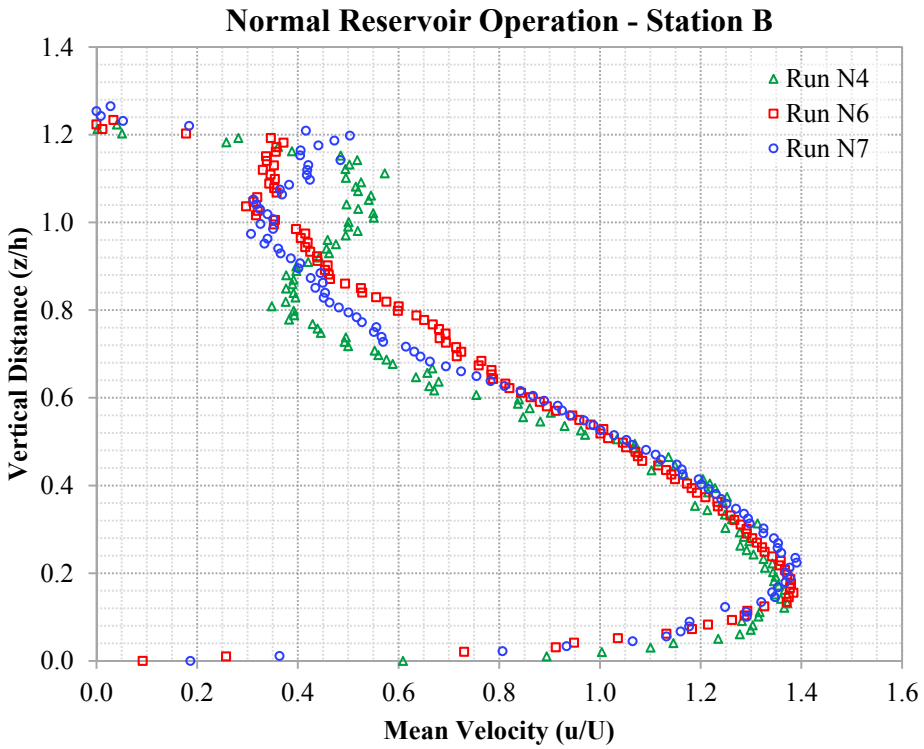

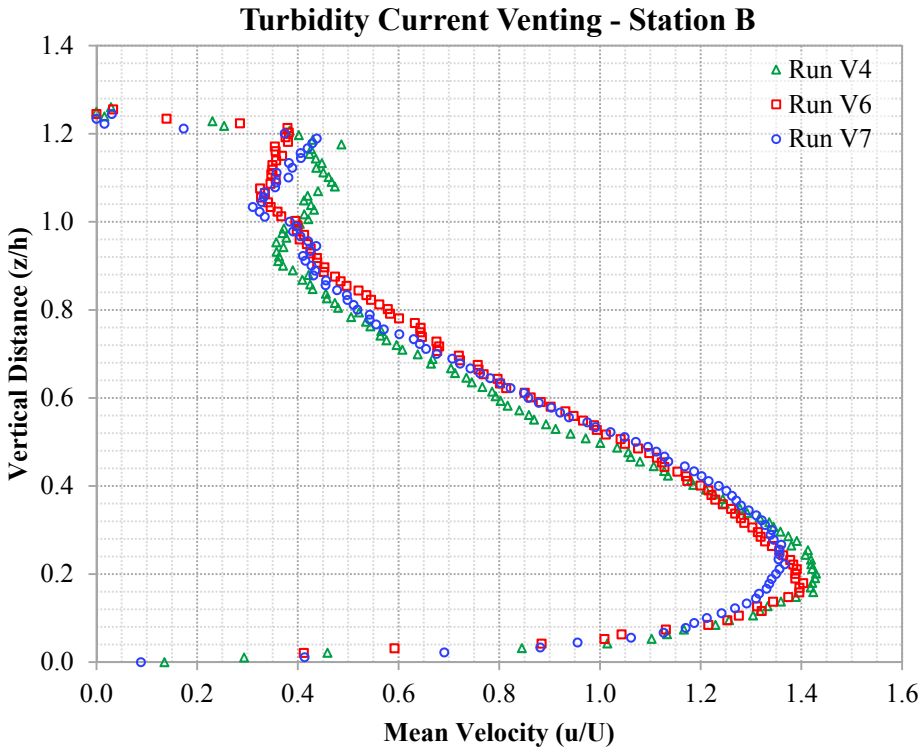

Figure 22. Normalized velocity profiles at Station B - 183 cm of distance from the dam.

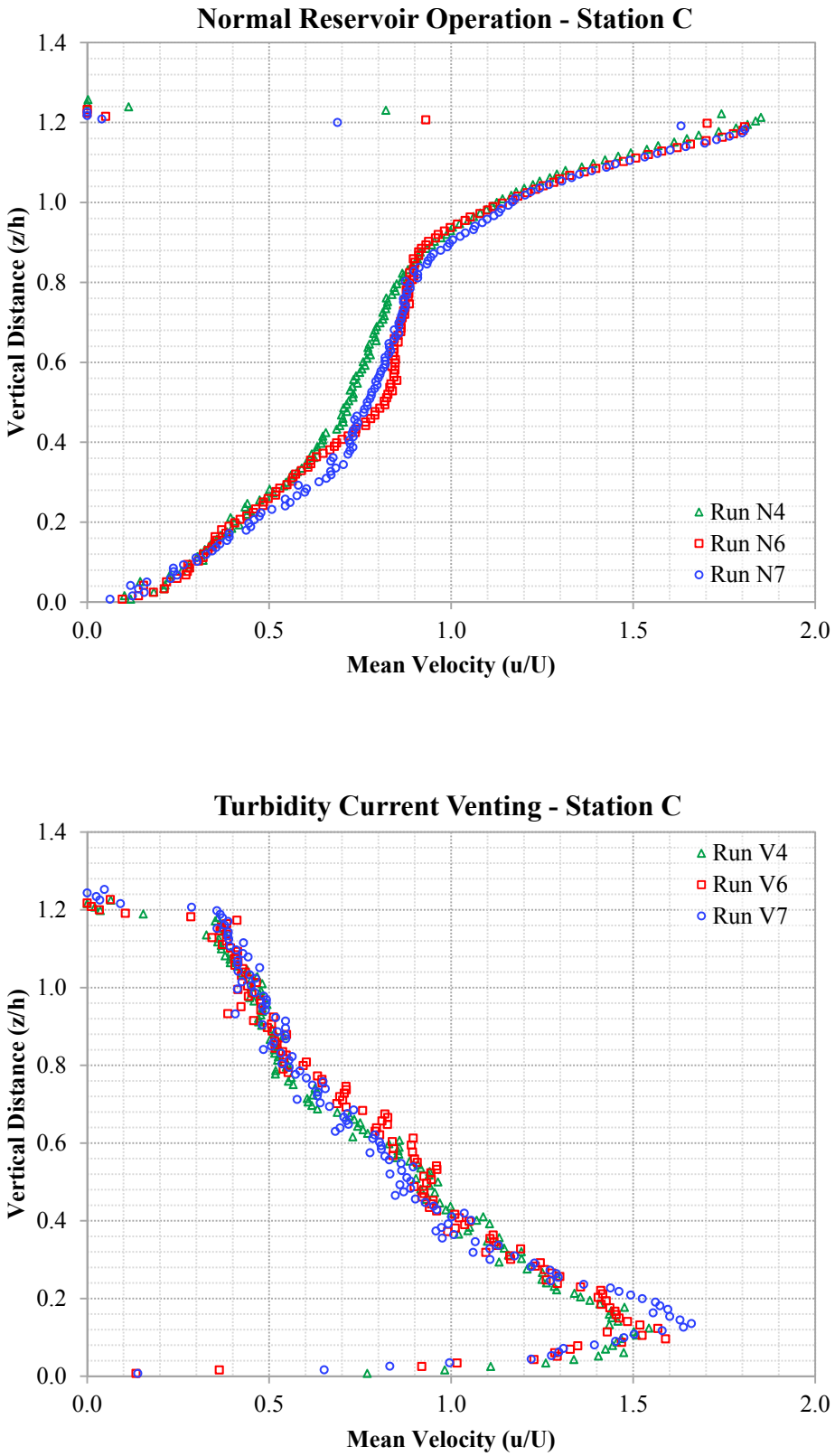

Figure 23. Normalized velocity profiles at Station C – near the dam.

The normalization of velocity profiles shows a good fit between the velocity profiles of both sediment management techniques. In Figure 24, the normalized profiles of both scenarios at Station A are plotted together to show the similarities between them.

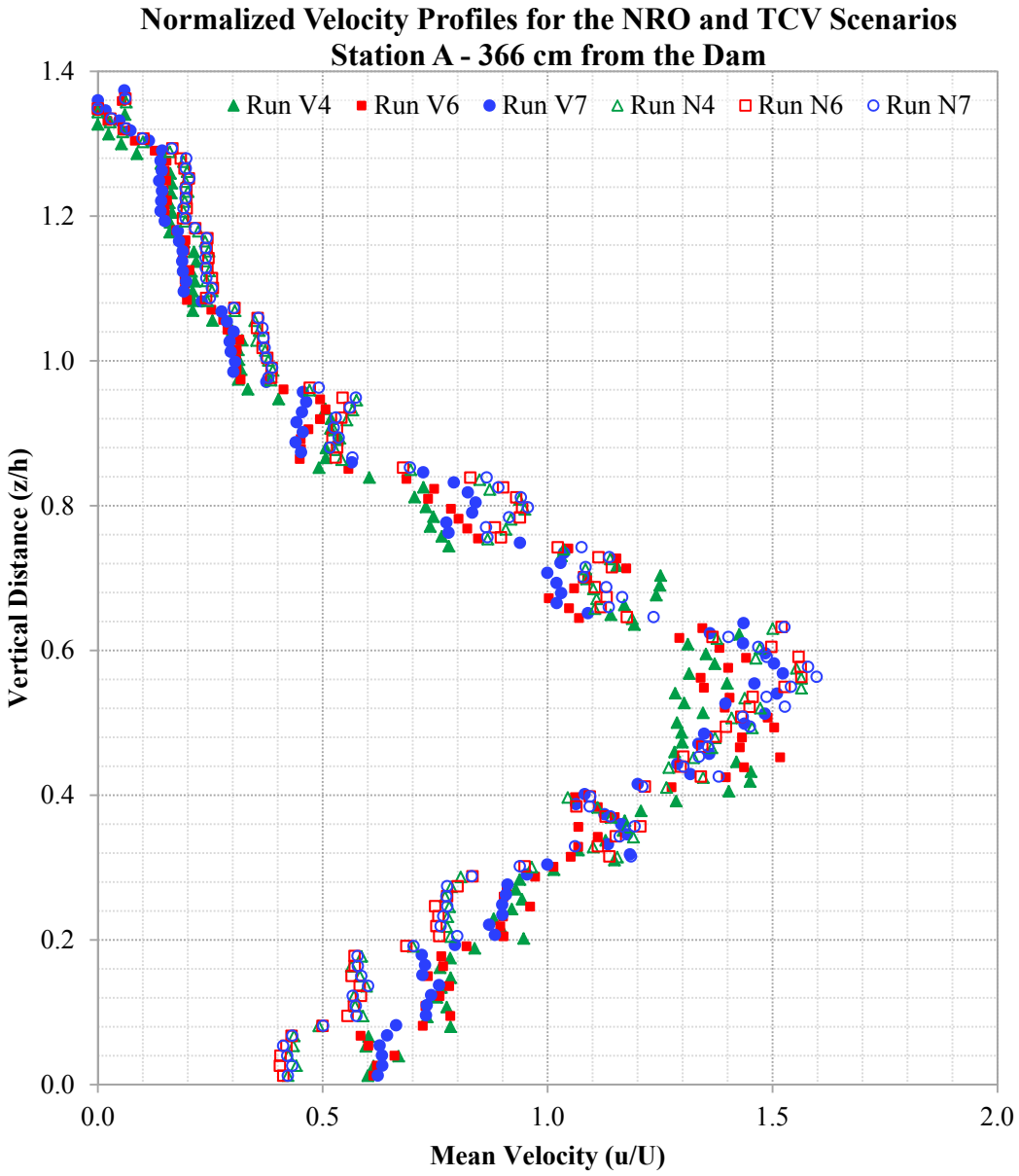

Figure 24. Normalized velocity profiles from the Normal Reservoir Operation and Turbidity Current Venting scenarios at Station A.

Velocity profiles at Station B have a great fit between both scenarios, as it can be appreciated in Figure 25 profiles seem to merge together as one where the current is identified.

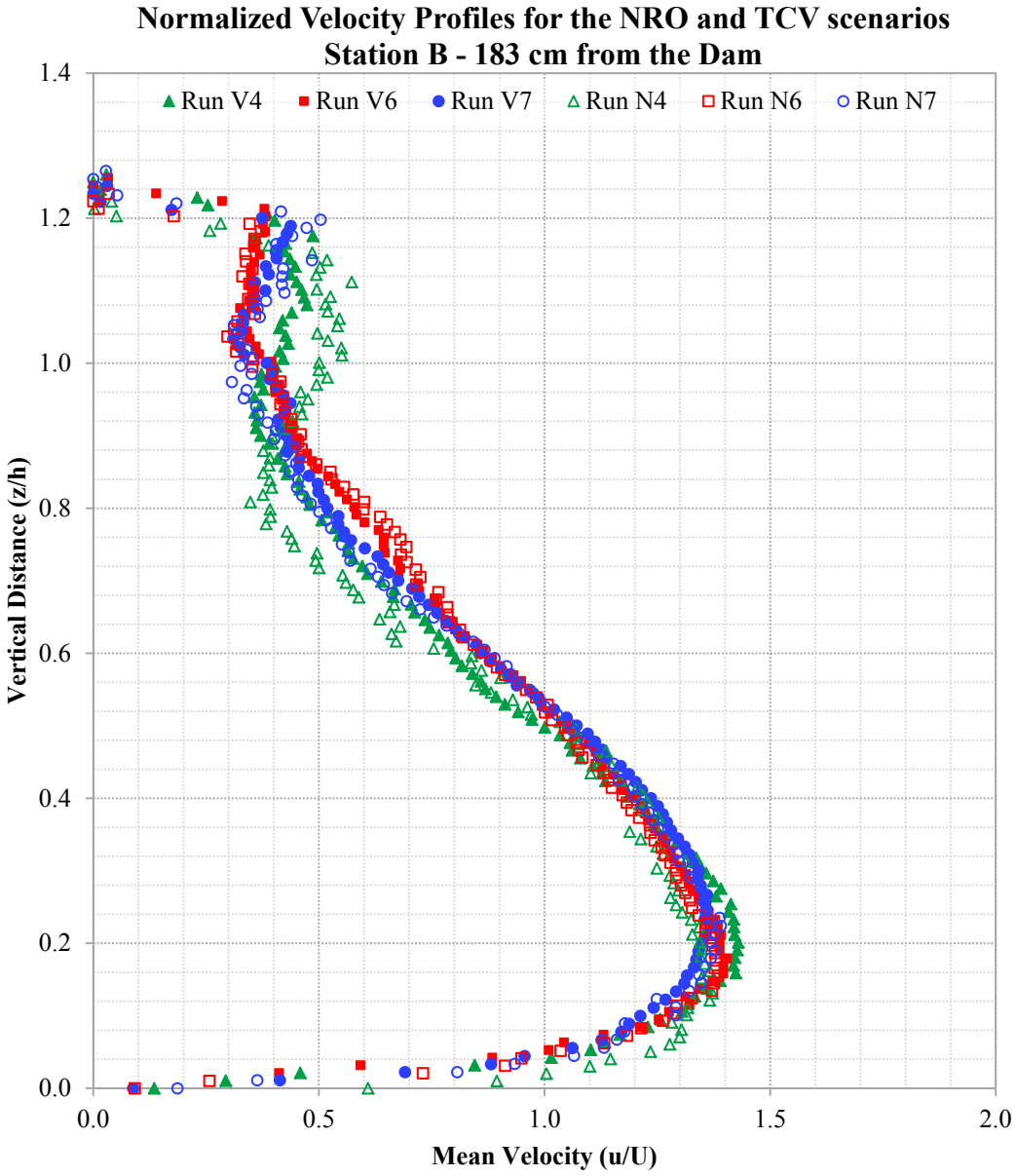

Figure 25. Normalized velocity profiles from the Normal Reservoir Operation and Turbidity Current Venting scenarios at Station B.

In Figure 26, it could be pointed out that all normalized velocity profiles at Station C reach a height of about 1.2, and the profiles cross at around 0.6. Some similarities can be attributed on the pattern or shape of the profile too, though it would be the inverse.

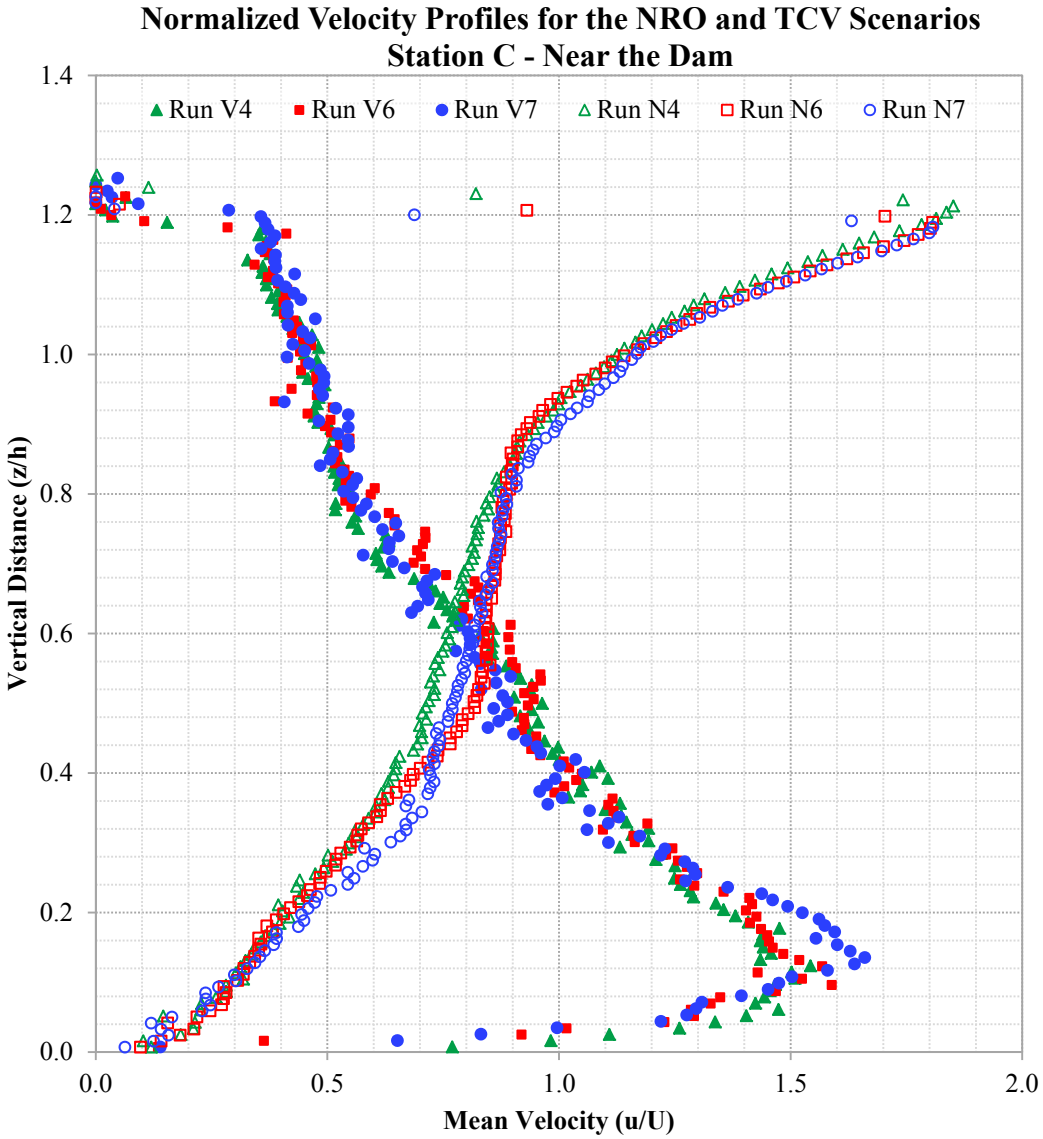

Figure 26. Normalized velocity profiles from the Normal Reservoir Operation and Turbidity Current Venting scenarios at Station C.

5.4.2 Suspended Sediment Concentration

Three sets of siphons were placed inside the storage pool, near the measuring stations A, B and C mentioned on Section 5.4.1 of this study, to collect samples of the suspended sediment and water mix at different elevations. The siphon set closer to the plunging point, Set A, was placed at about 366 cm upstream of the dam and it was composed of six siphons. Moving in the downstream direction, Set B was located at about 183 cm upstream of the dam, and had seven siphons. For Set C, the location was 23 cm upstream of the dam. It contained eight siphons. Table 9 presents the vertical distance at which the siphons were positioned before each experimental run. For this, all the siphon sets were raised until the lowest siphon was 1.25 cm from the new bed elevation formed by the sediment deposited during the previous run.

Table 9. Distance above the bed of siphon sets used to measure suspended sediment concentration.

Distance from the bed (cm)			
Siphon	**Station A**	**Station B**	**Station C**
8	--	--	24.45
7	--	21.90	21.60
6	18.40	16.85	16.85
5	13.65	13.00	12.40
4	9.55	9.20	8.90
3	5.70	6.00	5.70
2	3.20	3.20	3.20
1	1.25	1.25	1.25

Concentration samples were taken at Runs 1, 2, 4, and 6 for each scenario (see values in Appendix C). At each run, the first sample was taken at the moment when the turbidity current reached the location of each measuring station, with a reference time of t = 0; and the second and third samples were taken after 10 and 20 minutes, respectively. Figures 27 to 29 present how the suspended sediment concentration profiles changed as the turbid inflow continued contaminating the fresh water of the storage pool. The concentration profiles were obtained from the three samples taken at the three measuring stations. An average based on the four experimental runs of each scenario was calculated.

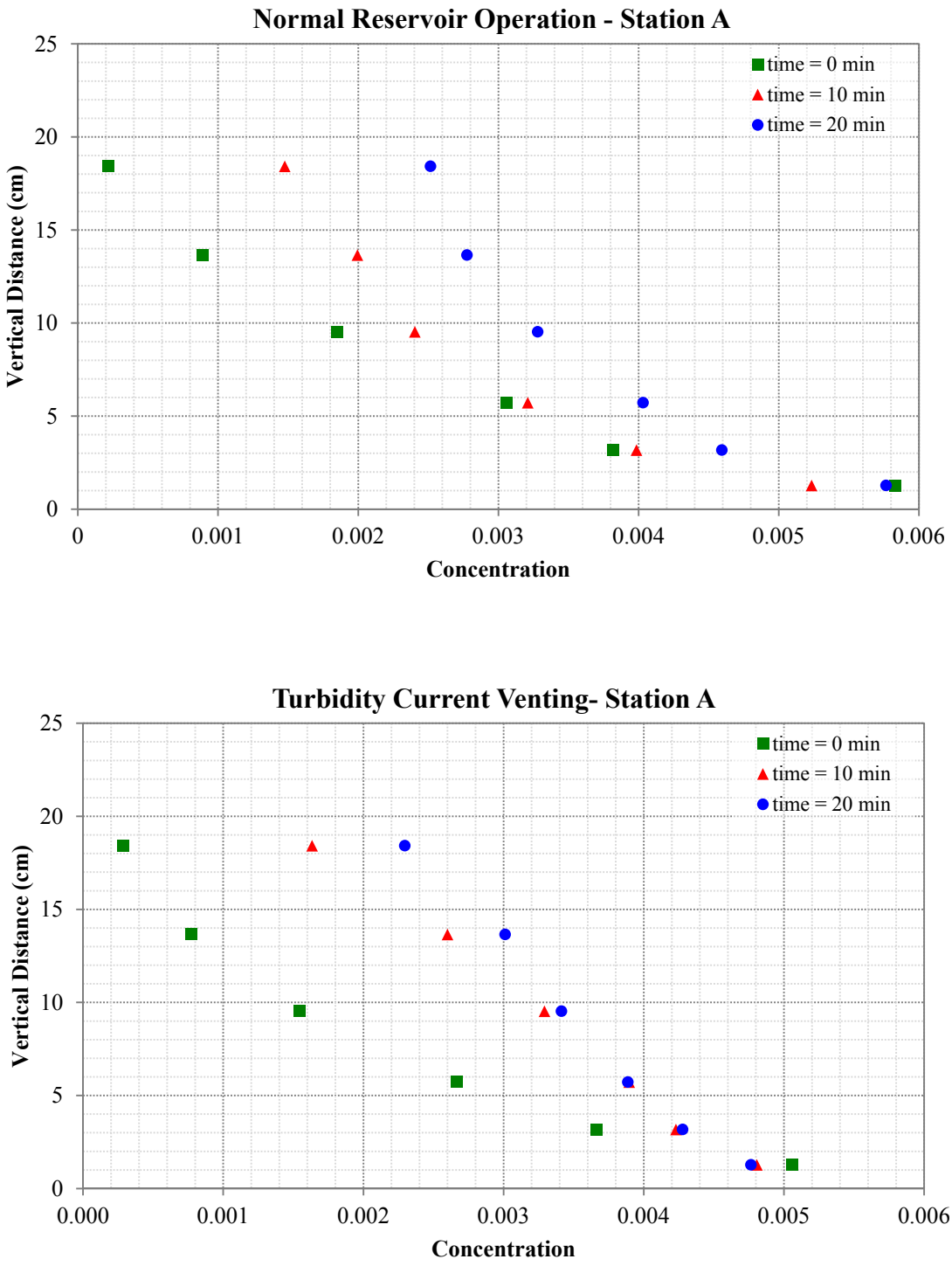

Figure 27. Progression in time of the suspended sediment profile at Station A – 366 cm upstream of the dam.

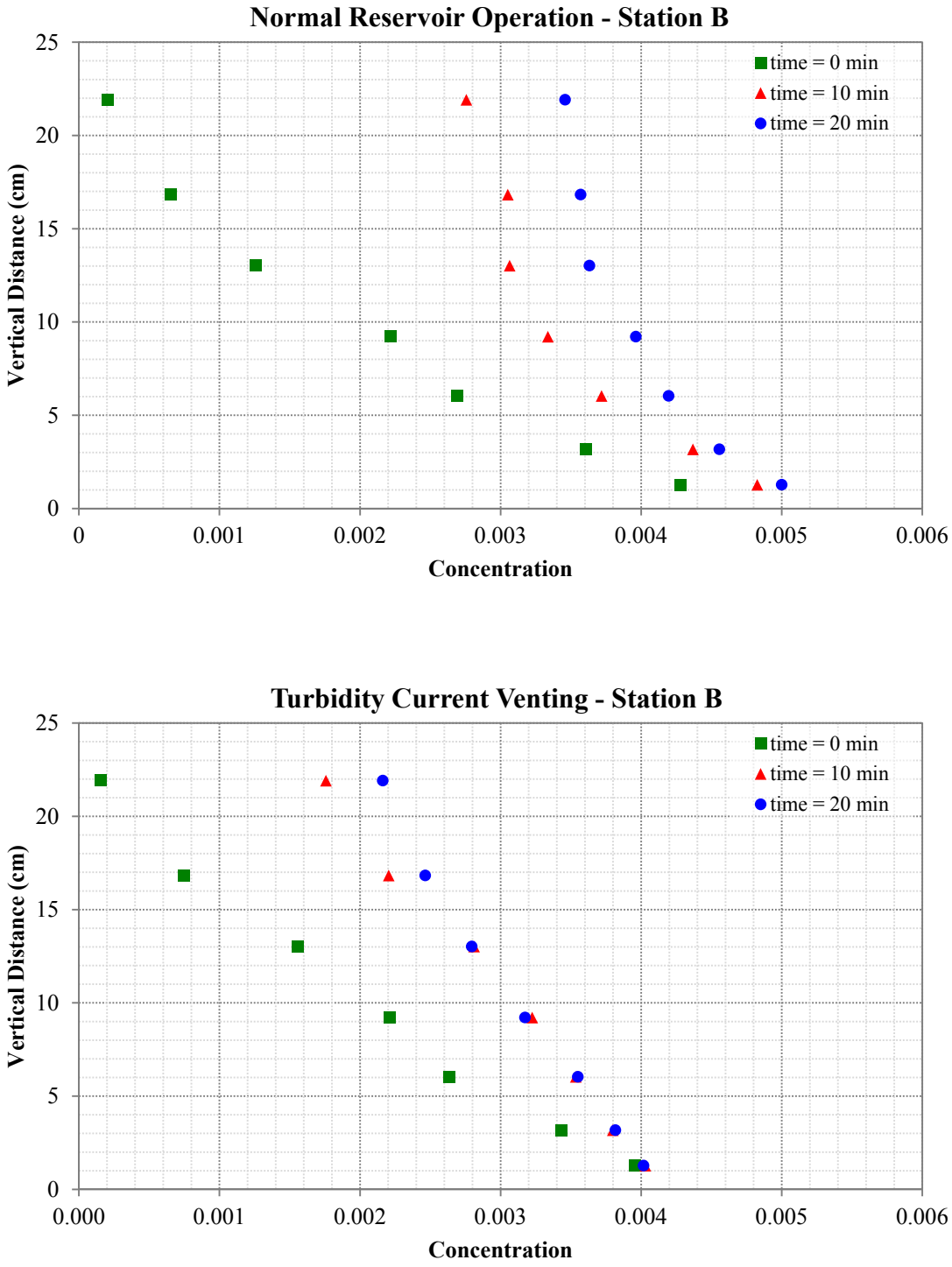

Figure 28. Progression in time of the suspended sediment profile at Station B – 183 cm upstream of the dam.

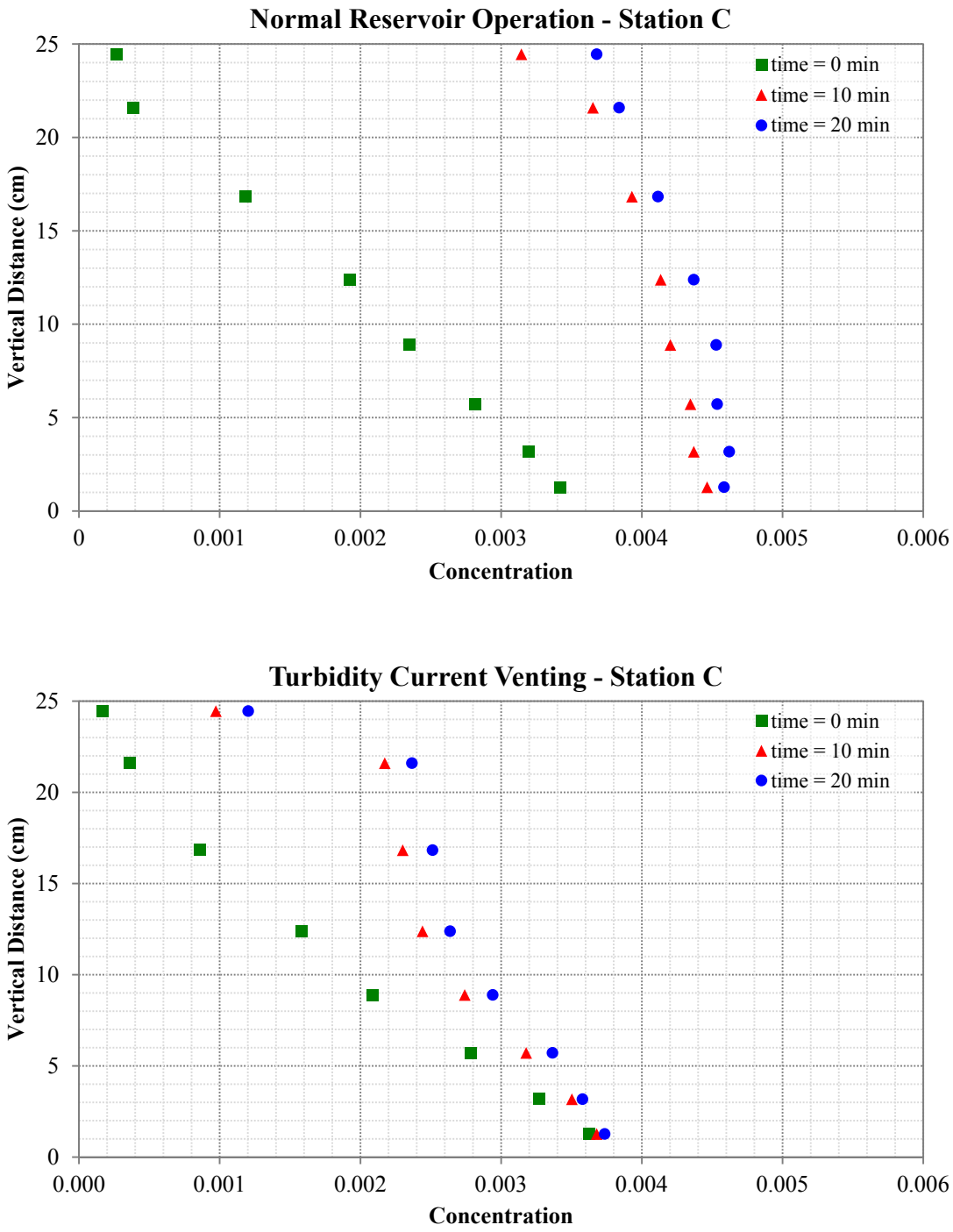

Figure 29. Progression in time of the suspended sediment profile at Station C – 23 cm upstream of the dam.

Moving in time from t = 0 min to t = 20 min, the suspended sediment concentration became more uniform in the vertical column at the three stations, especially at Station C. The difference in the concentration profiles between the NRO and TCV scenarios increased as the turbidity current moved closer to the dam, from Station A to Station C. The highest concentration values were found at Station C for the Normal Reservoir Operation, where the turbid flow is obstructed at the dam and clean water is released at the top. To explore the evolution and differences in sediment concentration between both scenarios, the layer-averaged suspended sediment concentration *C* was calculated using Equation 66. It was calculated for the three sediment samples collected per run at the three measuring stations, as presented in Table 10 and Figure 30.

$$UCh = \int_0^\infty uc\, dz \qquad \text{Equation 66}$$

Table 10. Layer-averaged suspended sediment concentration *C* values from the Normal Reservoir Operation and Turbidity Current Venting scenarios.

Sediment Management Technique	Location	Layer-Averaged Suspended Sediment Concentration *C*		
		***t* = 0 min**	***t* = 10 min**	***t* = 20 min**
Normal Reservoir Operation	Station A	0.0041	0.0047	0.0058
	Station B	0.0024	0.0037	0.0041
	Station C	0.0012	0.0037	0.0040
Turbidity Current Venting	Station A	0.0024	0.0036	0.0037
	Station B	0.0024	0.0033	0.0033
	Station C	0.0021	0.0028	0.0030

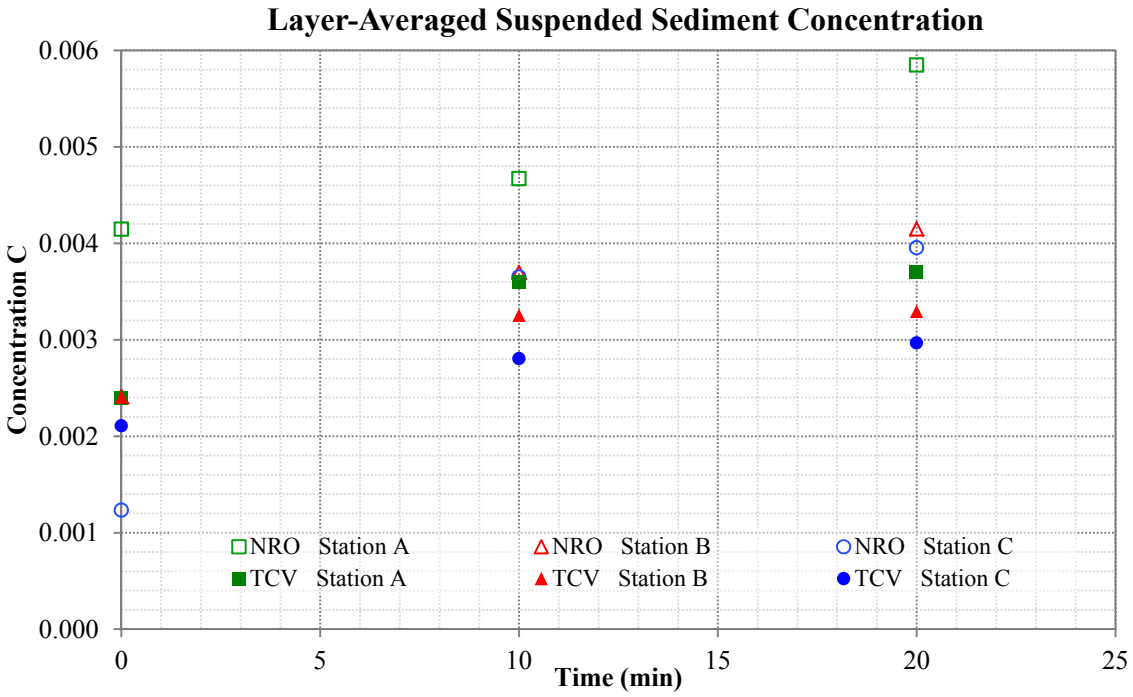

Figure 30. Time progression of the layer-averaged suspended sediment concentration *C*, calculated at measuring stations A, B and C, for the Normal Reservoir Operation (NRO) and Turbidity Current Venting (TCV) scenarios.

As expected in the suspended sediment concentration data presented above, a higher concentration of sediment was accumulated inside the storage pool for the NRO sediment management technique, and since the initial concentration C_o was the same for both study cases, it should translate into lower suspended sediment concentration on the outflow. Table 11 and Figure 31 present the outflow suspended sediment concentration for both sediment management techniques, where it shows that the outflow concentration from the TCV scenario was higher than the concentration from the NRO, for all sampled times and at all measured runs. For both sediment management techniques, there is a significant increment of sediment concentration from the initial samples to the samples at 10 min. The increment on outflow sediment concentration from the 10 min to the 20 min data collection was lower; however, it still was higher for the TCV technique compared to the NRO.

Table 11. Outflow Suspended Sediment Concentration.

Sediment Management Technique	Run	Outflow Suspended Sediment Concentration *C*		
		t = 0 min	*t* = 10 min	*t* = 20 min
Normal Reservoir Operation	N1	0.0019	0.0033	0.0034
	N2	0.0021	0.0032	0.0035
	N4	0.0023	0.0031	0.0036
	N6	0.0023	0.0033	0.0036
Turbidity Current Venting	V1	0.0033	0.0044	0.0049
	V2	0.0039	0.0047	0.0052
	V4	0.0030	0.0045	0.0052
	V6	0.0040	0.0049	0.0054

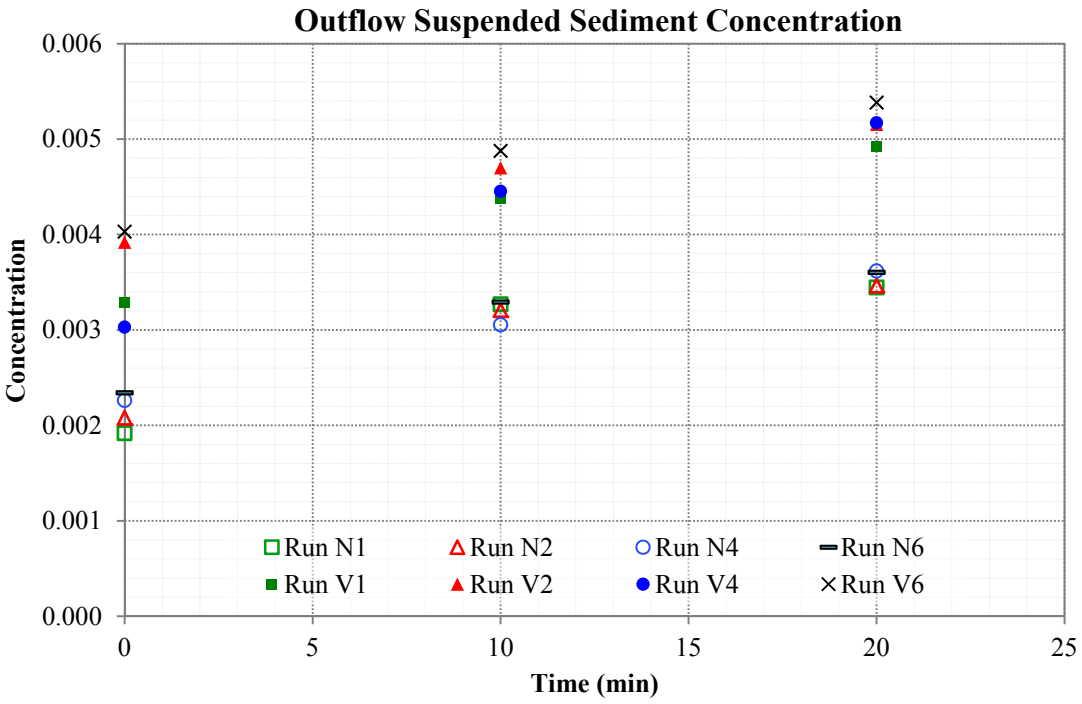

Figure 31. Suspended sediment concentration from the outflow of both studied sediment management techniques, Normal Reservoir Operation and Turbidity Current Venting.

5.5 Sediment Deposition

Turbidity currents were reproduced for a total time of 240 minutes for each sediment management technique scenario selected for this study, NRO and TCV. For both scenarios, the sediment-laden inflow produced sediment deposition from the inlet to the dam. Figure 32 and Table 12 present the location of fourteen spots where sediment deposition per unit area was measured after each run, including measurements at the topset and bottomset.

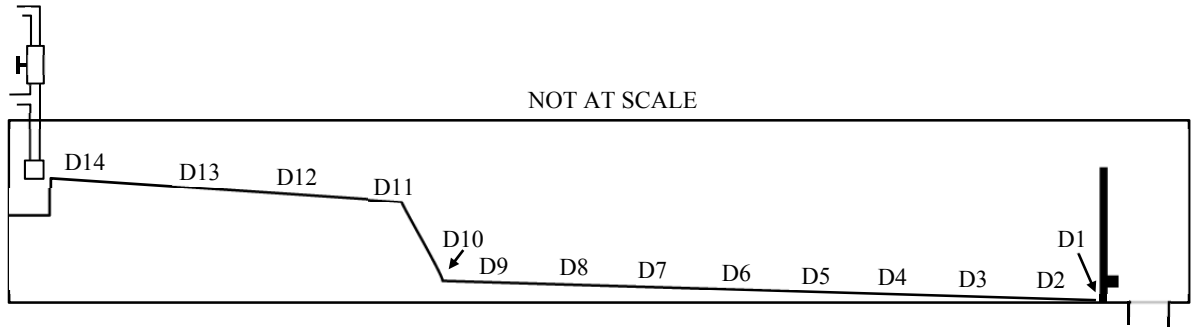

Figure 32. Schematic of the flume showing the location of the sediment deposition measurements.

Table 12. Location of sediment deposition per unit area measurements

	Measurement Point	Distance from the Dam (cm)	Distance from the Dam (ft)
Bottomset (Inside the Storage Pool)	D1	0.00	0.00
	D2	30.48	1.00
	D3	76.20	2.50
	D4	121.92	4.00
	D5	167.64	5.50
	D6	213.36	7.00
	D7	261.62	8.58
	D8	307.34	10.08
	D9	353.06	11.58
	D10	381.00	12.50
Plunging Point	D11	403.86	13.25
Topset	D12	487.68	16.00
	D13	563.88	18.50
	D14	640.08	21.00

The deposited sediment was preserved after every run using its surface from the previous run as the initial bed for the next run. Figure 33 presents the sediment deposition for the Reservoir Normal Operation scenario from the experimental runs N4, N6 and N7 representing the 1st, 2nd and 3rd Time Intervals. The sediment deposition for the Turbidity Current Venting scenario is provided in Figure 34, presenting the results of the experimental runs V4, V6 and V7. In order to compare the sediment deposition, Figure 35 provides the sediment deposition from both sediment management techniques, and the data is available in Appendix D. Significantly more deposition accumulated in the NRO scenario compared with the TCV scenario, from the inlet to the dam. At the end of the last run, the bottom outlets were partially covered with deposited sediment on the NRO scenario.

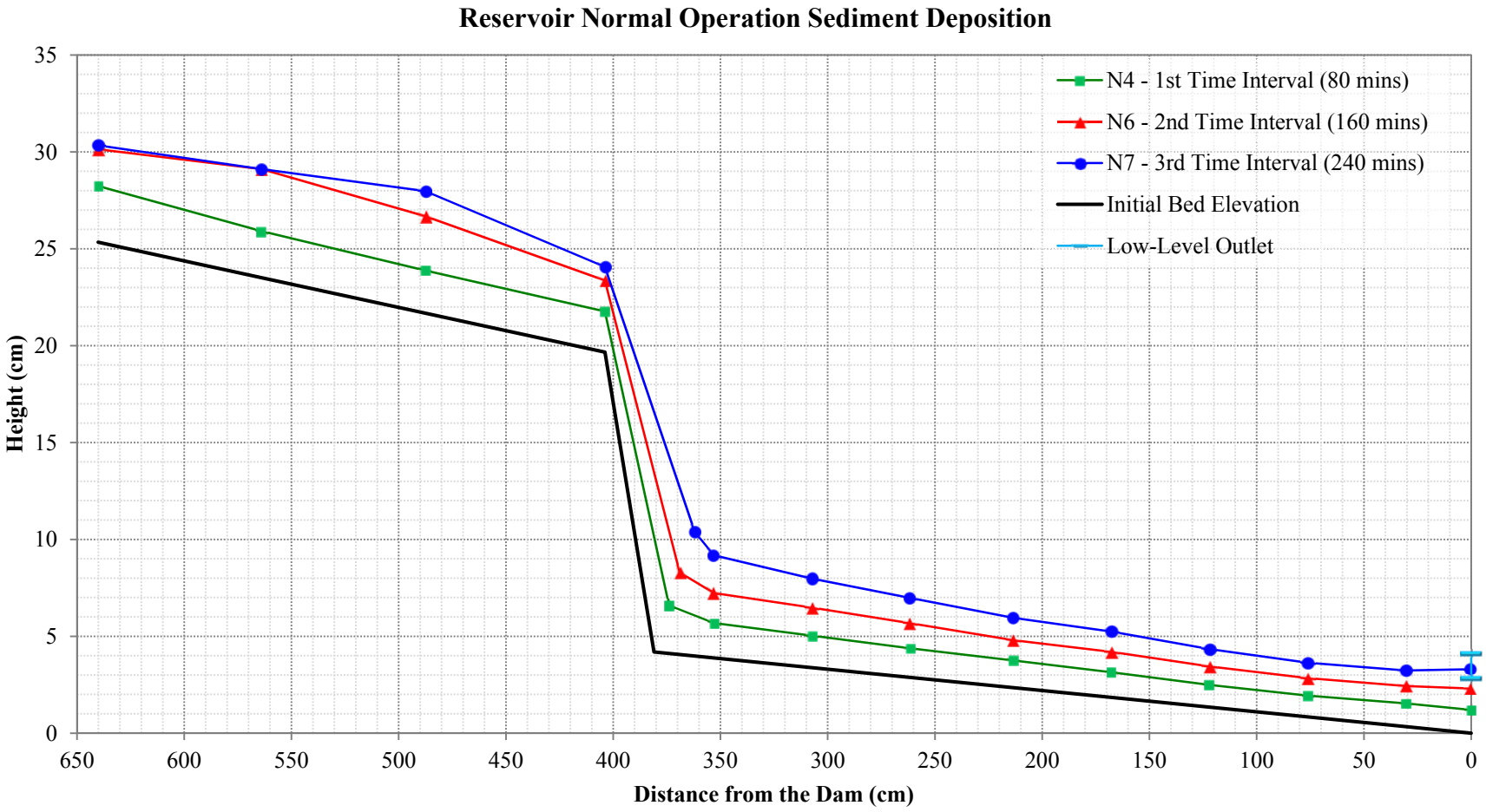

Figure 33. Reservoir Normal Operation sediment deposition in intervals of 80 minutes, using the results of the experimental runs N4, N6 and N7.

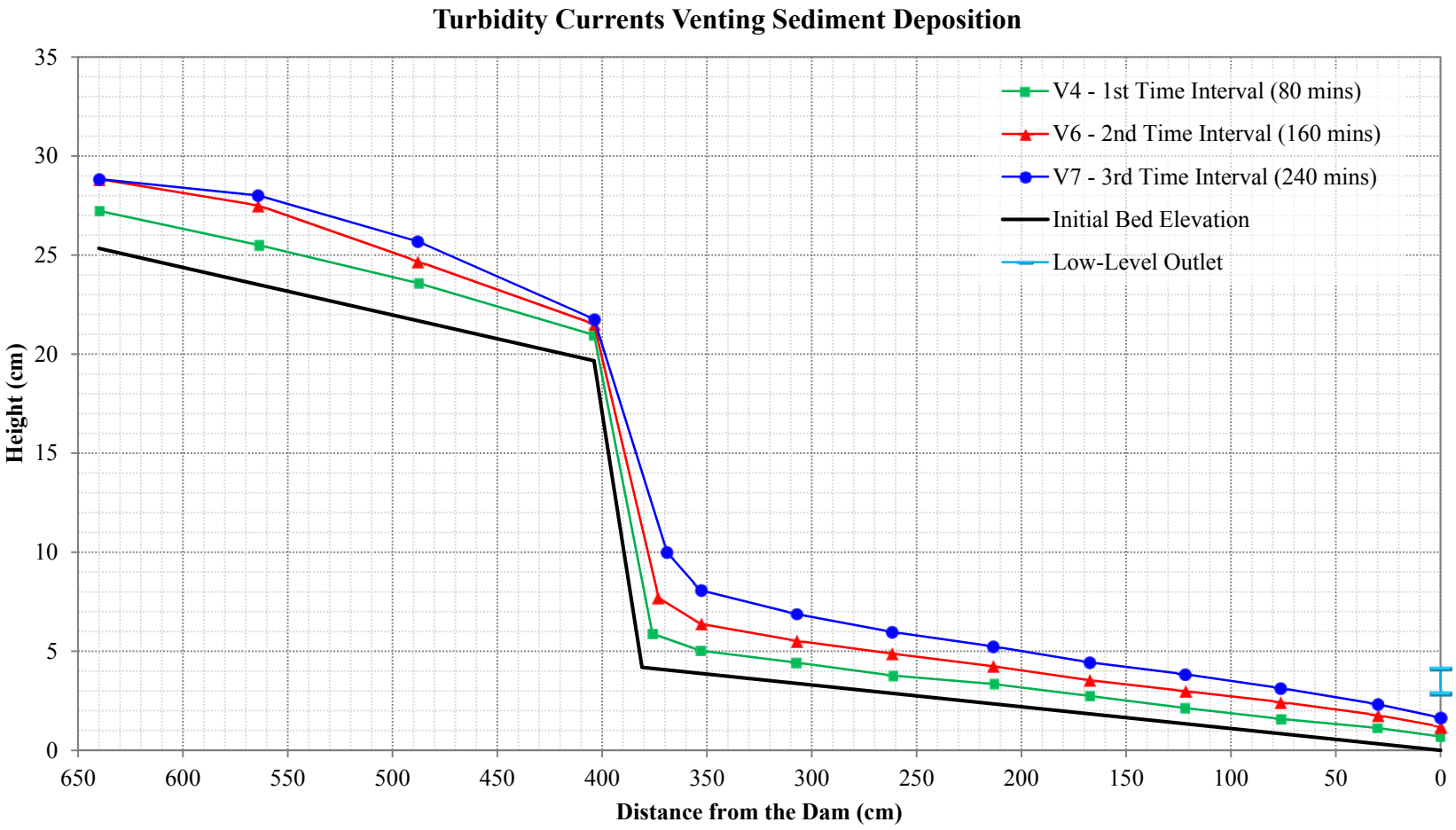

Figure 34. Turbidity Current Venting sediment deposition in intervals of 80 minutes, using the results of the experimental runs V4, V6 and V7.

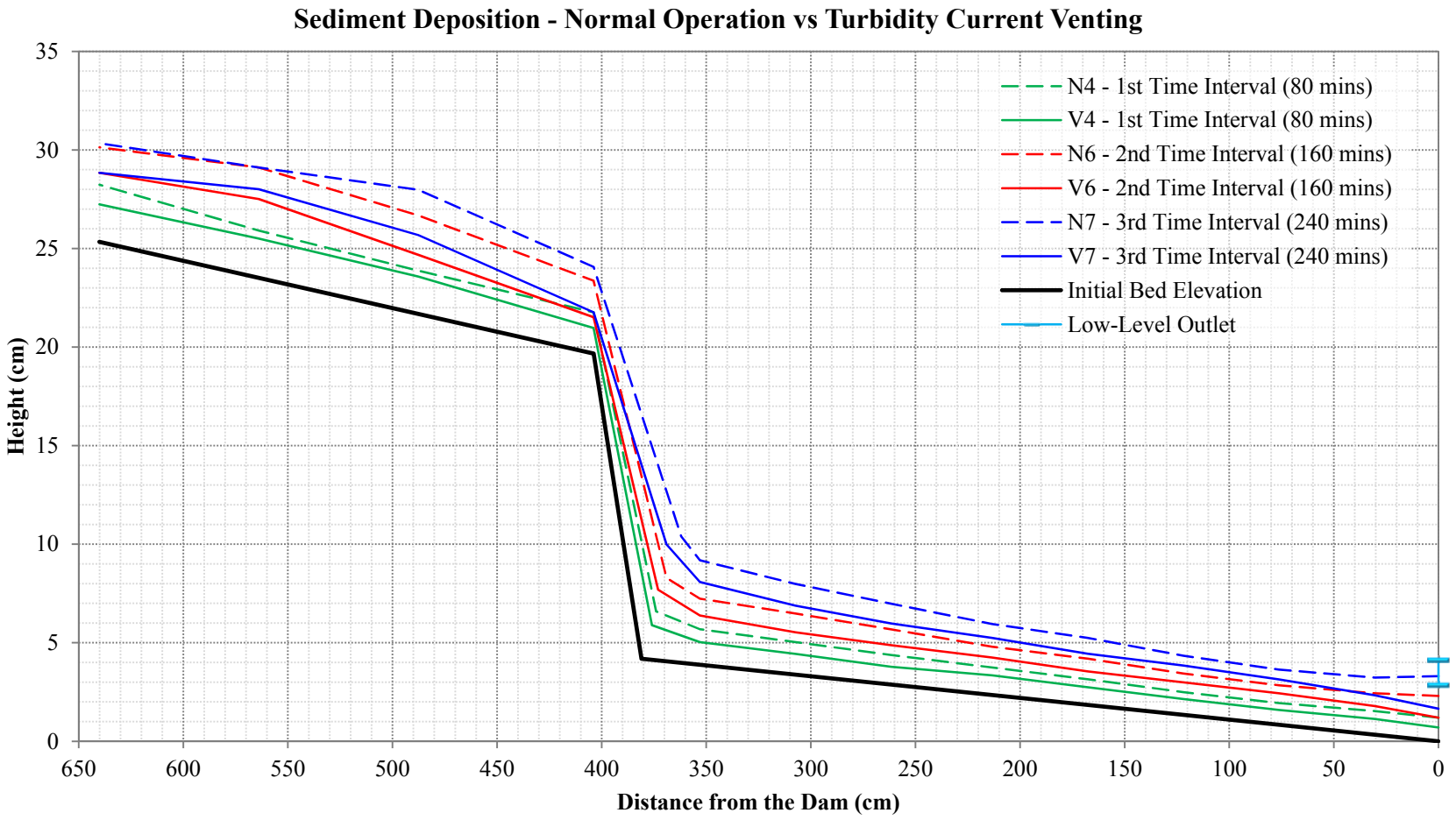

Figure 35. Comparison of sediment deposition between the Reservoir Normal Operation and Turbidity Current Venting sediment management techniques.

The following analyses and calculations based on the sediment deposition information are focused on the storage pool, from points D1 to D10 as presented on Table 12.

Sediment deposition rates were calculated based on the deposition information of experimental runs N4, N6 and N7, and V4, V6 and V7, representing the culmination of the 1st, 2nd, and 3rd Time Intervals. Figure 36 presents the average sediment deposition rates by accumulation, calculated using the following equation for each measuring point:

$$r_{d\,i} = \frac{d_i}{t_a} \qquad \text{Equation 67}$$

where $r_{d\,i}$ denotes the average deposition rate for location *i*, t_a denotes the accumulated time, and d_i denotes the accumulated sediment deposit at location *i*. These calculations present the averaged rate taking into account the accumulated deposition and time. For the 2nd Time Interval, the accumulated deposition up to the end of Run 6 is divided by 160 minutes. Similarly for the 3rd Time Interval, the total accumulation of deposited sediment from the seven runs is divided by 240 minutes. The sediment deposition rate data is available in Appendix D.

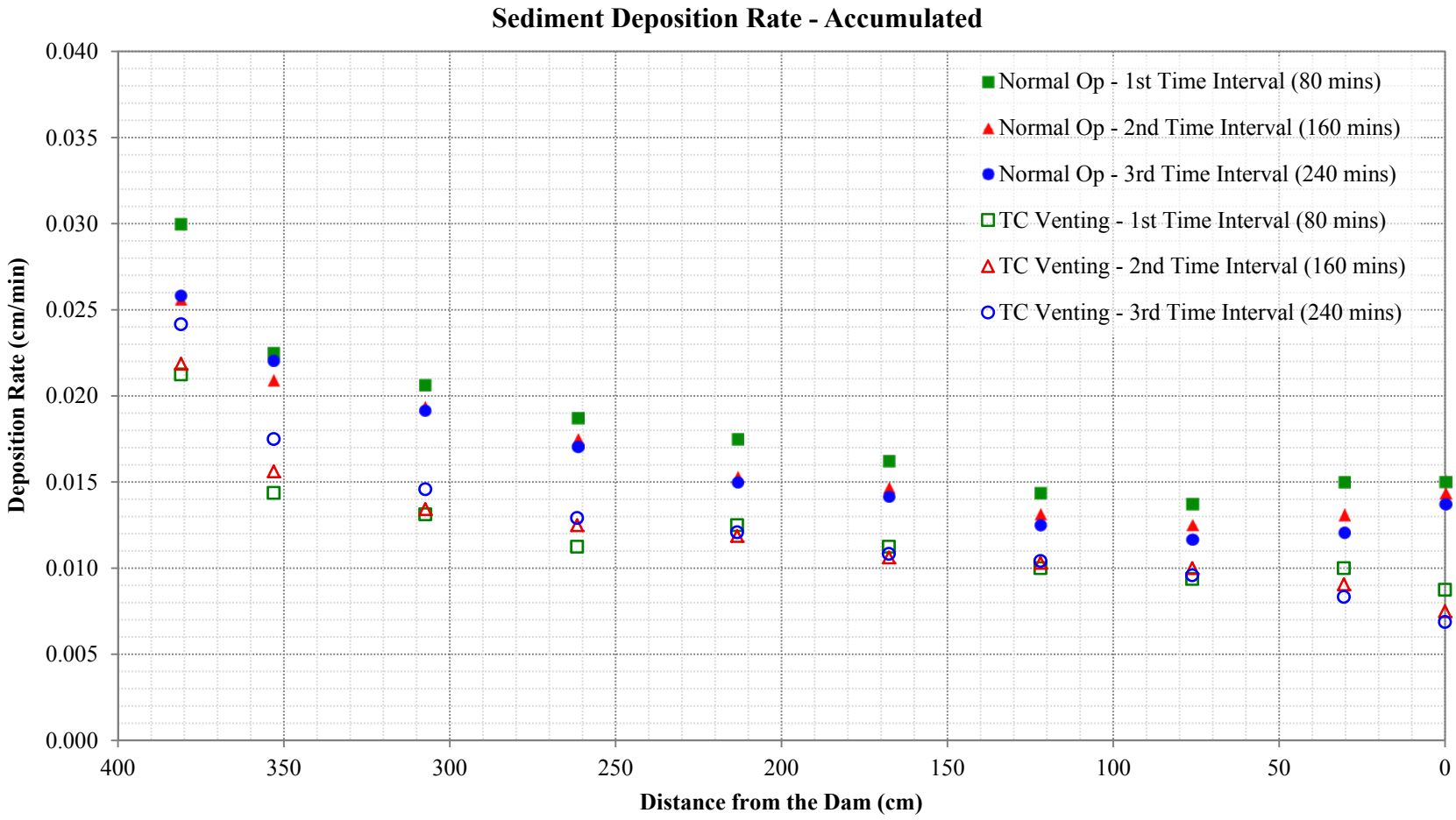

Figure 36. Sediment deposition rate at the storage pool, based on the accumulated deposition including all previous runs from the respective sediment management technique.

Along time, the accumulated average deposition rates are higher for the NRO scenario at all measuring points. The average deposition rate values for each scenario appear to be consistent over time, being higher near the plunging point and smoothly decreasing as the turbidity current moves closer to the dam. For the NRO scenario, the deposition rate increased near the dam because the dam intercepts the turbidity current and its velocity decreases. On the contrary, the deposition rate for the TCV scenario reached its minimum value near the dam due to the flow aspiration produced by the opened low-level outlets.

For a better understanding of how the deposition rate changed in time, a second calculation was made where the deposition rate was averaged over the deposition and duration of each time interval, using Equation 68.

$$r_{d_i} = \frac{d_{n_i} - d_{(n-1)_i}}{80\ mins} \qquad \text{Equation 68}$$

where d_{n_i} is the is the deposition accumulated up to the current time interval, and $d_{(n-1)_i}$ is the deposition accumulated up to the last experimental run of the previous time interval. The denominator of Equation 68 is 80 minutes because that is the extent of all time interval periods. The results are shown on Figure 37, and the data is available at Appendix D.

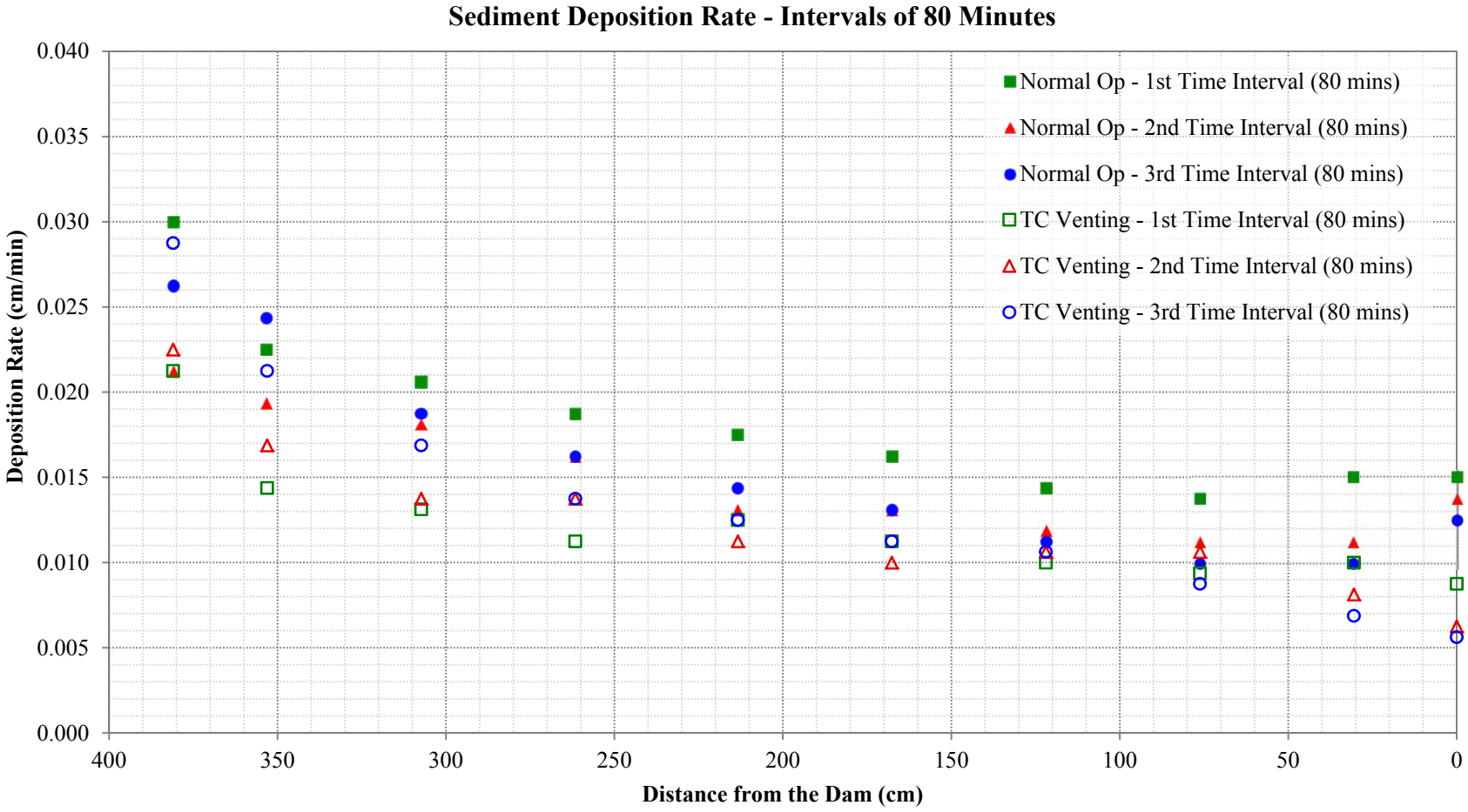

Figure 37. Sediment deposition rate at the storage pool, based on the deposition and time per time interval of 80 minutes each.

Using the sediment management technique of venting, it is expected to hydraulically route some or almost all inflowing sediment load beyond the storage pool. In the experiments of this study we managed to route some of the sediment load, as shown in Figure 35; and yet, an important aspect to consider is how effective the venting technique would be by extending the useful life of the impoundment. Figure 38 presents the projection of storage capacity, in percent, of the scale reservoir used for this study. Implementing the use of turbidity current venting in the designed scenario helped extend the useful life of the storage pool. The storage capacity decreases even when the turbid inflow is being vented, but the capacity loss rate is significantly smaller. Tables 13 and 14 present the progression of the storage capacity loss over time for both scenarios. The third column provides the volume of deposited sediment at the end of each time interval and the projection up to when the storage pool would be filled with sediment. The fourth and fifth columns provide the projection of available storage capacity, and the storage capacity loss is provided on the last column. Table 15 presents the remaining storage capacity for both scenarios as sediment is deposited by the turbid inflow along time. It also includes the difference between the storage capacities.

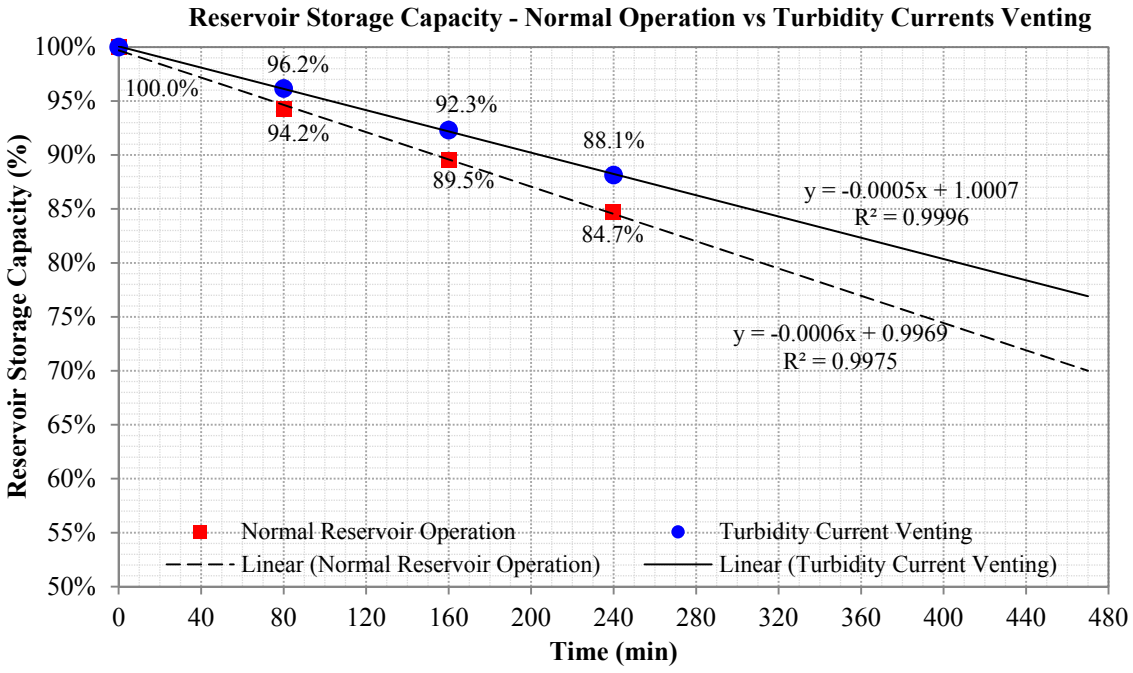

Figure 38. Evaluation of reservoir storage capacity loss along time.

Table 13. Normal Reservoir Operation – Projection of Storage Capacity Loss.

Reservoir Normal Operation Scenario					
Run	**Time (min)**	**Sediment Deposition (cm^3)**	**Storage Capacity (L)**	**Storage Capacity (%)**	**Storage Capacity Loss (%)**
Initial Bed	0.0	0.00	155.21	100.0	0.0
N4	80.0	8,980.63	146.23	94.2	5.8
N6	160.0	16,279.32	138.93	89.5	10.5
N7	240.0	23,721.24	131.49	84.7	15.3
Projection	500.0	47,044.67	108.17	69.7	30.3
	1000.0	93,608.19	61.60	39.7	60.3
	1661.5	155,211.72	0.00	0.0	100.0

Table 14. Turbidity Current Venting – Projection of Storage Capacity Loss.

Turbidity Currents Venting Scenario					
Run	**Time (min)**	**Sediment Deposition (cm^3)**	**Storage Capacity (L)**	**Storage Capacity (%)**	**Storage Capacity Loss (%)**
Initial Bed	0.0	0.00	155.21	100.0	0.0
V4	80.0	5,956.44	149.26	96.2	3.8
V6	160.0	11,940.94	143.27	92.3	7.7
V7	240.0	18,404.48	136.81	88.1	11.9
Projection	500.0	38,694.28	116.52	75.1	24.9
	1000.0	77,497.21	77.71	50.1	49.9
	1,661.5	128,833.48	26.38	17.0	83.0
	2,001.4	155,211.72	0.00	0.0	100.0

Table 15. Storage capacity difference between the applied sediment management techniques.

Time (min)	**Storage Capacity (%)**		**Difference (%)**
	NRO	**TCV**	
0	100.0	100.0	0.0
80	94.2	96.2	1.9
160	89.5	92.3	2.8
240	84.7	88.1	3.4
500	69.7	75.1	5.4
1,000	39.7	50.1	10.4
1,661.5	0.0	17.0	17.0
2,001.4	--	0.0	--

5.6 Deposition Grain Size Distribution

As mentioned in section 4.4, the solid material used for the sediment-laden inflow in this research study was silica flour Sil-Co-Sil® 106, which comes from quartz and has a specific gravity (S.G.) of 2.65. Samples of the accumulated sediment deposition were collected at eight locations along the bed after all the experimental runs from each of the two sediment management techniques applied on this study, Normal Reservoir Operation and Turbidity Current Venting, as presented in Figure 39 and Table 16. The sampling locations include samples at the topset, plunging point, foreset and bottomset with the last one just upstream of the dam. The samples were used to conduct grain size distribution (GSD) analysis according to the ASTM D422 Standard Test Method, the same analysis conducted on the sediment before the experiments were conducted. Further analysis of the GSD results was conducted to obtain a better understanding of deposition patterns along the bed, and how it compares between both applied scenarios.

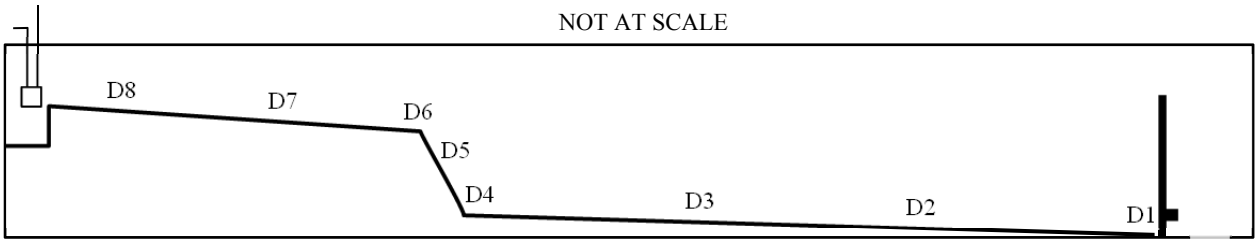

Figure 39. Schematic of the flume showing the location on the deposited sediment samples.

Table 16. Distance from the dam of the deposited sediment samples.

	Measurement Point	Distance from the Dam (cm)	Distance from the Dam (ft)
Bottomset (Inside the Storage Pool)	D1	0.0	0.0
	D2	127.0	4.2
	D3	254.0	8.3
	D4	381.0	12.5
Foreset	D5	394.0	12.9
Plunging Point	D6	407.0	13.3
Topset	D7	534.0	17.5
	D8	661.0	21.7

Tables 17 and 18 present the grain diameter sizes D_{84}, D_{50}, and $D_{16,}$ calculated from the GSD analysis, which are the sediment grain diameter sizes of which the 84%, the 50% and the 16% by weight of each sample consisted on finer grains. In both scenarios, the coarser sediment was quickly deposited at the foreset, measuring stations D8 and D7. Figures 40 to 42 show that the deposited sediment for the Normal Reservoir Operation technique contained finer grain sizes at the eight measuring locations, as compared to the Turbidity Current Venting technique. Inside the storage pool, the Normal Reservoir Operation scenario shows that the finer sediment was deposited near the dam (station D1), while the Turbidity Current Venting has coarser values on that location compared to measuring station D2. On the Turbidity Current Venting, the finer sediment was eliminated by discharge through the low-level outlets. A guideline was added to the plots showing the respective diameter size value of the analyzed sample from the original sediment sample before the experiments.

Table 17. Normal Reservoir Operation – Sediment grain diameter sizes of which the 84%, the 50% and the 16% by weight of each sample consisted on finer grains.

Normal Reservoir Operation Scenario			
Measurement Point	D_{84} **(µm)**	D_{50} **(µm)**	D_{16} **(µm)**
D1	50.62	24.06	4.44
D2	59.71	31.75	6.72
D3	59.09	31.41	7.99
D4	59.81	27.22	10.93
D5	70.30	30.98	16.73
D6	71.20	34.62	21.41
D7	84.31	40.04	22.55
D8	105.17	50.07	25.08

Table 18. Turbidity Current Venting – Sediment grain diameter sizes of which the 84%, the 50% and the 16% by weight of each sample consisted on finer grains.

Turbidity Current Venting Scenario			
Measurement Point	D_{84} (µm)	D_{50} (µm)	D_{16} (µm)
D1	59.33	37.60	8.97
D2	59.13	36.44	8.94
D3	66.95	33.31	11.48
D4	75.34	37.82	11.77
D5	77.99	32.38	14.46
D6	82.86	37.54	24.59
D7	108.11	68.12	28.69
D8	111.31	65.93	29.93

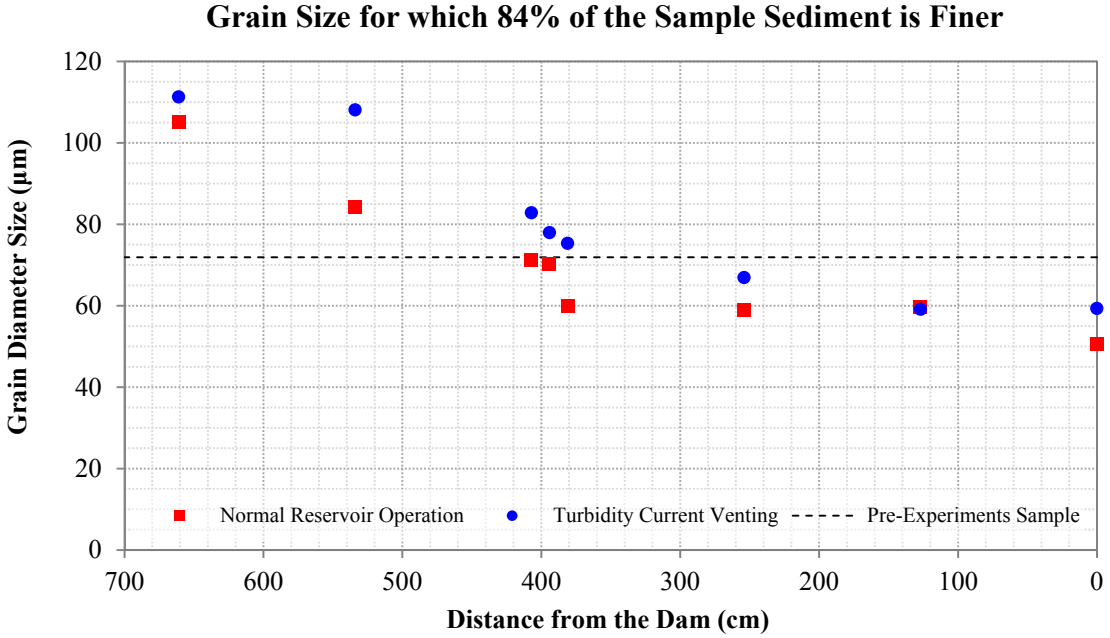

Figure 40. Sediment grain diameter sizes for which the 84% by weight of each sample consisted of finer grains, for the NRO and TCV scenarios.

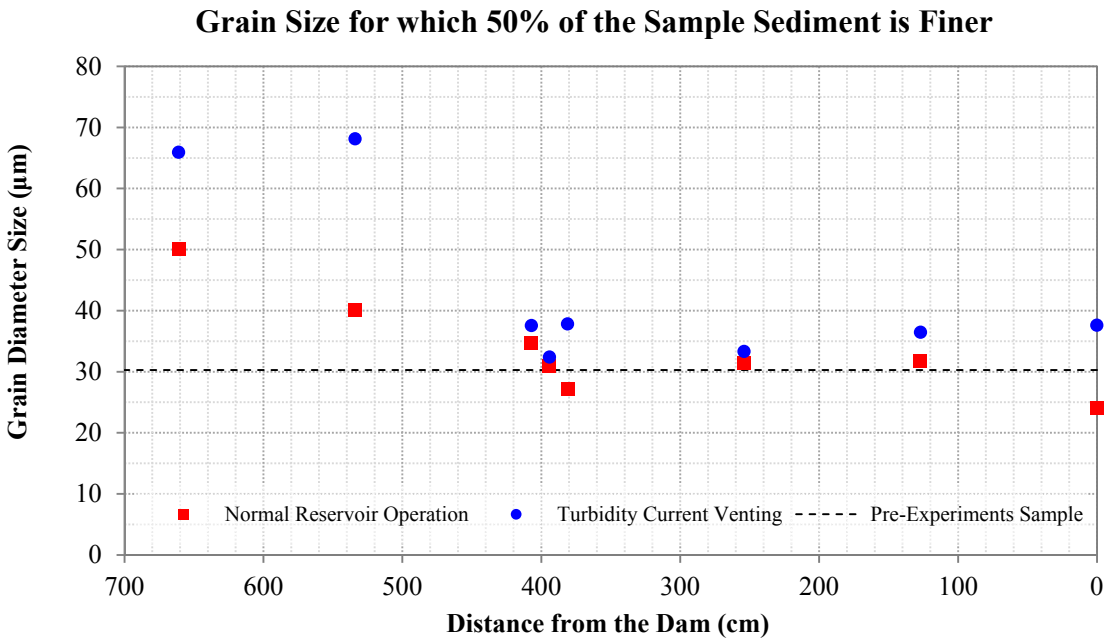

Figure 41. Sediment grain diameter sizes for which the 50% by weight of each sample consisted of finer grains, for the NRO and TCV scenarios.

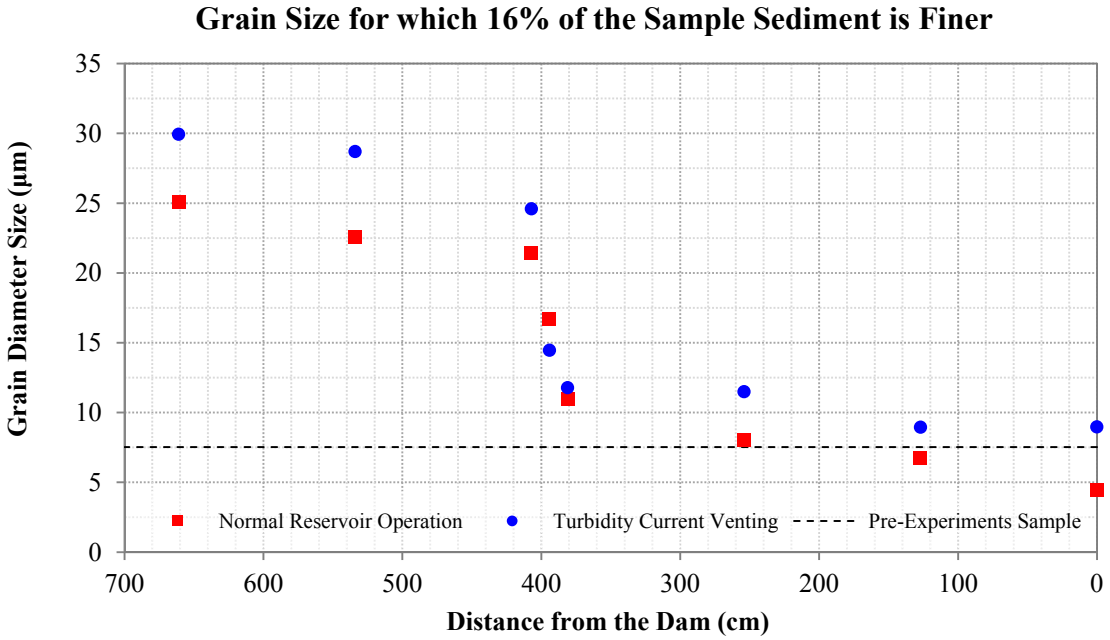

Figure 42. Sediment grain diameter sizes for which the 16% by weight of each sample consisted of finer grains, for the NRO and TCV scenarios.

The sedimentological mean grain size Φ_m was also calculated, as a means to obtain the geometric mean size D_g and the geometric standard deviation σ_g of each deposition sample (Tables 19 and 20). Inside the storage pool, the deposited sediment was classified as *coarse silt* according to Φ_m and D_g for both sediment management techniques applied. The geometric standard deviation σ_g was higher than 1.6 at all measuring points from both scenarios, which means the sediment material is considered poorly-sorted for all samples.

The same analysis was conducted on the original sample before the experiments were conducted, as presented on Section 4.4 of this report. It resulted in Φ_m = 5.40 and D_g = 23.71 μm, with a classification of *medium silt*. These values were also included on Figures 43 and 44 as guidelines to compare with the values from the sediment from the deposition. The standard deviation σ_g was 3.14 showing that the sediment was poorly-sorted before being used for the experiments. It is also higher than all the σ_g values from the samples of the Normal Reservoir Operation and the Turbidity Current Venting sediment management technique (Figure 45).

Table 19. Characteristics of the sediment deposited during the Normal Reservoir Operation experimental runs.

Normal Reservoir Operation					
Measurement Point	**Φ_m**	**D_g (μm)**	**Classification**	**σ_g**	**Classification**
D1	4.67	39.34	Coarse silt	2.28	Poorly sorted
D2	4.49	44.46	Coarse silt	2.17	Poorly sorted
D3	4.48	44.79	Coarse silt	2.19	Poorly sorted
D4	4.56	42.38	Coarse silt	2.13	Poorly sorted
D5	4.34	49.40	Coarse silt	1.92	Poorly sorted
D6	4.35	49.17	Coarse silt	1.89	Poorly sorted
D7	4.06	60.06	Coarse silt	1.94	Poorly sorted
D8	3.80	71.67	Very fine sand	2.00	Poorly sorted

Table 20. Characteristics of the sediment deposited during the Turbidity Current Venting experimental runs.

Turbidity Current Venting					
Measurement Point	**Φ_m**	**D_g (µm)**	**Classification**	**σ_g**	**Classification**
D1	4.83	35.17	Coarse silt	2.34	Poorly sorted
D2	4.95	32.41	Coarse silt	2.43	Poorly sorted
D3	4.60	41.26	Coarse silt	2.22	Poorly sorted
D4	4.30	50.75	Coarse silt	2.10	Poorly sorted
D5	4.41	47.06	Coarse silt	2.18	Poorly sorted
D6	4.17	55.49	Coarse silt	2.03	Poorly sorted
D7	3.83	70.14	Very fine sand	1.93	Poorly sorted
D8	3.85	69.25	Very fine sand	2.11	Poorly sorted

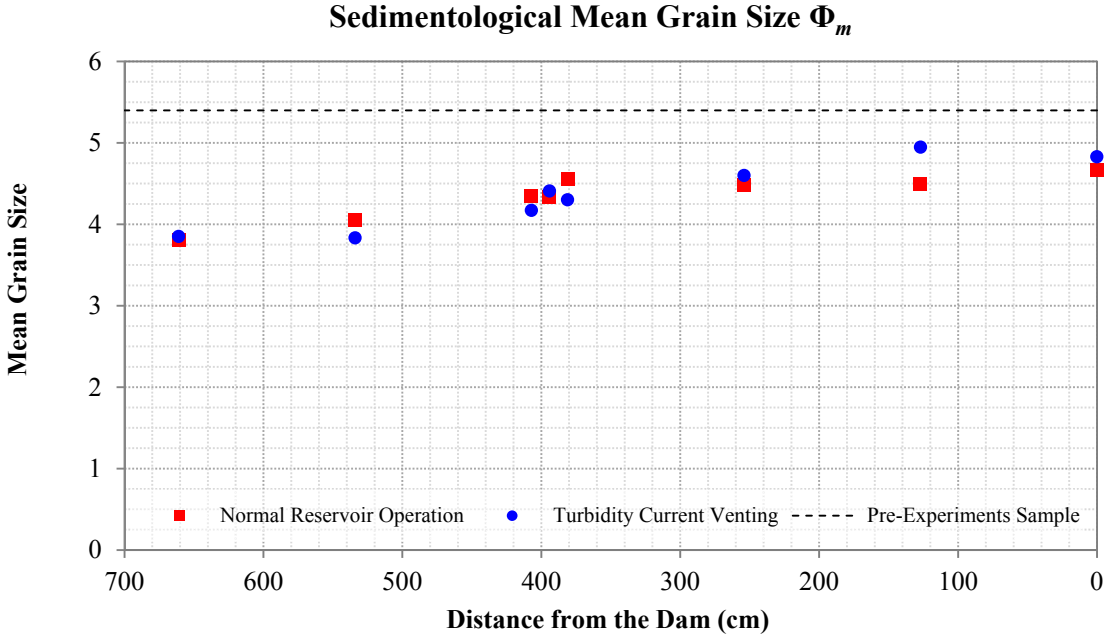

Figure 43. Sedimentological mean grain size of the accumulated sediment deposition after the experimental runs. The sedimentological scale Φ provides a sediment classification system according to the grain size.

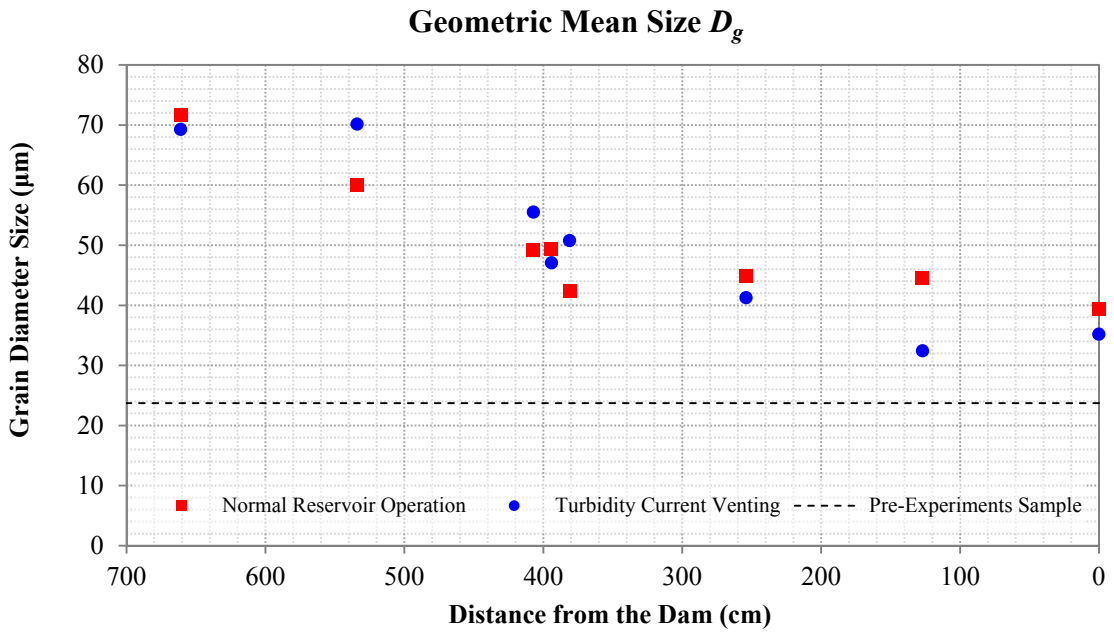

Figure 44. Geometric mean size of the accumulated sediment deposition after the experimental runs. It represents the analytical most frequent particle size on the sediment sample, based on mass.

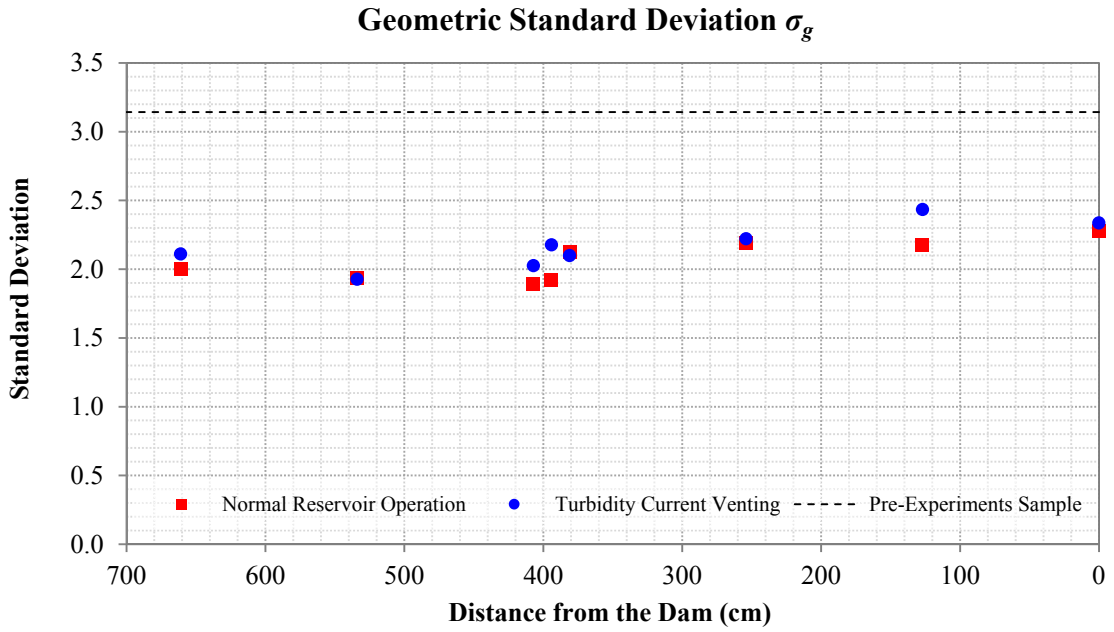

Figure 45. Geometric standard deviation of the accumulated sediment deposition after the experimental runs. Sediment samples with values of σ_g in excess of 1.6 are considered to be poorly-sorted.

CHAPTER 6: SUMMARY & CONCLUSIONS

For this study, a series of experiments were conducted in a laboratory flume to analyze the behavior of turbidity currents while using the pass-through sediment management technique of venting. The main focus was to explore and develop a better understanding of the streamwise flow velocity and suspended sediment concentration vertical profiles, and the sediment deposition patterns while the turbidity currents are vented. For this, two sediment management conditions or scenarios were recreated: the Turbidity Currents Venting (TCV) scenario, where sediment-laden underflow was intended to be released through the low-level outlets of the scaled dam; and the Normal Reservoir Operation (NRO) scenario, where the bottom outlets were closed and the discharge flowed over the dam. The later was considered the control scenario.

The results from the collected data show similar streamwise flow velocity profiles for both scenarios along the bed inside the impoundment, except near the dam. Due to the difference in outflow discharge operations, the maximum velocity in the vertical column at the dam area was near the bottom outlets level for the TCV condition, while the maximum velocity from the NRO was at the top of the dam. Higher flow velocities are expected to provide higher sediment transport capacity, and if the higher velocity in the vertical column occurs near the bottom, more sediment is likely to be maintained in suspension and/or entrained.

The initial suspended sediment concentration in the reservoir was similar for both scenarios, decreasing as the turbidity current moved downstream along the bed due to sediment deposition. Moving in time, the concentration profiles and layer-averaged concentration from the TCV were lower than the concentration measured from the NRO condition at all location inside the reservoir. On the other hand, the outflow sediment concentration was significantly higher for the TCV condition for all the samples along the bed and in time. Since the higher velocities at the dam area for the TCV condition were near the bed, higher concentrations of sediment were maintained in suspension and discharged through the bottom outlets. For the NRO condition, the outflow was located at the top of the dam. Since the sediment concentration is higher near the bottom of the dam, the water at the top is clearer, resulting in lower sediment concentration in the outflow.

The sediment deposition rate was also lower on the TCV condition along the bed as compared to the NRO, especially near the dam where the bottom outlets were partially obstructed with accumulated sediment at the end of the experimental runs for the NRO. The velocity near the bed for the NRO condition was close to zero, which led to more sediment deposition. For both scenarios, the location with the highest sediment deposition rate was the plunging point.

The efficiency of the turbidity currents venting technique varies for each case depending on the geometry, and sedimentological and hydrological characteristics. In this study, the flow velocities related to the turbidity currents recreated by the experimental design did not have the capacity to maintain all the inflowing sediment in suspension. Therefore, significant deposition occurred along the bed, reducing the suspended sediment concentration in the turbidity currents reaching the dam. Even though venting did not eliminate sediment deposition completely, results show that the useful life of the storage pool was extended by applying the turbidity currents venting technique. This supports the theory that the application of this technique is expected to reduce sediment deposition inside the storage pool.

Although the results presented here have demonstrated that applying the turbidity currents venting could reduce the sedimentation of reservoirs, there are areas of opportunity to further analyze this technique. Incorporating different geometry, sedimentological and hydrological characteristics will provide more information about its efficiency. The geometry characteristics to vary may include bed slope, initial delta, storage pool dimensions, dam geometry, and bottom outlets shape, dimensions and location on the dam. For the sedimentological characteristics, the variations could include the sediment material, grain size distribution, and mean grain size. The inflow volume could also be varied to study the effectiveness of turbidity current venting.

CHAPTER 7: REFERENCES

Abd El-Gawad, S. M. *3-D Numerical Modeling of Turbidity Currents.* Ph.D Dissertation, University of South Carolina, 2011.

Abid, A. "Transported Sediments and Drawing Off at the Nebeur Dam on the Mallegue Wadi during the Period 1 May 1954 to 30 April 1980." *International Seminar of Experts on Reservoir Desiltation, Tunis* (1980).

Ackerman, K. V., Mixon, D. M., Sundquist, E. T., Stallard, R. F., Schwarz, G. E. and Stewart, D. W. *RESIS-II: an updated version of the original reservoir sedimentation survey information system (RESIS) database*. US Geological Survey No. 434 (2009). Available only online at http://pubs.usgs.gov/ds/ds434

Akiyama, J. and Fukushima, Y. "Entrainment of noncohesive bed sediment into suspension." *Proceedings of 3rd International Symposium on River Sedimentation* (1986): 804–813

Akiyama, J. and Stefan, H. G. "Plunging flow into a reservoir: Theory." *Journal of Hydraulic Engineering* 110.4 (1984): 484-499.

Akiyama, J. and Stefan, H. G. "Turbidity current with erosion and deposition." *Journal of Hydraulic Engineering*, 111.12 (1985): 1473-1496.

Akiyama, J. and Stefan, H. G. "Turbidity current simulation in a diverging channel." *Water Resources Research* 24.4 (1988): 579-587.

Altinakar, M. S., Graf, W. H. and Hopfinger, E. J. "Weakly depositing turbidity current on a small slope." *Journal of Hydraulic Research* 28.1 (1990): 55-80.

Altinakar, M. S., Graf, W. H. and Hopfinger, E. J. "Flow structure in turbidity currents." *Journal of Hydraulic Research* 34.5 (1996): 713-718.

an Luthi, S. (1981). "Experiments on non-channelized turbidity currents and their deposits." *Marine Geology* 40.3 (1981): M59-M68.

Annandale, G. W. "Reservoir Sedimentation." *Encyclopedia of Hydrological Sciences*. (2006).

Ashida, K. and Michiue, M. "Laboratory study of suspended load discharge in alluvial channels." *Disaster Prevention Research Institute Annuals* (1964).

Ashida, K. and Egashira, S. "Basic study of turbidity currents." *Proceedings of Japan Society of Civil Engineers* 237 (1975): 37-50.

ASTM Standard D422, 1935 (2007), "Standard Test Method for Particle-Size Analysis of Soils." *ASTM International*, West Conshohocken, PA (2007) DOI: 10.1520/D0422-63R07, www.astm.org.

Bata, G. L. "Recirculation of cooling water in rivers and canals." *Journal of the Hydraulics Division* 83.3 (1957): 1-27.

Bell, H. S. *Stratified flow in reservoirs and its use in prevention of silting*. No. 491. US Department of Agriculture, 1942.

Boillat, J. L. and Delley, P. *Transformation de la prise d" eau de Malvaglia-Etude sur modèles et réalisation*. Laboratory of Hydraulic Constructions No. 1992-001 (1992): 145-151.

Brown, C. B. *The control of reservoir silting*. United States Department of Agriculture No. 521 (1944): 65-74.

Brune, G. M. "Trap Efficiency of Reservoirs." *Eos, Transactions American Geophysical Union* 34.3 (1953): 407-418.

Bruk, S. *Methods of computing sedimentation in lakes and reservoirs*. Unesco, Paris (1985): 224.

Bryant, P. J. and Wood, I. R. "Selective withdrawal from a layered fluid." *Journal of Fluid Mechanics* 77.3 (1976): 581-591.

Cao, S. *Laboratory Studies on Retrogressive Erosion of Fine Sediment Deposits*, M.S. Thesis, China Institute of Water Resources and Hydropower Research, Beijing (1981).

Cao, R., Ren, S. and Lu, Y. "Analysis of Conditions of Formation and Maintenance of High Sediment Concentration Density Currents." *Journal of Sediment Research* 2 (1984): 59-64.

Carmack, E. C. "Combined influence of inflow and lake temperatures on spring circulation in a riverine lake." *Journal of Physical Oceanography* 9.2 (1979): 422-434.

Celik, I. and Rodi, W. *A deposition-entrainment model for suspended sediment transport.* Universität Karlsruhe, 1984.

Chang, H. H., Harrison, L. L., Lee, W. and Tu, S. "Numerical modeling for sediment-pass-through reservoirs." *Journal of Hydraulic Engineering* 122.7 (1996): 381-388.

Chikita, K "Sedimentation by Turbidity Currnts." *Journal of the Faculty of Science, Hokkaido University. Series 7, Geophysics* 6.2 (1980): 255-300.

Chikita, K. "A field study on turbidity currents initiated from spring runoffs." *Water Resources Research* 25.2 (1989): 257-271.

Chikita, K. "Sedimentation by river-induced turbidity currents: field measurements and interpretation." *Sedimentology* 37.5 (1990): 891-905.

Chu, F. H., Pilkey, W. D. and Pilkey, O. H. "An analytical study of turbidity current steady flow." *Marine Geology* 33.3-4 (1979): 205-220.

Churchill, M. A., 1948. "Discussion of 'Analysis and Use of Reservoir Sedimentation Data'." by L. C. Gottschalk, *Proceedings of the Federal Interagency Sedimentation Conference. Bureau of Reclamation, US Department of the Interior, Washington, DC* (1948): 139-140.

Churchill, M. A. "Effects of storage impoundments on water quality." *Journal of the Sanitary Engineering Division* 83.1 (1957): 1-48.

Craya, A. “Loi de la Hauteur Limite d' Aspiration dan Deux Fluides de Densitis Differentes.” *Comptes Rendus.* Academie de Sciences, Paris, T. 222 (1946): 1159-1160.

Craya, A. “Recherches theoriques sur l'ecoulement de couches superposees de fluides de densites differentes.” *La Houille Blanche* 1 (1949): 44-55.

Crowder, B. M. “Economic Costs of Reservoir Sedimentation: A Regional Approach to Estimating Cropland Erosion Damages.” *Journal Soil and Water Conservation.* 42.3 (1987): 194-197.

Dai, A. and García, M. H. “Energy Dissipative Plunging Flows.” *Journal of Hydraulic Engineering* 136.8 (2009): 519-523.

Daly, R. A. “Origin of submarine canyons.” *American Journal of Science* 186 (1936): 401-420.

De Cesare, G. and Schleiss, A. “Turbidity current monitoring in a physical model flume using ultrasonic Doppler method.” *2nd International Symposium on Ultrasonic Doppler Methods for Fluid Mechanics and Fluid Engineering* (1999).

De Cesare, G., Oehy, C. and Schleiss, A. “Experiments on turbidity currents influenced by solid and permeable obstacles and water jet screens.” *6th ISUD-International Symposium on Ultrasonic Doppler Methods for Fluid Mechanics and Fluid Engineering*. Laboratory of Hydraulic Constructions No. 2008-066 (2008).

De Cesare, G., Schleiss, A. and Hermann, F. “Impact of turbidity currents on reservoir sedimentation.” *Journal of Hydraulic Engineering* 127 (2001): 6-16.

Dendy, F. E., Champion, W. A., and Wilson, R. B., 1973. “Reservoir Sedimentation Surveys in the United States.” In W. C. Ackermann, G. F. White, and E. B. Worthington (Editors), *Man-made Lakes: Their Problems and Environmental Effects,* Geophysical Monograph No. 17 (1973): 349-357. American Geophysical Union, Washington, D.C.

de Villiers, G., Kleinhans, M. G., van Breemen, D. M. O., Postma, G. and Hauber, E. “Experiments on sedimentation in wide reservoirs and erosion following dam removal.” *Proceedings of River Flow 2010 Conference* Vol. 2. 2010.

Duquennois, H. “Bilan des Operations de Soutirage des Vases au Barrage d'Iril Emda (Algeria).” *Collogue de Liege* (1959).

Edmonds, D. A., Shaw, J. B. and Mohrig, D. “Topset-dominated deltas: A new model for river delta stratigraphy.” *Geology* 39.12 (2011): 1175-1178.

Edwards, T. K. and Glysson, G. D. “Field Methods for Measurement of Fluvial Sediment.” *Department of the Interior, US Geological Survey Open-file Report* (1988): 86-531.

Eftekharzadeh, S. and Laursen, E. M. “A New Method for Removing Sediment from Reservoirs.” *Hydro Review* 9.1 (1990): 80-84.

Einstein, H. A. “The bed-load function for sediment transportation in open channel flows.” *US Department of Agriculture* 1026 (1950).

Ellison, T. H. and Turner, J. S. “Turbulent entrainment in stratified flows.” *Journal of Fluid*

Mechanics 6 (1959): 423-448. doi:10.1017/S0022112059000738

Engelund, F. and Fredsøe, J. "A sediment transport model for straight alluvial channels." *Hydrology Research* 7.5 (1976): 293-306.

Engelund, F. and Fredsøe, J. "Hydraulic theory of alluvial rivers." *Advances In Hydroscience, Academic Press, New York, NY* 13 (1982): 187-215.

Fan, J. "Experimental studies on density currents." *Water and Energy International* 17.4 (1960): 706-729.

Fan, J. "Experimental Studies on Density Currents." *Scientia Sinica, Chinese Academy of Sciences* 9.2 (1960): 275-303 (in Chinese).

Fan, J. "Methods of preserving reservoir capacity." *Methods of computing sedimentation in lakes and reservoirs, Paris: Unesco* (1985): 56-164.

Fan. J. "Turbid Density Currents in Reservoirs." *Water International* 11.3 (1986): 107-116.

Fan, J. "Density Currents in Reservoirs." *Workshop on Management of Reservoir Sedimentation, New Delhi* (1991).

Fan, J. and Morris, G.L. "Reservoir sedimentation. I: Delta and density current deposits." *Journal of Hydraulic Engineering* 118.3 (1992a): 354-369.

Fan, J. and Morris, G. L. "Reservoir Sedimentation. II: Reservoir desiltation and long-term storage capacity." *Journal Hydraulic Engineering ASCE* 118.3 (1992b): 370-384.

Farrell, G. J. and Stefan, H. G. "Buoyancy Induced Plunging Flow Into Reservoirs and Costal Regions" (1986). Retrieved from the University of Minnesota Digital Conservancy, http://purl.umn.edu/113341.

Farrell, G. J. and Stefan, H. G. "Mathematical modeling of plunging reservoir flows." *Journal of Hydraulic Research* 26.5 (1988): 525-537.

Fiock, L. R. "Records of silt carried by the Rio Grande and its accumulation in Elephant Butte Reservoir." *Eos, Transactions American Geophysical Union*15.2 (1934): 468-473.

Forbes, L. K. and Hocking, G. C. "Flow caused by a point sink in a fluid having a free surface." *The Journal of the Australian Mathematical Society. Series B. Applied Mathematics* 32.02 (1990): 231-249.

Forel, F. A. "Les ravins sous-lacustres des fleuves glaciaires." *Comptes Rendus de l'Académie des Sciences* 101 (1885): 725–28

Frenette, M. and Julien, P. Y. "Advances in Predicting Reservoir Sedimentation." *River Sedimentation* 3 (1986): 26.

Fry, A. S., Churchill, M. A., and Elder, R. A. "Significant Effects Of Density Currents In TVA's Integrated Reservoir And River System." *Proceedings of Minnesota International Hydraulic Convention* ASCE (1953): 335-354.

Fukushima, Y., Parker, G. and Pantin, H. M. "Prediction of ignitive turbidity currents in Scripps Submarine Canyon." *Marine Geology* 67.1-2 (1985): 55-81.

García, M. H. *Experimental Study of Turbidity Currents*, M.S. Thesis, Department of Civil and Mineral Engineering, University of Minnesota (September, 1985).

García, M. H. *Depositing and eroding sediment-driven flows: Turbidity currents*, Ph.D. Thesis, University of Minneapolis, Minneapolis (1989).

García, M. H. "Hydraulic jumps in sediment-driven bottom currents." *Journal of Hydraulic Engineering* 119.10 (1993): 1094-1117.

García, M. H. "Depositional turbidity currents laden with poorly sorted sediment." *Journal of hydraulic engineering* 120.11 (1994): 1240-1263.

García, M.H., Editor. *Sedimentation Engineering: Processes, Measurements, Modeling, and Practice.* American Society of Civil Engineers (ASCE) Manual of Engineering Practice 110 (2008).

García, M. H. and Parker, G. "On the numerical prediction of turbidity currents." *Third International Symposium on River Sedimentation, Mississippi: The University of Mississippi* (1984): 1556–1565.

García, M.H., and Parker, G. "Entrainment of Bed Sediment into Suspension." *ASCE Journal of Hydraulic Engineering* 117.4 (April 1991): 414-435.

Gariel, P. "Sur la Loi de la Hauteur Limite d'Aspiration dans Deux Fluides de Densite Differentes." *Comptes Rendus.* Academie de Sciences, Paris, T. 222 (1946): 781-783.

Gariel, P. "Recherches Experimentales sur l'ecoulement de couches superposees de fluides de densites differentes." *La Houille Blanche* 1 (1949): 56-64.

Georgoulas, A. N., Angelidis, P. B., Panagiotidis, T. G. and Kotsovinos, N. E. "3D numerical modelling of turbidity currents." *Environmental fluid mechanics* 10.6 (2010): 603-635.

Gilbert, G. K. *The topographic features of lake shores*. US Government Printing Office, 1885.

Gladstone, C., Ritchie, L. J., Sparks, R. S. J. and Woods, A. W. "An experimental investigation of density-stratified inertial gravity currents." *Sedimentology* 51.4 (2004): 767-789.

Grover, N. C. and Howard, S. C. "The passage of turbid water through Lake Mead." Transactions of the American Society of Civil Engineers 103.1 (1938): 720-781.

Hamblin, P. F., and Carmack, E. C. "River-induced currents in a Fjord Lake." *Journal of Geophysical Research: Oceans* 83.C2 (1978): 885-899.

Harleman, D. R. F., Morgan, R. L. and Purple, R. A. "Selective withdrawal from a vertically stratified fluid." *Proceedings of International Association for Hydraulic Research, Eighth Congress*. Vol. 1 (1959).

Harrison, L. L., Lee, W. H. and Tu, S. *Sediment pass-through, an alternative to reservoir*

dredging No. CONF-9507190--. American Society of Civil Engineers, New York, NY, 1995.

Hauenstein, W. and Dracos, T. H. "Investigation of plunging density currents generated by inflows in lakes." *Journal of Hydraulic Research* 22.3 (1984): 157-179.

Hakanson, L., and Jansson, M. *Principles of lake sedimentology*. National Swedish Environmental Protection Board, Uppsala, 1983.

Hakanson, L., and Jansson, M. *Principles of lake sedimentology*. 2nd Ed. (2002).

Hinze, J. O. "On the hydrodynamics of turbidity currents." *Geol. Mijnbouw*39.1 (1960): 18-25.

Hosseini, S. A., Shamsai, A. and Ataie-Ashtiani, B. "Synchronous measurements of the velocity and concentration in low density turbidity currents using an Acoustic Doppler Velocimeter." *Flow Measurement and Instrumentation* 17.1 (2006): 59-68.

Huang, H., Imran, J. and Pirmez, C. "Numerical model of turbidity currents with a deforming bottom boundary." *Journal of Hydraulic Engineering* 131.4 (2005): 283–293.

Huang, H., Imran, J. and Pirmez, C. "Numerical modeling of poorly sorted depositional turbidity currents." *Journal of Geophysical Research* 112.C1 (2007).

Huang, H., Imran, J. and Pirmez, C. "Numerical study of turbidity currents with sudden-release and sustained-inflow mechanisms." *Journal of Hydraulic Engineering* 134.9 (2008): 1199–1209.

ICOLD (International Commission on Large Dams). *World Register of Dams. Version updates 2011*. Lucerne: ICOLD (2011). Available online at www.icold-cigb.net.

Itakura, T. and Kishi, T. "Open channel flow with suspended sediments." *Journal of the Hydraulics Division* 106.8 (1980): 1325-1343.

Jirka, G. H. and Katavola, D. S. "SUPERCRITICAL WITHDRAWAL FROM TWO-LAYERED FLUID SYSTEMS: Part 2: Three-dimensional flow into round intake." *Journal of Hydraulic Research* 17.1 (1979): 53-62.

Johnson, J. W. *Underflow Studies at Lake Issaqueena*. Civil Engineering Vol. 12 (September 1942): 513-516.

Julien, P. Y. *Erosion and sedimentation*. Cambridge University Press, 2010.

Kantoush, S. A. "Symmetric or asymmetric flow patterns in shallow rectangular basins with sediment transport." *Proceedings of 32nd IAHR biennial congress, Venice, Italy*. 2007.

Kantoush, S. A. and Sumi, T. "River morphology and sediment management strategies for sustainable reservoir in Japan and European Alps." *Annuals of Disaster Prevention Research Institute, Kyoto University* 53 (2010): 821-839.

Kostic, S. and Parker, P. "Progradational sand-mud deltas in lakes and reservoirs. Part 1. Theory and numerical modeling." *Journal of Hydraulic Research* 41.2 (2003): 127-140.

Kostic, S. and Parker, P. “Progradational sand-mud deltas in lakes and reservoirs. Part 2. Experiment and numerical simulation.” *Journal of Hydraulic Research* 41.2 (2003): 141-152.

Krumbein, W. C. “Size frequency distributions of sediments.” *Journal of Sediment and Petrology* 4 (1934): 65-77.

Kuelegan, G. H. “Laws of Turbulent Flow in Open Channels.” *US Department of Commerce* 21 (1938).

Kuenen, P. H. and Migliorini, C. I. “Turbidity currents as a cause of graded bedding.” *The Journal of Geology* 58 (1950):91–127.

Lambert, A. "Turbidity currents from the Rhine River on the bottom of Lake Constance." (1982): 1-4.

Lane, E. W. *Some Hydraulic Engineering Aspects of Density Currents*, Hydraulic Laboratory Report No. Hyd-373. US Bureau of Reclamation: Denver, CO (1954).

Lawrence, G. A. and Imberger, J. “Selective withdrawal through a point sink in a continuously stratified fluid with a pycnocline.” *Univ. of Western Australia, Centre for Water Research, Environmental Dynamics Report* (1979).

Lee, H. Y. and Yu, W. S. “Experimental study of reservoir turbidity current.” *Journal of Hydraulic Engineering* 123.6 (1997): 520-528.

Lee, F. Z., Lai, J. S., Tan, Y. C. and Sung, C. C. “Turbid density current venting through reservoir outlets.” *KSCE Journal of Civil Engineering* 18.2 (2014): 694-705.

Lewis, A. D. *Silting of four large reservoirs in South Africa*. Second Congress on Large Dams, Communication No. 5 (1936).

Mahmood, K. “Reservoir sedimentation: Impact, extent and mitigation.” *Technical paper* No.71, The World Bank, Washington D.C. (1987).

Middleton, G. V. “Experiments on density and turbidity currents: III. Deposition of sediment.” *Canadian Journal of Earth Sciences* 4.3 (1967): 475-505.

Middleton, G. V. “Sediment deposition from turbidity currents.” *Annual Review of Earth and Planetary Sciences* 21 (1993): 89-114.

Mohammadnezhad, B. A. and Shamsai, A. “Effects of Density Currents on Sedimentation in Reservoirs.” *Scientia Iranica* 14.5 (2007): 395-404.

Morris, G. L. and Fan, J. *Reservoir Sedimentation Handbook: Design and management of dams, reservoirs, and watersheds for sustainable use*. McGraw Hill Professional, NY (1998).

Morris, G.L., Annandale, G. and Hotchkiss, R. “Reservoir Sedimentation.” In: García, M. H. (Ed.), *Sedimentation Engineering: Processes, Measurements, Modeling, and Practice.* Chapter 12 in American Society of Civil Engineers (ASCE) Manual of Engineering Practice 110 (2008).

Müller, Philippe Jan, and Giovanni De Cesare. "Sedimentation problems in the reservoirs of the Kraftwerke Sarganserland–Venting of turbidity currents as the essential part of the solution." *Proceedings (on CD) of the 23rd Congress of the Int. Commission on Large Dams CIGB-ICOLD*. Vol. 2. No. EPFL-CONF-148588 (2009).

Necker, F., Härtel, C., Kleiser, L., and Meiburg, E. "High-resolution simulations of particle-driven gravity currents." *International Journal of Multiphase Flow* 28.2 (2002): 279-300.

Necker, F., Härtel, C., Kleiser, L., and Meiburg, E. "Mixing and dissipation in particle-driven gravity currents." *Journal of Fluid Mechanics* 545 (2005): 339-372.

Normark, W. R., and Dickson, F. H. "Man-made turbidity currents in Lake Superior." *Sedimentology*, *23*.6 (1976): 815-831.

Oberle, R., Dubas, C., Gardet. A., Charpie, J., and Decoppet, H. P. "Protection contre l'Ensemblement du Bassin d'Accumulation de l'Aménagement Hydroélectrique de la Massa," *9th ICOLD* Q.33, R.37 (1967): 665-688.

Pantin, H. M. "Interaction between velocity and effective density in turbidity flow: phase-plane analysis, with criteria for autosuspension." *Marine Geology* 31.1 (1979): 59-99.

Parker, G. "Conditions for the ignition of catastrophically erosive turbidity currents." *Marine Geology* 46.3-4 (1982): 307-327.

Parker, G., Fukushima, Y. and Pantin, H. M. "Self-accelerating turbidity currents." *Journal of Fluid Mechanics* 171 (1986): 145-181.

Parker, G., García, M., Fukushima, Y. and Yu, W. "Experiments on turbidity currents over an erodible bed." *Journal of Hydraulic Research* 25.1 (1987): 123-147.

Parker, G., and Toniolo, H. "Note on the analysis of plunging of density flows." *Journal of Hydraulic Engineering* 133.6 (2007): 690-694.

Plapp, J. E., and Mitchell, J. P. "A hydrodynamic theory of turbidity currents." *Journal of Geophysical Research* 65.3 (1960): 983-992.

Rijn, L. C. V. "Sediment transport, part II: suspended load transport." *Journal of Hydraulic Engineering* 110.11 (1984): 1613-1641.

Savage, S. B., and Brimberg, J. "Analysis of plunging phenomena in water reservoirs." *Journal of Hydraulic Research* 13.2 (1975): 187-205.

Sequeiros, O. E., Cantero, M. I., and García, M. H. "Sediment management by jets and turbidity currents with application to a reservoir for flood and pollution control in Chicago, Illinois." *Journal of Hydraulic Research* 47.3 (2009): 340-348.

Sequeiros, O.E., Naruse, H., Endo, N., García, M.H. and Parker, G. "Experimental study on self-accelerating turbidity currents." *Journal of Geophysical Research: Oceans* 114.C5 (2009).

Sequeiros, O.E., Spinewine, B., Beaubouef, R.T., Sun, T., García, M.H. and Parker, G. "Characteristics of velocity and excess density profiles of saline underflows and turbidity

currents flowing over a mobile bed." *Journal of Hydraulic Engineering* 136.7 (2010): 412-433.

Shiklomanov, I. A. "World Fresh Water Resources." In: Gleick, P. H. (Ed.), *Water in Crisis: A guide to world fresh water resources.* Oxford University Press, New York.

Singh, B., and Shan, C. R. "Plunging Phenomena of Density Currents in Reservoirs." *La Houille Blanche* 1(1971): 59-64.

Smith, J. D., and McLean, S. R. "Spatially averaged flow over a wavy surface." *Journal of Geophysical research* 82.12 (1977): 1735-1746.

Soltero, R. A., Wright, J. C., and Horpestad, A. A. "Physical limnology of Bighorn Lake--Yellowtail Dam, Montana: internal density currents." *Northwest Science* (1974).

Stefan, H. "High concentration turbidity currents in reservoirs." *Proceedings of 15th Conference IAHR* Vol. 1 (1973): 341-352.

Stow, D. A. and Bowen, A. J. "A physical model for the transport and sorting of fine-grained sediment by turbidity currents." *Sedimentology* 27.1 (1980): 31-46.

Sundborg, A. and Jansson, M. B. "Present and future conditions of reservoir sedimentation." *Sedimentological Studies in the Cachí Reservoir, Costa Rica: Sediment Inflow, Reservoir Sedimentation, and Effects of Flushing, MB Jansson and A. Rodríguez (Eds.), UNGI Rapport* 81 (1992): 157-164.

Takahara, T. and Matsumura, K. "Experimental study of the sediment trap effect of steel grid-type sabo dams." *International Journal of Erosion Control Engineering* 1.2 (2008): 73-78.

Tesaker, E. *Uniform turbidity current experiments.* Ph.D. Thesis, Norway Technological University (1969).

Tokyay, T. E. and García, M. H. "Effect of initial excess density and discharge on constant flux gravity currents propagating on a slope." *Environmental Fluid Mechanics* 14.2 (2014): 409-429.

Training Course on Reservoir Sedimentation. "Lecture Notes of the Training Course on Reservoir Sedimentation." Beijing (1985).

Turner, J. S. "Buoyancy effects in fluids." *Cambridge Univ* (1973).

Water Scarcity. *World Wildlife Fund's website*. Retrieved 12 January, 2015, from http://www.worldwildlife.org/threats/water-scarcity

White, W. R. *Evacuation of Sediment from Reservoirs*. Thomas Telford: London, 2001.

Wiebe, A. H. "Density currents in Norris reservoir." *Ecology* 20.3 (1939): 446-450.

World Commission on Dams. *Dams and development a new framework for decision-making. The Report of the World Commission on Dams*. Earthscan, London, 2000.

Wood, I. R. "Selective withdrawal from two-layer fluid." *Journal of the Hydraulics Division*

104.12 (1978): 1647-1659.

Wunderlich, W. O. and Elder, R. A. “Mechanics of Flow Through Man-Made Lakes.” *Man-made lakes: their problems and environmental effects* (1973): 300-310.

Yellow River Conservancy Commission. “Proceedings of symposium on density flow investigation.” *Yellow River Water Conservancy Publishing House*. (2006).

Young, D. L., and Lin, Q. H. “Density currents during a storm in Te-Chi reservoir of Taiwan.” *Proceedings of 24th IAHR Conference of International Association for Hydraulic Research*. Delft, The Netherlands, 1991.

Yu, W. S., Lee, H. Y. and Hsu, S. M. “Experiments on deposition behavior of fine sediment in a reservoir.” *Journal of Hydraulic Engineering* 126.12 (2000): 912-920.

Zhang, Y., Hu, C. and Wang, Y. “1-D MATHEMATICAL MODEL FOR HEAVILY SEDIMENT–LADEN RIVERS AND ITS APPLICATIONS.” *US-China Workshop on Advanced Computational Modelling in Hydroscience & Engineering, September* (19-21).

APPENDIX A: PHOTOS OF THE EXPERIMENTAL RUNS

A1. Photo Sequence of a Normal Reservoir Operation Typical Run

The scaled reservoir was initially filled with clean water. Then the turbidity current plunged inside and moves downstream along the bed until it reached the dam. All the water on the reservoir became cloudy, so red and blue dye was added to the turbidity current make it visible.

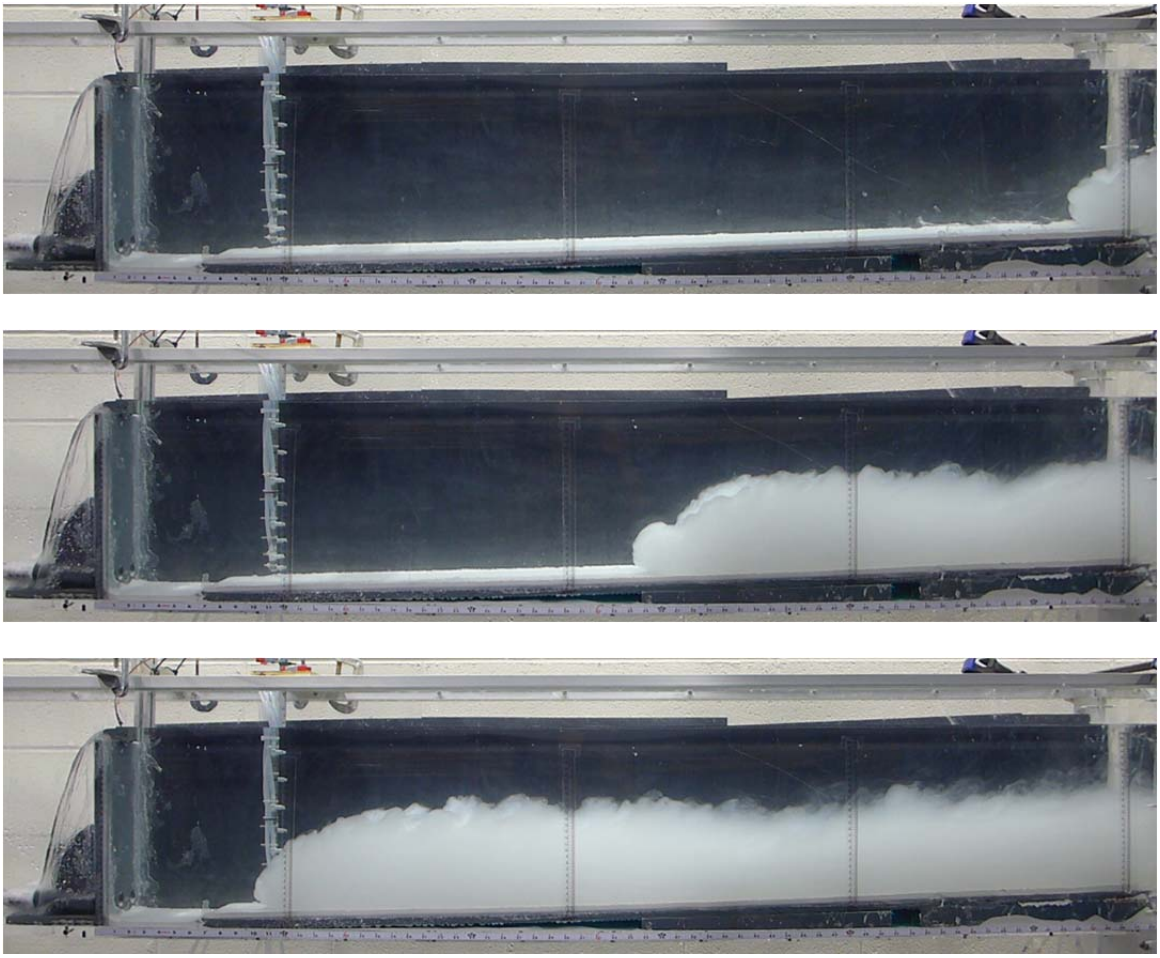

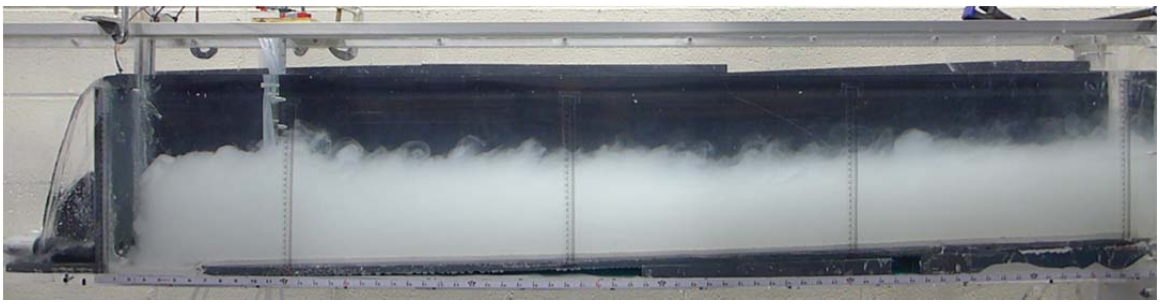

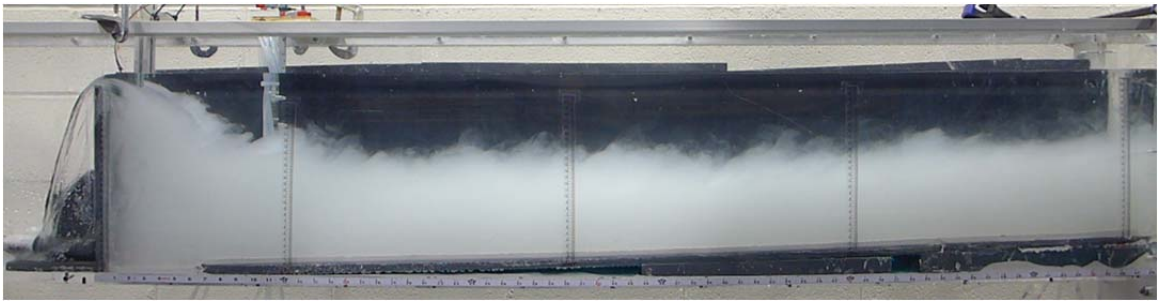

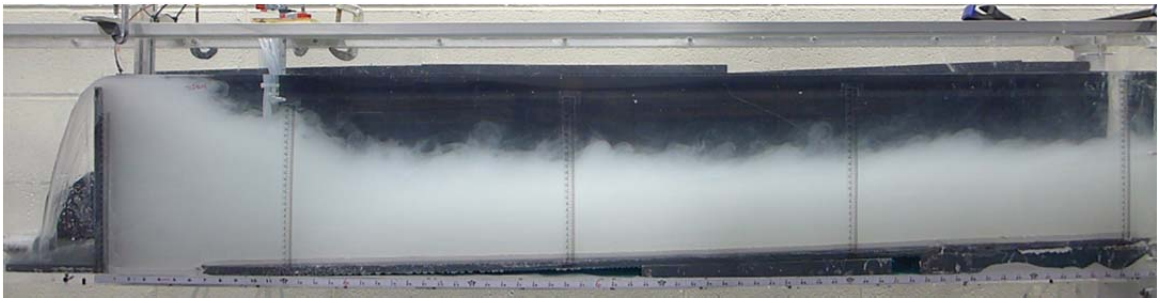

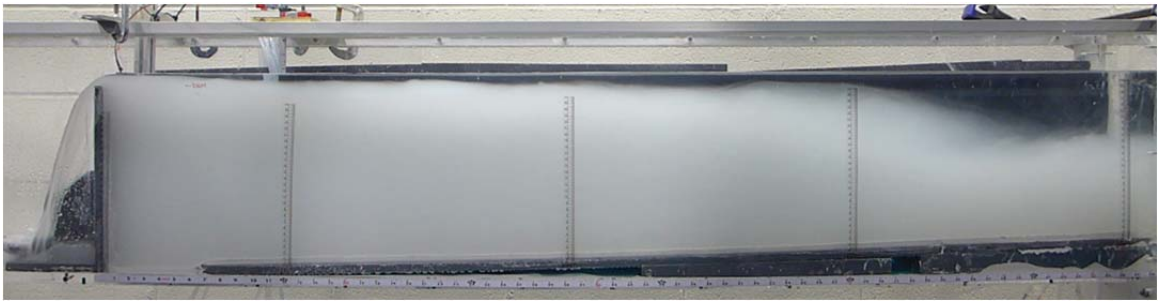

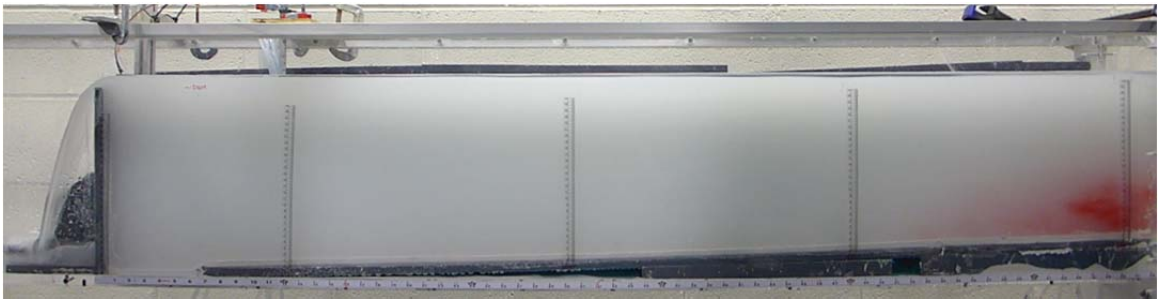

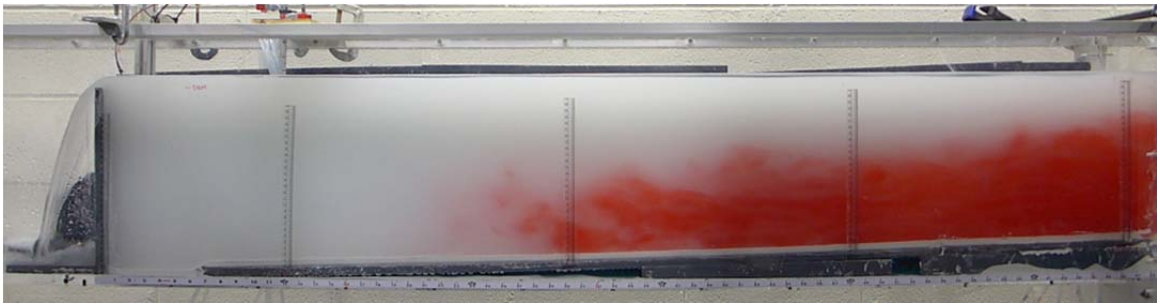

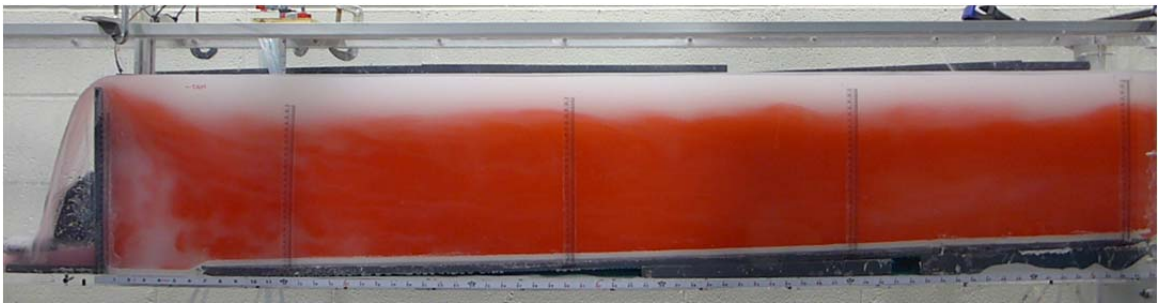

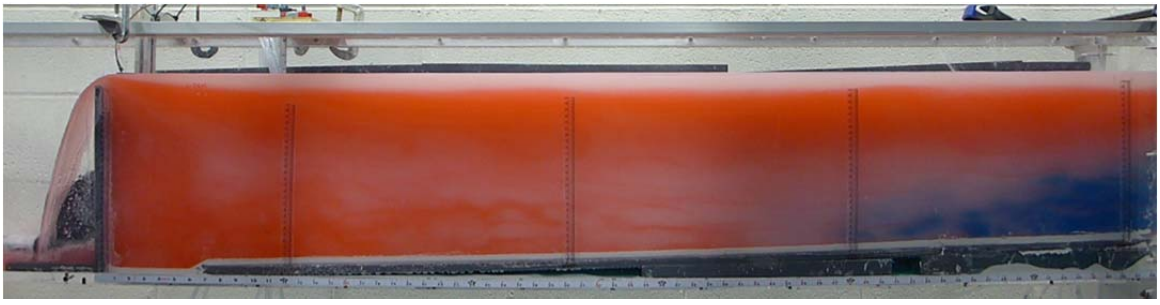

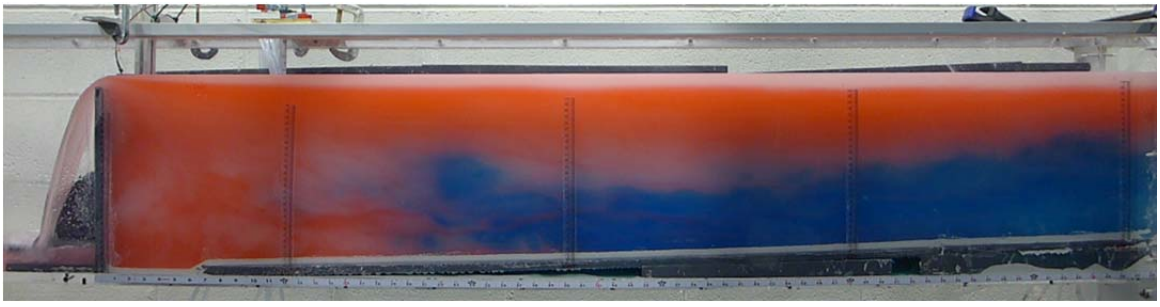

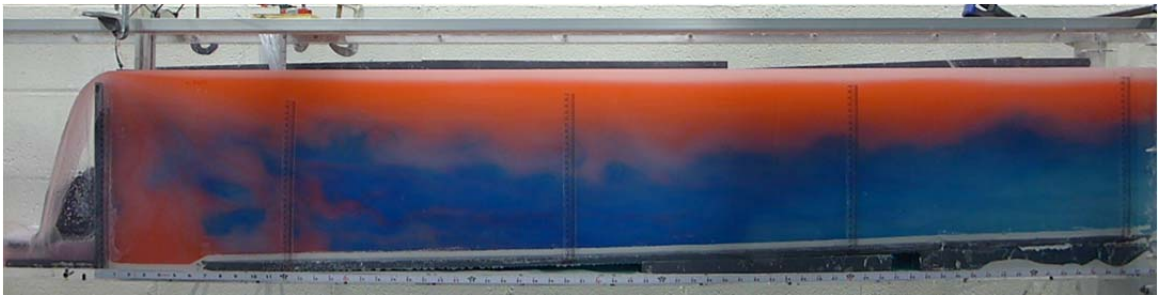

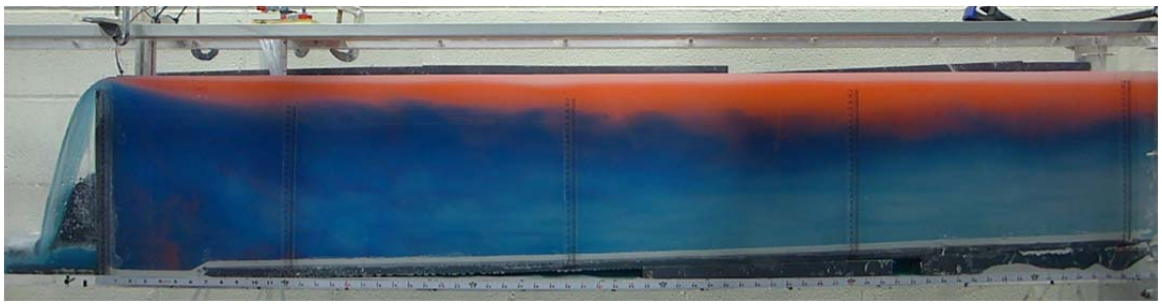

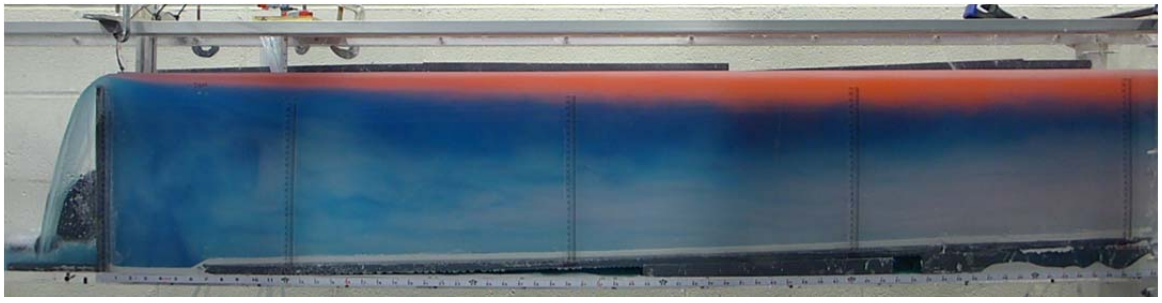

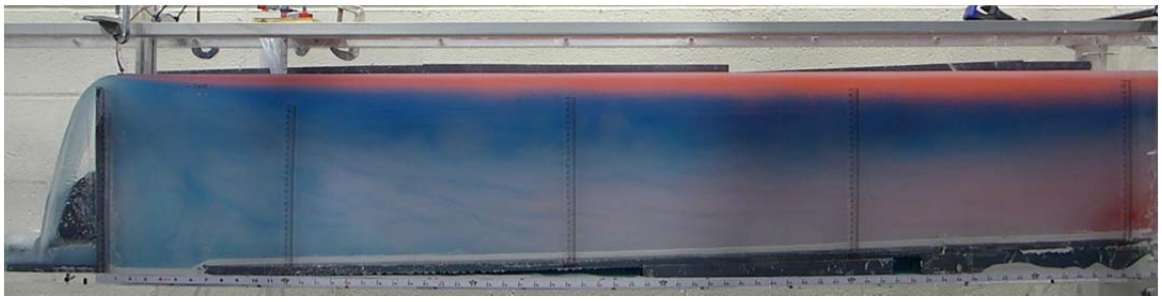

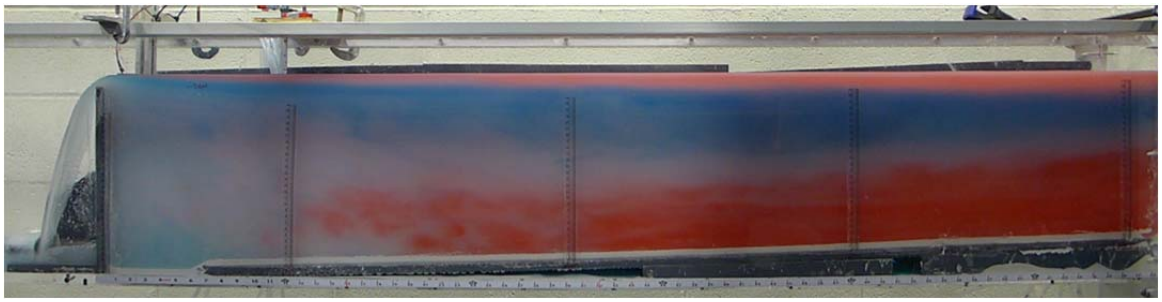

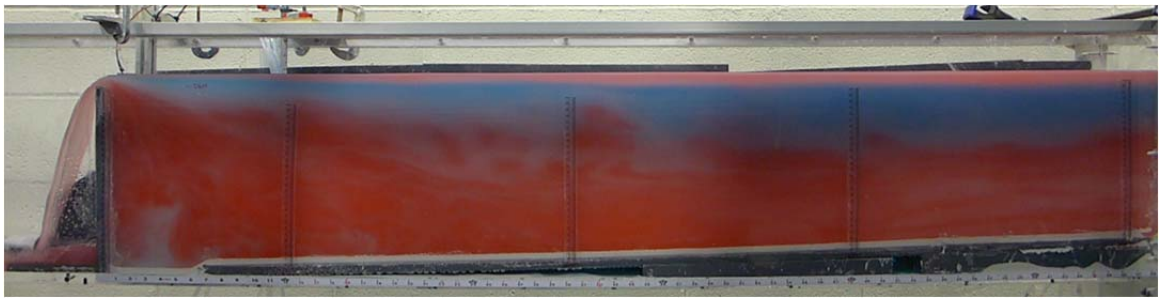

A2. Photo Sequence of a Turbidity Current Venting Typical Run

The scaled reservoir was initially filled with clean water. Then the turbidity current plunged inside and moved downstream along the bed until it reached the dam. When the turbidity current was about 61 cm (2 ft) from the dam, the low-level outlets were opened to extract the current. Red and blue dye was added to the turbidity current make it visible.

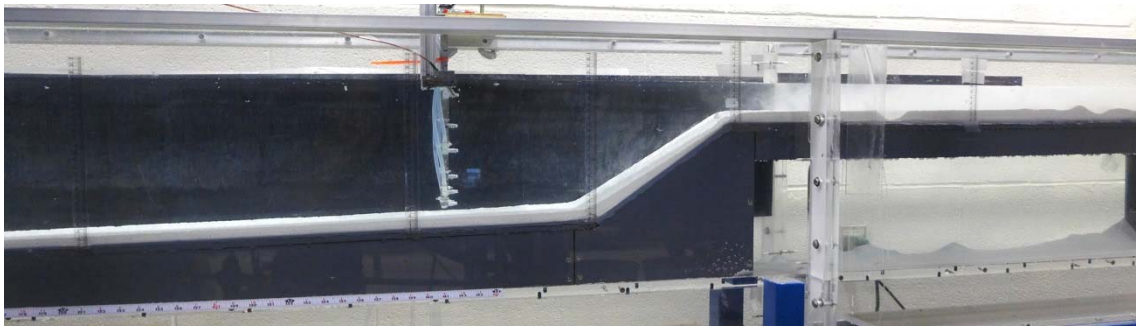

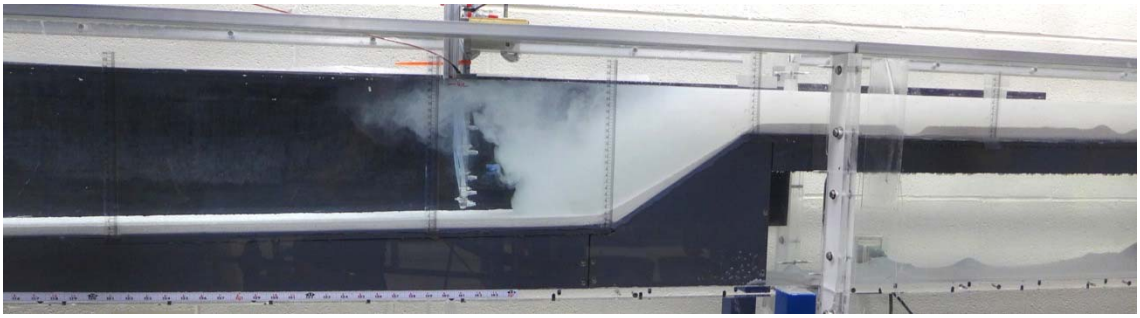

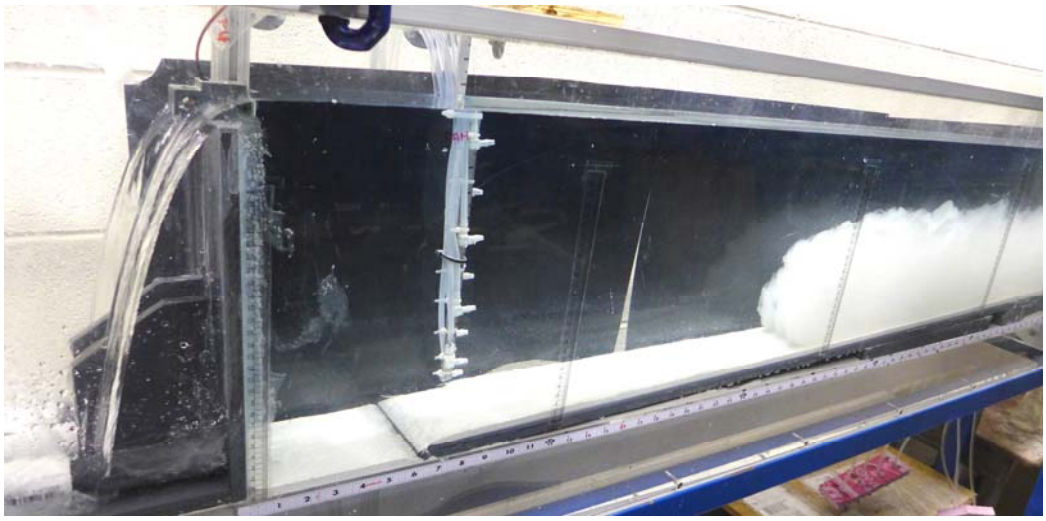

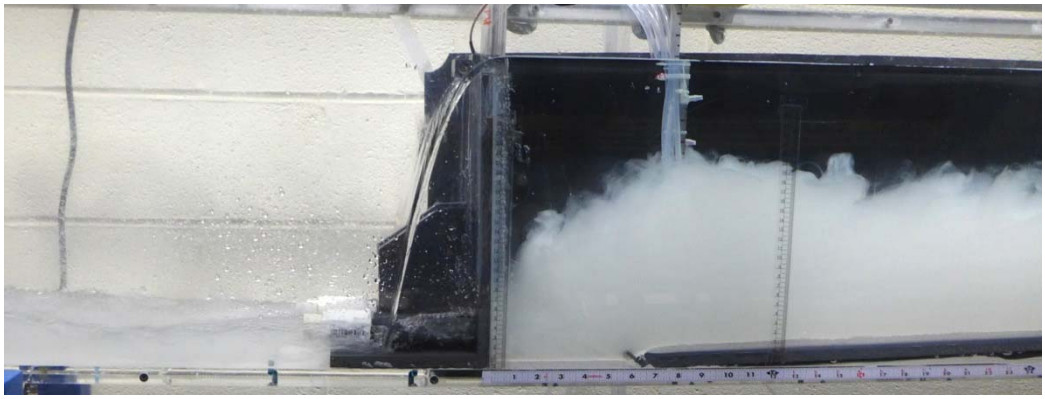

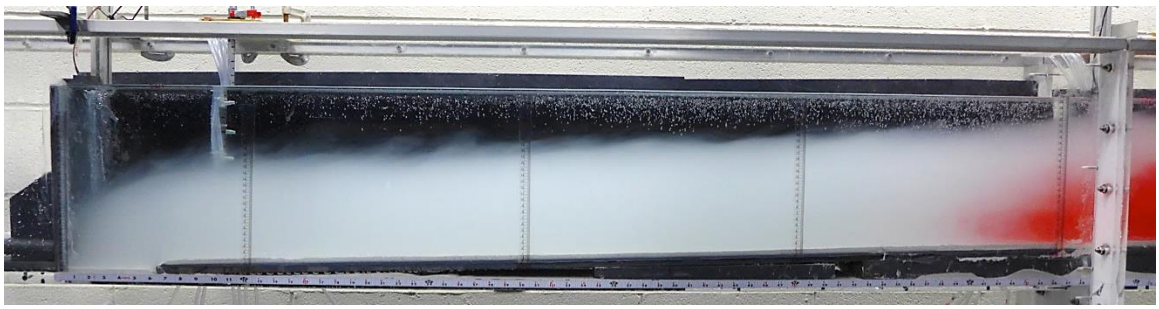

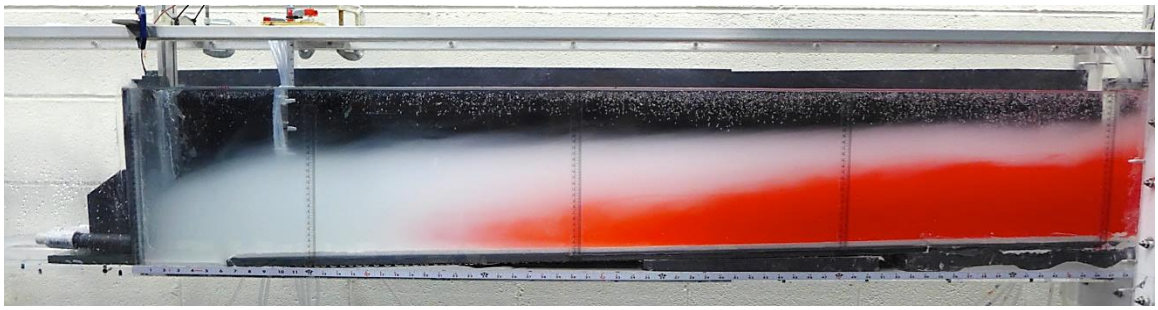

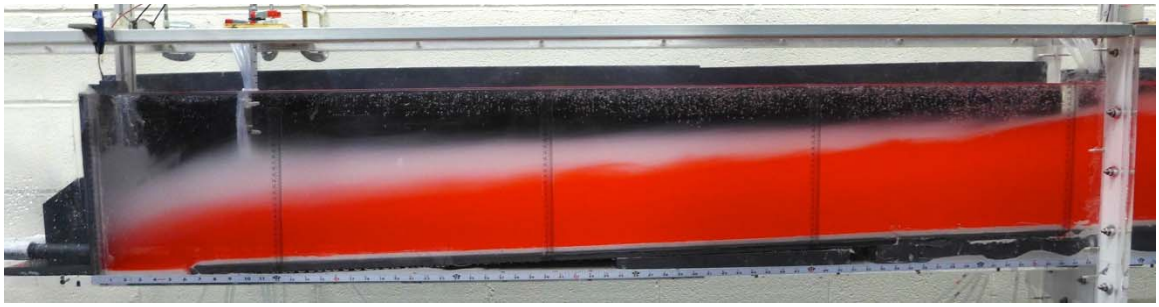

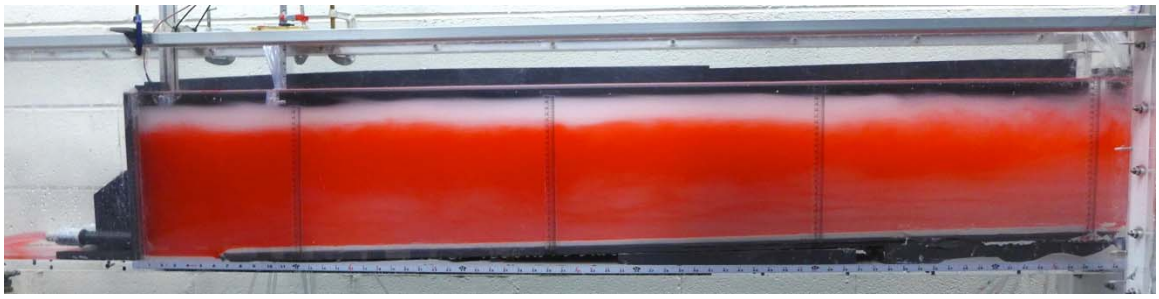

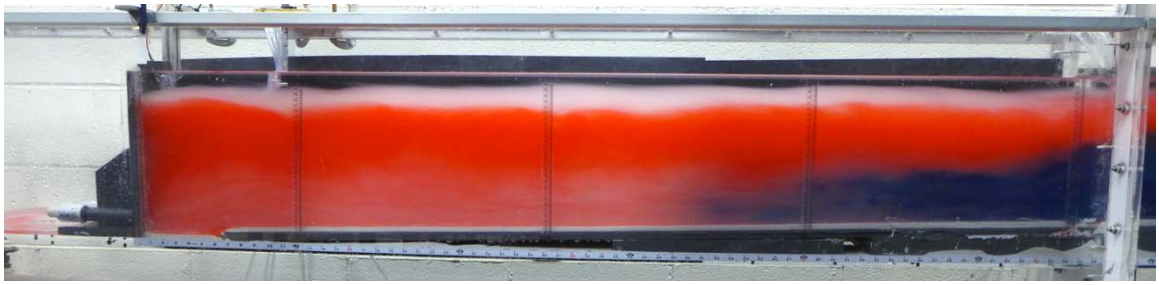

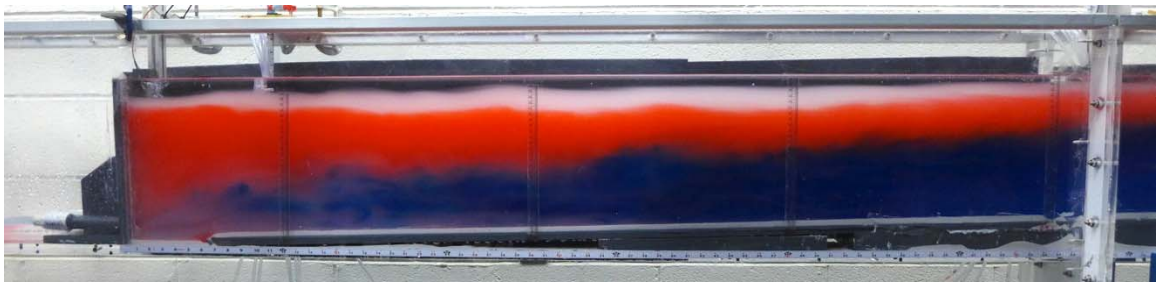

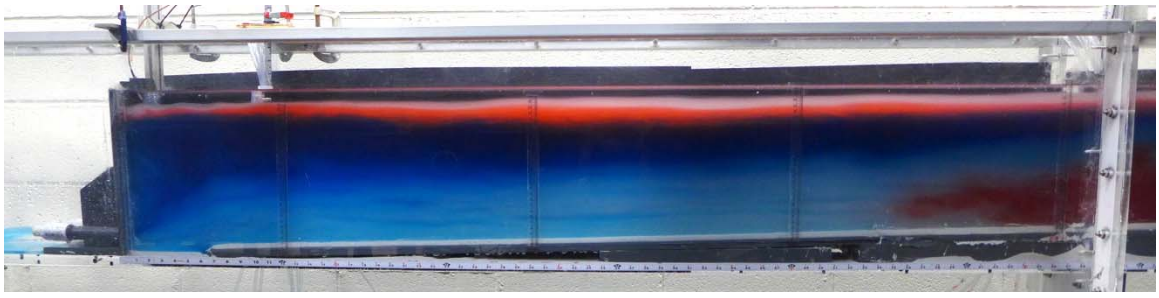

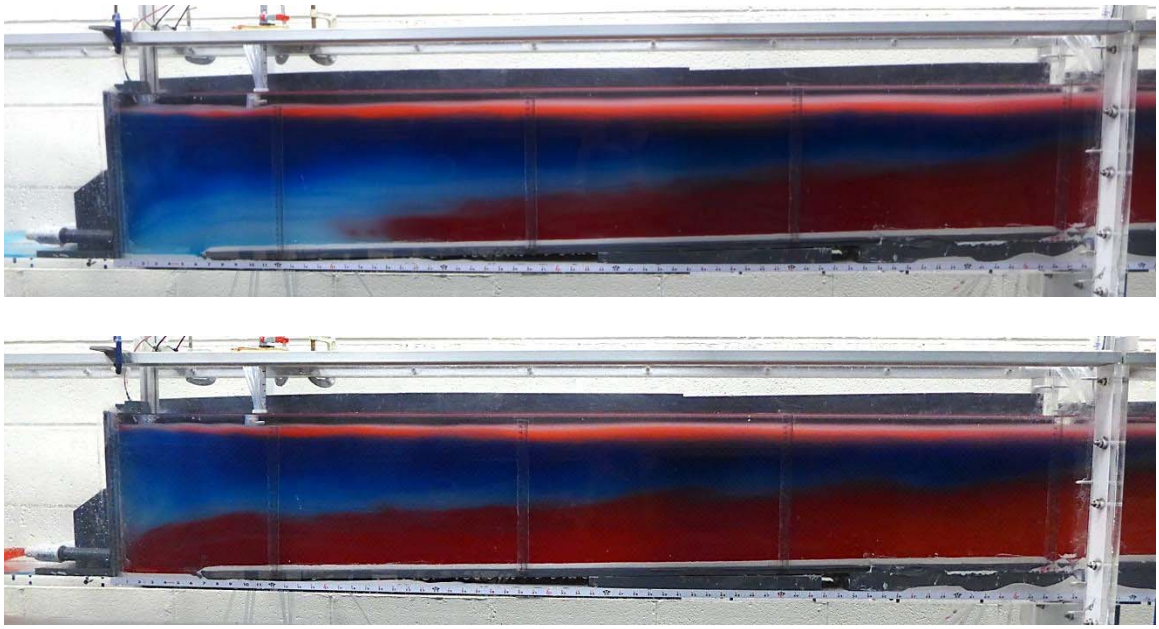

A3. Turbidity Current Extracted Through The Low Level Outlets.

The turbidity current inside the reservoir was dyed with red coloring. It can be appreciated in the picture that the outflow matches the color of the turbidity current, which was extracted through the low-level outlets.

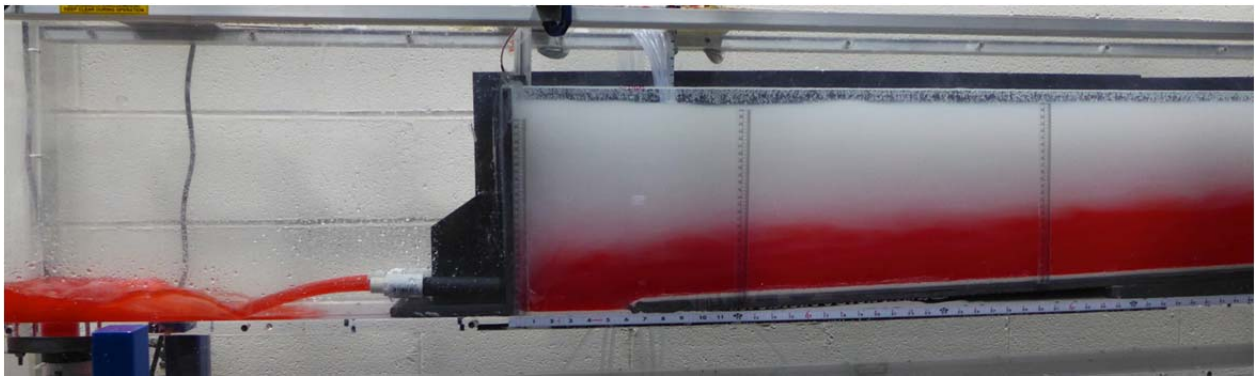

APPENDIX B: STREAMWISE VELOCITY DATA

B1. Normal Reservoir Operation - Location A

Normal Reservoir Operation - Location A											
Run N4				Run N6				Run N7			
Measured		Normalized		Measured		Normalized		Measured		Normalized	
h (cm)	u (cm/s)	z/h	u/U	h (cm)	u (cm/s)	z/h	u/U	h (cm)	u (cm/s)	z/h	u/U
19.02	0.04	1.36	0.06	19.02	0.04	1.36	0.06	19.02	0.04	1.36	0.06
18.83	0.00	1.34	0.00	18.83	0.00	1.35	0.00	18.83	0.00	1.35	0.00
18.63	0.02	1.33	0.03	18.63	0.02	1.33	0.03	18.63	0.02	1.34	0.02
18.44	0.04	1.32	0.05	18.44	0.04	1.32	0.06	18.44	0.04	1.32	0.04
18.25	0.07	1.30	0.10	18.25	0.07	1.31	0.10	18.25	0.07	1.31	0.06
18.06	0.11	1.29	0.16	18.06	0.11	1.29	0.17	18.06	0.11	1.29	0.10
17.86	0.13	1.28	0.19	17.86	0.13	1.28	0.18	17.86	0.13	1.28	0.13
17.67	0.13	1.26	0.20	17.67	0.13	1.27	0.19	17.67	0.13	1.27	0.12
17.48	0.13	1.25	0.19	17.48	0.14	1.25	0.20	17.48	0.14	1.25	0.13
17.29	0.14	1.23	0.20	17.29	0.13	1.24	0.20	17.29	0.13	1.24	0.12
17.10	0.13	1.22	0.19	17.10	0.13	1.22	0.20	17.10	0.13	1.22	0.12
16.90	0.13	1.21	0.19	16.90	0.13	1.21	0.20	16.90	0.13	1.21	0.12
16.71	0.13	1.19	0.19	16.71	0.13	1.20	0.19	16.71	0.13	1.20	0.12
16.52	0.15	1.18	0.22	16.52	0.15	1.18	0.22	16.52	0.15	1.18	0.14
16.33	0.16	1.17	0.24	16.33	0.17	1.17	0.24	16.33	0.16	1.17	0.15
16.13	0.17	1.15	0.25	16.13	0.16	1.16	0.24	16.13	0.16	1.16	0.15
15.94	0.16	1.14	0.24	15.94	0.17	1.14	0.25	15.94	0.16	1.14	0.15
15.75	0.17	1.12	0.25	15.75	0.17	1.13	0.24	15.75	0.16	1.13	0.15
15.56	0.16	1.11	0.24	15.56	0.17	1.11	0.25	15.56	0.16	1.11	0.15
15.37	0.17	1.10	0.25	15.37	0.17	1.10	0.26	15.37	0.17	1.10	0.16
15.17	0.16	1.08	0.24	15.17	0.16	1.09	0.24	15.17	0.17	1.09	0.16
14.98	0.21	1.07	0.30	14.98	0.21	1.07	0.30	14.98	0.21	1.07	0.19
14.79	0.24	1.06	0.35	14.79	0.24	1.06	0.36	14.79	0.24	1.06	0.23
14.60	0.24	1.04	0.36	14.60	0.24	1.05	0.35	14.60	0.25	1.05	0.23
14.40	0.24	1.03	0.35	14.40	0.25	1.03	0.37	14.40	0.25	1.03	0.24
14.21	0.25	1.01	0.37	14.21	0.25	1.02	0.37	14.21	0.25	1.02	0.24
14.02	0.26	1.00	0.38	14.02	0.26	1.00	0.38	14.02	0.25	1.00	0.24
13.83	0.26	0.99	0.39	13.83	0.26	0.99	0.39	13.83	0.26	0.99	0.25
13.64	0.26	0.97	0.38	13.64	0.26	0.98	0.39	13.64	0.26	0.98	0.24
13.44	0.32	0.96	0.47	13.44	0.32	0.96	0.47	13.44	0.33	0.96	0.31
13.25	0.39	0.95	0.58	13.25	0.37	0.95	0.54	13.25	0.39	0.95	0.37
13.06	0.38	0.93	0.57	13.06	0.38	0.94	0.56	13.06	0.38	0.94	0.36
12.87	0.37	0.92	0.55	12.87	0.37	0.92	0.54	12.87	0.36	0.92	0.34
12.67	0.35	0.90	0.52	12.67	0.36	0.91	0.53	12.67	0.36	0.91	0.33

Cont. of Normal Reservoir Operation - Location A											
Run N4				Run N6				Run N7			
Measured		Normalized		Measured		Normalized		Measured		Normalized	
h (cm)	u (cm/s)	z/h	u/U	h (cm)	u (cm/s)	z/h	u/U	h (cm)	u (cm/s)	z/h	u/U
12.48	0.36	0.89	0.53	12.48	0.35	0.89	0.52	12.48	0.36	0.89	0.34
12.29	0.36	0.88	0.53	12.29	0.36	0.88	0.53	12.29	0.35	0.88	0.33
12.10	0.37	0.86	0.54	12.10	0.36	0.87	0.53	12.10	0.38	0.87	0.36
11.90	0.47	0.85	0.70	11.90	0.46	0.85	0.68	11.90	0.47	0.85	0.44
11.71	0.57	0.84	0.85	11.71	0.56	0.84	0.83	11.71	0.59	0.84	0.55
11.52	0.59	0.82	0.87	11.52	0.61	0.83	0.90	11.52	0.61	0.83	0.57
11.33	0.63	0.81	0.94	11.33	0.63	0.81	0.93	11.33	0.64	0.81	0.60
11.14	0.64	0.79	0.95	11.14	0.64	0.80	0.94	11.14	0.65	0.80	0.61
10.94	0.62	0.78	0.92	10.94	0.64	0.78	0.94	10.94	0.62	0.78	0.58
10.75	0.61	0.77	0.91	10.75	0.60	0.77	0.88	10.75	0.59	0.77	0.55
10.56	0.59	0.75	0.87	10.56	0.61	0.76	0.90	10.56	0.59	0.76	0.55
10.37	0.70	0.74	1.04	10.37	0.70	0.74	1.02	10.37	0.73	0.74	0.69
10.17	0.77	0.73	1.14	10.17	0.76	0.73	1.11	10.17	0.77	0.73	0.73
9.98	0.73	0.71	1.08	9.98	0.78	0.72	1.14	9.98	0.74	0.72	0.69
9.79	0.73	0.70	1.09	9.79	0.73	0.70	1.08	9.79	0.73	0.70	0.69
9.60	0.74	0.69	1.10	9.60	0.75	0.69	1.10	9.60	0.77	0.69	0.72
9.41	0.75	0.67	1.11	9.41	0.77	0.67	1.13	9.41	0.79	0.67	0.74
9.21	0.75	0.66	1.10	9.21	0.76	0.66	1.12	9.21	0.77	0.66	0.73
9.02	0.80	0.64	1.19	9.02	0.80	0.65	1.18	9.02	0.84	0.65	0.79
8.83	1.01	0.63	1.50	8.83	1.03	0.63	1.52	8.83	1.04	0.63	0.97
8.64	0.93	0.62	1.38	8.64	0.93	0.62	1.37	8.64	0.95	0.62	0.90
8.44	0.99	0.60	1.47	8.44	1.02	0.60	1.50	8.44	1.00	0.61	0.94
8.25	0.99	0.59	1.46	8.25	1.06	0.59	1.56	8.25	1.01	0.59	0.95
8.06	1.05	0.58	1.55	8.06	1.06	0.58	1.56	8.06	1.07	0.58	1.01
7.87	1.06	0.56	1.56	7.87	1.06	0.56	1.56	7.87	1.09	0.56	1.02
7.68	1.06	0.55	1.56	7.68	1.04	0.55	1.53	7.68	1.05	0.55	0.98
7.48	0.97	0.53	1.44	7.48	0.99	0.54	1.46	7.48	1.01	0.54	0.95
7.29	0.99	0.52	1.47	7.29	0.98	0.52	1.45	7.29	1.04	0.52	0.98
7.10	0.95	0.51	1.41	7.10	0.97	0.51	1.43	7.10	0.97	0.51	0.92
6.91	0.98	0.49	1.45	6.91	0.95	0.49	1.40	6.91	0.99	0.49	0.93
6.71	0.93	0.48	1.37	6.71	0.93	0.48	1.37	6.71	0.92	0.48	0.87
6.52	0.92	0.47	1.36	6.52	0.91	0.47	1.34	6.52	0.92	0.47	0.87
6.33	0.89	0.45	1.32	6.33	0.88	0.45	1.30	6.33	0.91	0.45	0.85
6.14	0.86	0.44	1.27	6.14	0.88	0.44	1.30	6.14	0.89	0.44	0.83
5.94	0.91	0.42	1.35	5.94	0.91	0.43	1.34	5.94	0.94	0.43	0.88
5.75	0.85	0.41	1.26	5.75	0.83	0.41	1.22	5.75	0.82	0.41	0.77
5.56	0.71	0.40	1.04	5.56	0.74	0.40	1.09	5.56	0.74	0.40	0.70
5.37	0.75	0.38	1.11	5.37	0.72	0.38	1.06	5.37	0.74	0.38	0.70
5.18	0.77	0.37	1.14	5.18	0.77	0.37	1.13	5.18	0.77	0.37	0.73
4.98	0.79	0.36	1.17	4.98	0.82	0.36	1.21	4.98	0.81	0.36	0.76
4.79	0.80	0.34	1.19	4.79	0.78	0.34	1.15	4.79	0.79	0.34	0.74

Cont. of Normal Reservoir Operation - Location A											
Run N4				Run N6				Run N7			
Measured		Normalized		Measured		Normalized		Measured		Normalized	
h (cm)	u (cm/s)	z/h	u/U	h (cm)	u (cm/s)	z/h	u/U	h (cm)	u (cm/s)	z/h	u/U
4.60	0.74	0.33	1.10	4.60	0.76	0.33	1.11	4.60	0.72	0.33	0.68
4.41	0.78	0.31	1.15	4.41	0.77	0.32	1.14	4.41	0.81	0.32	0.76
4.21	0.65	0.30	0.96	4.21	0.64	0.30	0.95	4.21	0.64	0.30	0.60
4.02	0.54	0.29	0.81	4.02	0.57	0.29	0.83	4.02	0.56	0.29	0.53
3.83	0.53	0.27	0.79	3.83	0.54	0.27	0.80	3.83	0.53	0.27	0.50
3.64	0.52	0.26	0.77	3.64	0.53	0.26	0.78	3.64	0.53	0.26	0.49
3.45	0.53	0.25	0.78	3.45	0.51	0.25	0.75	3.45	0.53	0.25	0.50
3.25	0.53	0.23	0.78	3.25	0.51	0.23	0.76	3.25	0.52	0.23	0.49
3.06	0.52	0.22	0.78	3.06	0.51	0.22	0.75	3.06	0.52	0.22	0.49
2.87	0.53	0.20	0.78	2.87	0.52	0.21	0.76	2.87	0.54	0.21	0.51
2.68	0.47	0.19	0.70	2.68	0.47	0.19	0.69	2.68	0.48	0.19	0.45
2.48	0.40	0.18	0.59	2.48	0.39	0.18	0.57	2.48	0.39	0.18	0.37
2.29	0.38	0.16	0.56	2.29	0.39	0.16	0.57	2.29	0.39	0.16	0.37
2.10	0.39	0.15	0.58	2.10	0.38	0.15	0.56	2.10	0.40	0.15	0.37
1.91	0.40	0.14	0.60	1.91	0.40	0.14	0.58	1.91	0.41	0.14	0.38
1.72	0.38	0.12	0.57	1.72	0.40	0.12	0.58	1.72	0.39	0.12	0.36
1.52	0.39	0.11	0.57	1.52	0.39	0.11	0.57	1.52	0.39	0.11	0.37
1.33	0.40	0.09	0.59	1.33	0.38	0.10	0.55	1.33	0.39	0.10	0.37
1.14	0.33	0.08	0.49	1.14	0.34	0.08	0.50	1.14	0.34	0.08	0.32
0.95	0.29	0.07	0.44	0.95	0.29	0.07	0.43	0.95	0.29	0.07	0.28
0.75	0.29	0.05	0.43	0.75	0.29	0.05	0.42	0.75	0.28	0.05	0.26
0.56	0.29	0.04	0.42	0.56	0.28	0.04	0.41	0.56	0.29	0.04	0.27
0.37	0.30	0.03	0.44	0.37	0.28	0.03	0.40	0.37	0.29	0.03	0.28
0.18	0.29	0.01	0.42	0.18	0.28	0.01	0.41	0.18	0.29	0.01	0.27
-0.02	0.27	0.00	0.40	-0.02	0.27	0.00	0.40	-0.02	0.28	0.00	0.26

B2. Normal Reservoir Operation - Location B

Normal Reservoir Operation - Location B											
Run N4				Run N6				Run N7			
Measured		Normalized		Measured		Normalized		Measured		Normalized	
h (cm)	u (cm/s)	z/h	u/U	h (cm)	u (cm/s)	z/h	u/U	h (cm)	u (cm/s)	z/h	u/U
23.26	0.06	1.22	0.04	22.88	0.06	1.23	0.03	21.73	0.05	1.27	0.03
23.07	0.00	1.21	0.00	22.69	0.00	1.22	0.00	21.53	0.00	1.25	0.00
22.88	0.08	1.20	0.05	22.49	0.02	1.21	0.01	21.34	0.01	1.24	0.01
22.69	0.44	1.19	0.28	22.30	0.31	1.20	0.18	21.15	0.09	1.23	0.05
22.49	0.41	1.18	0.26	22.11	0.61	1.19	0.35	20.96	0.31	1.22	0.18
22.30	0.57	1.17	0.36	21.92	0.66	1.18	0.37	20.76	0.70	1.21	0.42
22.11	0.61	1.16	0.39	21.73	0.63	1.17	0.36	20.57	0.85	1.20	0.50
21.92	0.76	1.15	0.49	21.53	0.63	1.16	0.36	20.38	0.80	1.19	0.47
21.73	0.81	1.14	0.52	21.34	0.59	1.15	0.34	20.19	0.75	1.18	0.44
21.53	0.79	1.13	0.50	21.15	0.60	1.14	0.34	20.00	0.69	1.16	0.41
21.34	0.78	1.12	0.49	20.96	0.62	1.13	0.35	19.80	0.69	1.15	0.40
21.15	0.90	1.11	0.57	20.76	0.58	1.12	0.33	19.61	0.82	1.14	0.48
20.96	0.78	1.10	0.50	20.57	0.61	1.11	0.35	19.42	0.71	1.13	0.42
20.76	0.83	1.09	0.53	20.38	0.63	1.10	0.35	19.23	0.71	1.12	0.42
20.57	0.81	1.08	0.52	20.19	0.61	1.09	0.34	19.03	0.71	1.11	0.42
20.38	0.82	1.07	0.52	20.00	0.62	1.08	0.35	18.84	0.72	1.10	0.42
20.19	0.86	1.06	0.55	19.80	0.63	1.07	0.36	18.65	0.65	1.09	0.38
20.00	0.85	1.05	0.54	19.61	0.56	1.06	0.32	18.46	0.62	1.07	0.36
19.80	0.78	1.04	0.50	19.42	0.55	1.05	0.31	18.26	0.63	1.06	0.37
19.61	0.82	1.03	0.52	19.23	0.52	1.04	0.30	18.07	0.53	1.05	0.31
19.42	0.86	1.02	0.55	19.03	0.57	1.03	0.32	17.88	0.54	1.04	0.32
19.23	0.87	1.01	0.55	18.84	0.56	1.02	0.32	17.69	0.55	1.03	0.32
19.03	0.79	1.00	0.50	18.65	0.63	1.01	0.35	17.50	0.58	1.02	0.34
18.84	0.79	0.99	0.50	18.46	0.62	1.00	0.35	17.30	0.60	1.01	0.35
18.65	0.82	0.98	0.52	18.26	0.70	0.99	0.40	17.11	0.55	1.00	0.33
18.46	0.78	0.97	0.49	18.07	0.73	0.97	0.41	16.92	0.59	0.99	0.35
18.26	0.72	0.96	0.46	17.88	0.72	0.96	0.41	16.73	0.52	0.97	0.31
18.07	0.75	0.95	0.48	17.69	0.74	0.95	0.42	16.53	0.58	0.96	0.34
17.88	0.72	0.94	0.46	17.50	0.73	0.94	0.41	16.34	0.57	0.95	0.33
17.69	0.73	0.93	0.46	17.30	0.75	0.93	0.42	16.15	0.61	0.94	0.36
17.50	0.69	0.92	0.44	17.11	0.77	0.92	0.44	15.96	0.62	0.93	0.37
17.30	0.66	0.91	0.42	16.92	0.77	0.91	0.44	15.77	0.65	0.92	0.39
17.11	0.62	0.90	0.40	16.73	0.81	0.90	0.46	15.57	0.69	0.91	0.40
16.92	0.62	0.89	0.40	16.53	0.80	0.89	0.45	15.38	0.68	0.90	0.40
16.73	0.59	0.88	0.38	16.34	0.81	0.88	0.46	15.19	0.75	0.88	0.44
16.53	0.62	0.87	0.39	16.15	0.82	0.87	0.46	15.00	0.72	0.87	0.43
16.34	0.61	0.86	0.39	15.96	0.87	0.86	0.49	14.80	0.76	0.86	0.45
16.15	0.59	0.85	0.38	15.77	0.93	0.85	0.53	14.61	0.74	0.85	0.43
15.96	0.62	0.84	0.39	15.57	0.93	0.84	0.53	14.42	0.77	0.84	0.45

Cont. of Normal Reservoir Operation - Location B											
Run N4				Run N6				Run N7			
Measured		Normalized		Measured		Normalized		Measured		Normalized	
h (cm)	u (cm/s)	z/h	u/U	h (cm)	u (cm/s)	z/h	u/U	h (cm)	u (cm/s)	z/h	u/U
15.77	0.62	0.83	0.40	15.38	0.98	0.83	0.56	14.23	0.77	0.83	0.45
15.57	0.59	0.82	0.38	15.19	1.02	0.82	0.58	14.04	0.78	0.82	0.46
15.38	0.55	0.81	0.35	15.00	1.06	0.81	0.60	13.84	0.82	0.81	0.48
15.19	0.62	0.80	0.39	14.80	1.06	0.80	0.60	13.65	0.85	0.80	0.50
15.00	0.62	0.79	0.39	14.61	1.12	0.79	0.64	13.46	0.88	0.78	0.52
14.80	0.60	0.78	0.38	14.42	1.15	0.78	0.65	13.27	0.89	0.77	0.53
14.61	0.68	0.77	0.43	14.23	1.18	0.77	0.67	13.07	0.94	0.76	0.56
14.42	0.69	0.76	0.44	14.04	1.20	0.76	0.68	12.88	0.93	0.75	0.55
14.23	0.70	0.75	0.45	13.84	1.22	0.75	0.69	12.69	0.96	0.74	0.57
14.04	0.78	0.74	0.50	13.65	1.20	0.74	0.68	12.50	0.97	0.73	0.57
13.84	0.78	0.73	0.49	13.46	1.22	0.73	0.69	12.30	1.04	0.72	0.61
13.65	0.79	0.72	0.50	13.27	1.26	0.72	0.71	12.11	1.07	0.71	0.63
13.46	0.87	0.71	0.55	13.07	1.28	0.71	0.72	11.92	1.09	0.69	0.64
13.27	0.88	0.70	0.56	12.88	1.26	0.69	0.72	11.73	1.12	0.68	0.66
13.07	0.91	0.69	0.58	12.69	1.35	0.68	0.76	11.54	1.18	0.67	0.69
12.88	0.93	0.68	0.59	12.50	1.34	0.67	0.76	11.34	1.23	0.66	0.72
12.69	1.05	0.67	0.67	12.30	1.38	0.66	0.78	11.15	1.28	0.65	0.75
12.50	1.03	0.66	0.66	12.11	1.38	0.65	0.78	10.96	1.33	0.64	0.78
12.30	1.00	0.65	0.63	11.92	1.39	0.64	0.79	10.77	1.37	0.63	0.81
12.11	1.07	0.64	0.68	11.73	1.43	0.63	0.81	10.57	1.43	0.62	0.84
11.92	1.04	0.63	0.66	11.54	1.45	0.62	0.82	10.38	1.47	0.60	0.87
11.73	1.06	0.62	0.67	11.34	1.49	0.61	0.84	10.19	1.51	0.59	0.89
11.54	1.19	0.61	0.75	11.15	1.52	0.60	0.86	10.00	1.55	0.58	0.92
11.34	1.32	0.60	0.84	10.96	1.55	0.59	0.88	9.81	1.57	0.57	0.92
11.15	1.32	0.59	0.84	10.77	1.58	0.58	0.89	9.61	1.60	0.56	0.94
10.96	1.35	0.58	0.86	10.57	1.61	0.57	0.91	9.42	1.64	0.55	0.97
10.77	1.42	0.57	0.90	10.38	1.67	0.56	0.94	9.23	1.67	0.54	0.99
10.57	1.33	0.56	0.85	10.19	1.69	0.55	0.96	9.04	1.70	0.53	1.00
10.38	1.39	0.55	0.88	10.00	1.73	0.54	0.98	8.84	1.74	0.52	1.03
10.19	1.46	0.54	0.93	9.81	1.78	0.53	1.01	8.65	1.78	0.50	1.05
10.00	1.51	0.53	0.96	9.61	1.77	0.52	1.00	8.46	1.80	0.49	1.06
9.81	1.53	0.52	0.97	9.42	1.79	0.51	1.02	8.27	1.85	0.48	1.09
9.61	1.63	0.51	1.03	9.23	1.84	0.50	1.05	8.08	1.88	0.47	1.11
9.42	1.68	0.50	1.07	9.04	1.86	0.49	1.05	7.88	1.90	0.46	1.12
9.23	1.68	0.49	1.07	8.84	1.89	0.48	1.07	7.69	1.95	0.45	1.15
9.04	1.69	0.48	1.07	8.65	1.90	0.47	1.08	7.50	1.97	0.44	1.16
8.84	1.79	0.47	1.14	8.46	1.91	0.46	1.08	7.31	1.97	0.43	1.16
8.65	1.76	0.45	1.12	8.27	1.97	0.45	1.12	7.11	2.03	0.41	1.20
8.46	1.81	0.44	1.15	8.08	2.00	0.44	1.13	6.92	2.04	0.40	1.20
8.27	1.73	0.43	1.10	7.88	2.01	0.43	1.14	6.73	2.06	0.39	1.22
8.08	1.84	0.42	1.17	7.69	2.03	0.41	1.15	6.54	2.09	0.38	1.23

Cont. of Normal Reservoir Operation - Location B											
Run N4				Run N6				Run N7			
Measured		Normalized		Measured		Normalized		Measured		Normalized	
h (cm)	u (cm/s)	z/h	u/U	h (cm)	u (cm/s)	z/h	u/U	h (cm)	u (cm/s)	z/h	u/U
7.88	1.90	0.41	1.20	7.50	2.07	0.40	1.17	6.34	2.10	0.37	1.24
7.69	1.92	0.40	1.22	7.31	2.09	0.39	1.18	6.15	2.12	0.36	1.25
7.50	1.93	0.39	1.23	7.11	2.10	0.38	1.19	5.96	2.15	0.35	1.27
7.31	1.91	0.38	1.21	6.92	2.13	0.37	1.21	5.77	2.18	0.34	1.29
7.11	1.97	0.37	1.25	6.73	2.18	0.36	1.23	5.58	2.19	0.32	1.29
6.92	1.96	0.36	1.24	6.54	2.18	0.35	1.23	5.38	2.20	0.31	1.30
6.73	1.87	0.35	1.19	6.34	2.20	0.34	1.24	5.19	2.25	0.30	1.32
6.54	1.91	0.34	1.21	6.15	2.22	0.33	1.26	5.00	2.25	0.29	1.32
6.34	1.96	0.33	1.25	5.96	2.24	0.32	1.27	4.81	2.28	0.28	1.35
6.15	1.99	0.32	1.26	5.77	2.26	0.31	1.28	4.61	2.29	0.27	1.35
5.96	2.07	0.31	1.31	5.58	2.28	0.30	1.29	4.42	2.29	0.26	1.35
5.77	1.97	0.30	1.25	5.38	2.28	0.29	1.29	4.23	2.31	0.25	1.36
5.58	2.01	0.29	1.28	5.19	2.30	0.28	1.30	4.04	2.35	0.24	1.39
5.38	2.02	0.28	1.29	5.00	2.31	0.27	1.31	3.85	2.36	0.22	1.39
5.19	2.04	0.27	1.30	4.81	2.33	0.26	1.32	3.65	2.33	0.21	1.38
5.00	2.01	0.26	1.28	4.61	2.34	0.25	1.33	3.46	2.32	0.20	1.37
4.81	2.03	0.25	1.29	4.42	2.37	0.24	1.34	3.27	2.33	0.19	1.38
4.61	2.05	0.24	1.30	4.23	2.40	0.23	1.36	3.08	2.32	0.18	1.37
4.42	2.08	0.23	1.32	4.04	2.39	0.22	1.36	2.88	2.29	0.17	1.35
4.23	2.11	0.22	1.34	3.85	2.41	0.21	1.37	2.69	2.27	0.16	1.34
4.04	2.09	0.21	1.33	3.65	2.42	0.20	1.37	2.50	2.28	0.15	1.35
3.85	2.11	0.20	1.34	3.46	2.43	0.19	1.38	2.31	2.24	0.13	1.32
3.65	2.12	0.19	1.35	3.27	2.43	0.18	1.38	2.12	2.12	0.12	1.25
3.46	2.12	0.18	1.35	3.08	2.43	0.17	1.38	1.92	2.19	0.11	1.29
3.27	2.13	0.17	1.35	2.88	2.44	0.16	1.38	1.73	2.19	0.10	1.29
3.08	2.15	0.16	1.37	2.69	2.43	0.15	1.37	1.54	2.00	0.09	1.18
2.88	2.12	0.15	1.35	2.50	2.42	0.13	1.37	1.35	2.00	0.08	1.18
2.69	2.14	0.14	1.36	2.31	2.34	0.12	1.33	1.15	1.97	0.07	1.16
2.50	2.16	0.13	1.37	2.12	2.28	0.11	1.29	0.96	1.92	0.06	1.13
2.31	2.15	0.12	1.37	1.92	2.27	0.10	1.29	0.77	1.81	0.04	1.06
2.12	2.07	0.11	1.32	1.73	2.23	0.09	1.26	0.58	1.58	0.03	0.93
1.92	2.07	0.10	1.31	1.54	2.14	0.08	1.21	0.38	1.37	0.02	0.81
1.73	2.02	0.09	1.28	1.35	2.09	0.07	1.18	0.19	0.62	0.01	0.36
1.54	2.05	0.08	1.30	1.15	2.00	0.06	1.13	0.00	0.32	0.00	0.19
1.35	2.04	0.07	1.30	0.96	1.83	0.05	1.04				
1.15	2.01	0.06	1.28	0.77	1.67	0.04	0.95				
0.96	1.94	0.05	1.23	0.58	1.61	0.03	0.91				
0.77	1.80	0.04	1.15	0.38	1.29	0.02	0.73				
0.58	1.73	0.03	1.10	0.19	0.45	0.01	0.26				
0.38	1.58	0.02	1.00	0.00	0.16	0.00	0.09				
0.19	1.41	0.01	0.89								
0.00	0.96	0.00	0.61								

B3. Normal Reservoir Operation - Location C

Normal Reservoir Operation - Location C											
Run N4				Run N6				Run N7			
Measured		Normalized		Measured		Normalized		Measured		Normalized	
h (cm)	u (cm/s)	z/h	u/U	h (cm)	u (cm/s)	z/h	u/U	h (cm)	u (cm/s)	z/h	u/U
26.88	0.28	0.39	0.22	26.88	0.13	1.22	0.05	26.88	0.10	1.21	0.04
26.69	2.01	0.39	1.56	26.69	2.32	1.21	0.93	26.69	1.74	1.20	0.69
26.50	4.27	0.39	3.32	26.50	4.25	1.20	1.70	26.50	4.14	1.19	1.63
26.31	4.54	0.39	3.53	26.31	4.50	1.19	1.81	26.31	4.58	1.18	1.81
26.11	4.50	0.38	3.50	26.11	4.49	1.18	1.80	26.11	4.56	1.18	1.80
25.92	4.45	0.38	3.46	25.92	4.43	1.17	1.77	25.92	4.48	1.17	1.76
25.73	4.37	0.38	3.40	25.73	4.35	1.16	1.74	25.73	4.39	1.16	1.73
25.54	4.25	0.38	3.31	25.54	4.24	1.16	1.70	25.54	4.30	1.15	1.70
25.35	4.12	0.37	3.20	25.35	4.13	1.15	1.66	25.35	4.17	1.14	1.64
25.15	4.04	0.37	3.14	25.15	4.04	1.14	1.62	25.15	4.06	1.13	1.60
24.96	3.95	0.37	3.08	24.96	3.94	1.13	1.58	24.96	3.97	1.12	1.57
24.77	3.84	0.36	2.99	24.77	3.85	1.12	1.54	24.77	3.89	1.11	1.53
24.58	3.77	0.36	2.93	24.58	3.76	1.11	1.51	24.58	3.78	1.11	1.49
24.38	3.66	0.36	2.85	24.38	3.67	1.10	1.47	24.38	3.68	1.10	1.45
24.19	3.58	0.36	2.78	24.19	3.58	1.09	1.43	24.19	3.62	1.09	1.43
24.00	3.49	0.35	2.71	24.00	3.49	1.09	1.40	24.00	3.52	1.08	1.39
23.81	3.41	0.35	2.65	23.81	3.41	1.08	1.37	23.81	3.43	1.07	1.35
23.62	3.33	0.35	2.59	23.62	3.31	1.07	1.33	23.62	3.38	1.06	1.33
23.42	3.22	0.34	2.51	23.42	3.24	1.06	1.30	23.42	3.31	1.05	1.30
23.23	3.16	0.34	2.46	23.23	3.20	1.05	1.28	23.23	3.22	1.05	1.27
23.04	3.12	0.34	2.42	23.04	3.12	1.04	1.25	23.04	3.15	1.04	1.24
22.85	3.05	0.34	2.37	22.85	3.07	1.03	1.23	22.85	3.09	1.03	1.22
22.65	3.00	0.33	2.34	22.65	3.01	1.02	1.21	22.65	3.05	1.02	1.20
22.46	2.94	0.33	2.29	22.46	2.95	1.02	1.18	22.46	2.98	1.01	1.18
22.27	2.89	0.33	2.25	22.27	2.92	1.01	1.17	22.27	2.96	1.00	1.17
22.08	2.86	0.32	2.22	22.08	2.84	1.00	1.14	22.08	2.94	0.99	1.16
21.89	2.80	0.32	2.18	21.89	2.78	0.99	1.11	21.89	2.88	0.99	1.14
21.69	2.76	0.32	2.15	21.69	2.74	0.98	1.10	21.69	2.87	0.98	1.13
21.50	2.73	0.32	2.12	21.50	2.69	0.97	1.08	21.50	2.83	0.97	1.12
21.31	2.69	0.31	2.09	21.31	2.62	0.96	1.05	21.31	2.79	0.96	1.10
21.12	2.65	0.31	2.06	21.12	2.59	0.96	1.04	21.12	2.75	0.95	1.09
20.92	2.60	0.31	2.02	20.92	2.54	0.95	1.02	20.92	2.70	0.94	1.06
20.73	2.57	0.30	2.00	20.73	2.49	0.94	1.00	20.73	2.69	0.93	1.06
20.54	2.51	0.30	1.95	20.54	2.45	0.93	0.98	20.54	2.64	0.92	1.04
20.35	2.46	0.30	1.91	20.35	2.41	0.92	0.96	20.35	2.60	0.92	1.02
20.15	2.45	0.30	1.90	20.15	2.39	0.91	0.96	20.15	2.55	0.91	1.00
19.96	2.42	0.29	1.88	19.96	2.34	0.90	0.94	19.96	2.53	0.90	0.99
19.77	2.38	0.29	1.85	19.77	2.32	0.89	0.93	19.77	2.51	0.89	0.99
19.58	2.34	0.29	1.82	19.58	2.29	0.89	0.92	19.58	2.46	0.88	0.97

Cont. of Normal Reservoir Operation - Location C											
Run N4				Run N6				Run N7			
Measured		Normalized		Measured		Normalized		Measured		Normalized	
h (cm)	u (cm/s)	z/h	u/U	h (cm)	u (cm/s)	z/h	u/U	h (cm)	u (cm/s)	z/h	u/U
19.39	2.32	0.28	1.80	19.39	2.27	0.88	0.91	19.39	2.41	0.87	0.95
19.19	2.29	0.28	1.78	19.19	2.27	0.87	0.91	19.19	2.39	0.86	0.94
19.00	2.24	0.28	1.75	19.00	2.23	0.86	0.90	19.00	2.38	0.86	0.94
18.81	2.23	0.28	1.74	18.81	2.25	0.85	0.90	18.81	2.37	0.85	0.93
18.62	2.22	0.27	1.73	18.62	2.24	0.84	0.90	18.62	2.31	0.84	0.91
18.42	2.21	0.27	1.72	18.42	2.23	0.83	0.90	18.42	2.28	0.83	0.90
18.23	2.19	0.27	1.71	18.23	2.21	0.82	0.89	18.23	2.30	0.82	0.91
18.04	2.16	0.26	1.68	18.04	2.24	0.82	0.90	18.04	2.30	0.81	0.91
17.85	2.12	0.26	1.65	17.85	2.23	0.81	0.89	17.85	2.22	0.80	0.87
17.66	2.13	0.26	1.66	17.66	2.21	0.80	0.89	17.66	2.25	0.79	0.89
17.46	2.12	0.26	1.65	17.46	2.19	0.79	0.88	17.46	2.25	0.79	0.89
17.27	2.08	0.25	1.62	17.27	2.19	0.78	0.88	17.27	2.23	0.78	0.88
17.08	2.07	0.25	1.61	17.08	2.20	0.77	0.88	17.08	2.23	0.77	0.88
16.89	2.08	0.25	1.62	16.89	2.20	0.76	0.88	16.89	2.20	0.76	0.87
16.69	2.05	0.25	1.60	16.69	2.18	0.76	0.87	16.69	2.20	0.75	0.87
16.50	2.01	0.24	1.57	16.50	2.21	0.75	0.88	16.50	2.22	0.74	0.87
16.31	2.02	0.24	1.57	16.31	2.18	0.74	0.87	16.31	2.21	0.73	0.87
16.12	2.02	0.24	1.57	16.12	2.17	0.73	0.87	16.12	2.20	0.73	0.87
15.93	2.01	0.23	1.57	15.93	2.17	0.72	0.87	15.93	2.19	0.72	0.86
15.73	1.99	0.23	1.55	15.73	2.16	0.71	0.87	15.73	2.19	0.71	0.86
15.54	2.00	0.23	1.56	15.54	2.15	0.70	0.86	15.54	2.17	0.70	0.86
15.35	1.99	0.23	1.55	15.35	2.15	0.69	0.86	15.35	2.17	0.69	0.86
15.16	1.97	0.22	1.53	15.16	2.15	0.69	0.86	15.16	2.14	0.68	0.84
14.96	1.95	0.22	1.52	14.96	2.15	0.68	0.86	14.96	2.17	0.67	0.86
14.77	1.94	0.22	1.51	14.77	2.13	0.67	0.85	14.77	2.15	0.66	0.85
14.58	1.93	0.21	1.50	14.58	2.10	0.66	0.84	14.58	2.14	0.66	0.84
14.39	1.94	0.21	1.51	14.39	2.13	0.65	0.85	14.39	2.10	0.65	0.83
14.19	1.95	0.21	1.51	14.19	2.10	0.64	0.84	14.19	2.11	0.64	0.83
14.00	1.90	0.21	1.48	14.00	2.10	0.63	0.84	14.00	2.12	0.63	0.83
13.81	1.89	0.20	1.47	13.81	2.10	0.62	0.84	13.81	2.10	0.62	0.83
13.62	1.89	0.20	1.47	13.62	2.10	0.62	0.84	13.62	2.08	0.61	0.82
13.43	1.91	0.20	1.48	13.43	2.11	0.61	0.85	13.43	2.08	0.60	0.82
13.23	1.88	0.19	1.47	13.23	2.11	0.60	0.85	13.23	2.08	0.60	0.82
13.04	1.86	0.19	1.45	13.04	2.09	0.59	0.84	13.04	2.07	0.59	0.81
12.85	1.87	0.19	1.46	12.85	2.11	0.58	0.85	12.85	2.05	0.58	0.81
12.66	1.85	0.19	1.44	12.66	2.10	0.57	0.84	12.66	2.04	0.57	0.80
12.46	1.83	0.18	1.43	12.46	2.10	0.56	0.84	12.46	2.03	0.56	0.80
12.27	1.81	0.18	1.41	12.27	2.12	0.56	0.85	12.27	2.01	0.55	0.79
12.08	1.79	0.18	1.40	12.08	2.08	0.55	0.83	12.08	2.02	0.54	0.80
11.89	1.82	0.17	1.42	11.89	2.07	0.54	0.83	11.89	2.00	0.54	0.79
11.70	1.79	0.17	1.39	11.70	2.09	0.53	0.84	11.70	1.98	0.53	0.78

Cont. of Normal Reservoir Operation - Location C											
Run N4				Run N6				Run N7			
Measured		Normalized		Measured		Normalized		Measured		Normalized	
h (cm)	u (cm/s)	z/h	u/U	h (cm)	u (cm/s)	z/h	u/U	h (cm)	u (cm/s)	z/h	u/U
11.50	1.77	0.17	1.38	11.50	2.06	0.52	0.83	11.50	1.98	0.52	0.78
11.31	1.79	0.17	1.39	11.31	2.05	0.51	0.82	11.31	1.97	0.51	0.78
11.12	1.79	0.16	1.39	11.12	2.04	0.50	0.82	11.12	1.95	0.50	0.77
10.93	1.76	0.16	1.37	10.93	2.04	0.49	0.82	10.93	1.95	0.49	0.77
10.73	1.75	0.16	1.36	10.73	2.00	0.49	0.80	10.73	1.93	0.48	0.76
10.54	1.73	0.15	1.34	10.54	1.97	0.48	0.79	10.54	1.93	0.47	0.76
10.35	1.75	0.15	1.36	10.35	1.97	0.47	0.79	10.35	1.88	0.47	0.74
10.16	1.71	0.15	1.33	10.16	1.94	0.46	0.78	10.16	1.86	0.46	0.73
9.97	1.72	0.15	1.34	9.97	1.91	0.45	0.76	9.97	1.88	0.45	0.74
9.77	1.73	0.14	1.34	9.77	1.91	0.44	0.76	9.77	1.88	0.44	0.74
9.58	1.70	0.14	1.32	9.58	1.84	0.43	0.74	9.58	1.86	0.43	0.73
9.39	1.68	0.14	1.31	9.39	1.84	0.42	0.74	9.39	1.85	0.42	0.73
9.20	1.61	0.14	1.25	9.20	1.79	0.42	0.72	9.20	1.85	0.41	0.73
9.00	1.59	0.13	1.23	9.00	1.75	0.41	0.70	9.00	1.83	0.41	0.72
8.81	1.59	0.13	1.23	8.81	1.71	0.40	0.68	8.81	1.83	0.40	0.72
8.62	1.58	0.13	1.23	8.62	1.69	0.39	0.68	8.62	1.85	0.39	0.73
8.43	1.55	0.12	1.21	8.43	1.66	0.38	0.67	8.43	1.83	0.38	0.72
8.23	1.55	0.12	1.20	8.23	1.62	0.37	0.65	8.23	1.82	0.37	0.72
8.04	1.51	0.12	1.18	8.04	1.57	0.36	0.63	8.04	1.71	0.36	0.68
7.85	1.53	0.12	1.19	7.85	1.53	0.36	0.61	7.85	1.70	0.35	0.67
7.66	1.48	0.11	1.15	7.66	1.53	0.35	0.61	7.66	1.79	0.34	0.70
7.47	1.48	0.11	1.15	7.47	1.51	0.34	0.61	7.47	1.73	0.34	0.68
7.27	1.44	0.11	1.12	7.27	1.47	0.33	0.59	7.27	1.70	0.33	0.67
7.08	1.42	0.10	1.10	7.08	1.43	0.32	0.57	7.08	1.70	0.32	0.67
6.89	1.37	0.10	1.07	6.89	1.41	0.31	0.57	6.89	1.67	0.31	0.66
6.70	1.38	0.10	1.07	6.70	1.40	0.30	0.56	6.70	1.62	0.30	0.64
6.50	1.34	0.10	1.04	6.50	1.37	0.29	0.55	6.50	1.47	0.29	0.58
6.31	1.32	0.09	1.03	6.31	1.32	0.29	0.53	6.31	1.53	0.28	0.60
6.12	1.23	0.09	0.96	6.12	1.29	0.28	0.52	6.12	1.52	0.28	0.60
5.93	1.25	0.09	0.98	5.93	1.29	0.27	0.52	5.93	1.46	0.27	0.58
5.74	1.21	0.08	0.94	5.74	1.24	0.26	0.50	5.74	1.38	0.26	0.54
5.54	1.16	0.08	0.90	5.54	1.21	0.25	0.48	5.54	1.41	0.25	0.56
5.35	1.08	0.08	0.84	5.35	1.20	0.24	0.48	5.35	1.38	0.24	0.54
5.16	1.06	0.08	0.83	5.16	1.15	0.23	0.46	5.16	1.29	0.23	0.51
4.97	1.10	0.07	0.86	4.97	1.14	0.22	0.46	4.97	1.21	0.22	0.48
4.77	1.08	0.07	0.84	4.77	1.09	0.22	0.44	4.77	1.20	0.21	0.47
4.58	0.97	0.07	0.75	4.58	1.05	0.21	0.42	4.58	1.16	0.21	0.46
4.39	0.99	0.06	0.77	4.39	1.01	0.20	0.41	4.39	1.13	0.20	0.44
4.20	1.03	0.06	0.80	4.20	0.97	0.19	0.39	4.20	1.14	0.19	0.45
4.01	0.97	0.06	0.76	4.01	0.92	0.18	0.37	4.01	1.11	0.18	0.44
3.81	0.94	0.06	0.73	3.81	0.95	0.17	0.38	3.81	0.99	0.17	0.39

Cont. of Normal Reservoir Operation - Location C											
Run N4				Run N6				Run N7			
Measured		Normalized		Measured		Normalized		Measured		Normalized	
h (cm)	u (cm/s)	z/h	u/U	h (cm)	u (cm/s)	z/h	u/U	h (cm)	u (cm/s)	z/h	u/U
3.62	0.90	0.05	0.70	3.62	0.88	0.16	0.35	3.62	0.99	0.16	0.39
3.43	0.87	0.05	0.68	3.43	0.89	0.16	0.36	3.43	0.97	0.15	0.38
3.24	0.84	0.05	0.65	3.24	0.88	0.15	0.35	3.24	0.93	0.15	0.36
3.04	0.82	0.04	0.64	3.04	0.86	0.14	0.34	3.04	0.90	0.14	0.35
2.85	0.79	0.04	0.62	2.85	0.83	0.13	0.33	2.85	0.87	0.13	0.34
2.66	0.77	0.04	0.60	2.66	0.80	0.12	0.32	2.66	0.83	0.12	0.33
2.47	0.74	0.04	0.58	2.47	0.79	0.11	0.32	2.47	0.76	0.11	0.30
2.27	0.78	0.03	0.61	2.27	0.76	0.10	0.31	2.27	0.77	0.10	0.30
2.08	0.69	0.03	0.54	2.08	0.69	0.09	0.28	2.08	0.67	0.09	0.26
1.89	0.69	0.03	0.54	1.89	0.70	0.09	0.28	1.89	0.60	0.09	0.24
1.70	0.64	0.02	0.50	1.70	0.69	0.08	0.28	1.70	0.60	0.08	0.24
1.51	0.56	0.02	0.43	1.51	0.68	0.07	0.27	1.51	0.63	0.07	0.25
1.31	0.55	0.02	0.43	1.31	0.62	0.06	0.25	1.31	0.58	0.06	0.23
1.12	0.36	0.02	0.28	1.12	0.54	0.05	0.22	1.12	0.42	0.05	0.16
0.93	0.52	0.01	0.41	0.93	0.39	0.04	0.15	0.93	0.30	0.04	0.12
0.74	0.52	0.01	0.40	0.74	0.53	0.03	0.21	0.74	0.36	0.03	0.14
0.54	0.45	0.01	0.35	0.54	0.45	0.02	0.18	0.54	0.40	0.02	0.16
0.35	0.25	0.01	0.20	0.35	0.35	0.02	0.14	0.35	0.32	0.02	0.12
0.16	0.29	0.00	0.23	0.16	0.24	0.01	0.10	0.16	0.16	0.01	0.06

B4. Turbidity Current Venting - Location A

Turbidity Current Venting - Location A												
Run V4				Run V6				Run V7			
Measured		Normalized		Measured		Normalized		Measured		Normalized	
h (cm)	u (cm/s)	z/h	u/U	h (cm)	u (cm/s)	z/h	u/U	h (cm)	u (cm/s)	z/h	u/U
19.02	0.06	1.34	0.06	19.02	0.05	1.36	0.05	19.02	0.07	1.37	0.06
18.83	0.00	1.33	0.00	18.83	0.00	1.35	0.00	18.83	0.00	1.36	0.00
18.63	0.02	1.31	0.02	18.63	0.02	1.33	0.02	18.63	0.02	1.35	0.02
18.44	0.05	1.30	0.05	18.44	0.06	1.32	0.06	18.44	0.06	1.33	0.05
18.25	0.08	1.29	0.09	18.25	0.08	1.30	0.08	18.25	0.09	1.32	0.07
18.06	0.14	1.27	0.14	18.06	0.13	1.29	0.13	18.06	0.14	1.30	0.11
17.86	0.16	1.26	0.16	17.86	0.16	1.28	0.15	17.86	0.18	1.29	0.14
17.67	0.16	1.25	0.16	17.67	0.15	1.26	0.15	17.67	0.17	1.28	0.14
17.48	0.16	1.23	0.16	17.48	0.16	1.25	0.15	17.48	0.17	1.26	0.14
17.29	0.15	1.22	0.16	17.29	0.15	1.24	0.15	17.29	0.17	1.25	0.14
17.10	0.16	1.20	0.16	17.10	0.16	1.22	0.15	17.10	0.17	1.24	0.14
16.90	0.15	1.19	0.16	16.90	0.15	1.21	0.15	16.90	0.17	1.22	0.14
16.71	0.15	1.18	0.16	16.71	0.15	1.19	0.15	16.71	0.17	1.21	0.14
16.52	0.18	1.16	0.19	16.52	0.18	1.18	0.17	16.52	0.18	1.19	0.15
16.33	0.21	1.15	0.21	16.33	0.20	1.17	0.20	16.33	0.22	1.18	0.18
16.13	0.21	1.14	0.22	16.13	0.20	1.15	0.19	16.13	0.22	1.17	0.18
15.94	0.20	1.12	0.21	15.94	0.19	1.14	0.19	15.94	0.23	1.15	0.19
15.75	0.21	1.11	0.22	15.75	0.21	1.13	0.20	15.75	0.23	1.14	0.19
15.56	0.20	1.10	0.21	15.56	0.20	1.11	0.19	15.56	0.23	1.12	0.19
15.37	0.21	1.08	0.21	15.37	0.20	1.10	0.19	15.37	0.24	1.11	0.20
15.17	0.20	1.07	0.21	15.17	0.20	1.08	0.20	15.17	0.23	1.10	0.19
14.98	0.25	1.06	0.25	14.98	0.26	1.07	0.25	14.98	0.28	1.08	0.23
14.79	0.29	1.04	0.30	14.79	0.28	1.06	0.28	14.79	0.34	1.07	0.27
14.60	0.31	1.03	0.32	14.60	0.29	1.04	0.29	14.60	0.35	1.05	0.29
14.40	0.30	1.02	0.31	14.40	0.32	1.03	0.31	14.40	0.37	1.04	0.30
14.21	0.30	1.00	0.31	14.21	0.31	1.02	0.31	14.21	0.36	1.03	0.29
14.02	0.31	0.99	0.32	14.02	0.31	1.00	0.31	14.02	0.36	1.01	0.30
13.83	0.30	0.97	0.31	13.83	0.31	0.99	0.31	13.83	0.37	1.00	0.31
13.64	0.32	0.96	0.33	13.64	0.32	0.97	0.32	13.64	0.37	0.99	0.30
13.44	0.39	0.95	0.40	13.44	0.42	0.96	0.41	13.44	0.46	0.97	0.37
13.25	0.49	0.93	0.51	13.25	0.50	0.95	0.49	13.25	0.56	0.96	0.46
13.06	0.50	0.92	0.52	13.06	0.52	0.93	0.51	13.06	0.57	0.94	0.46
12.87	0.50	0.91	0.52	12.87	0.50	0.92	0.49	12.87	0.56	0.93	0.45
12.67	0.52	0.89	0.54	12.67	0.48	0.91	0.47	12.67	0.54	0.92	0.44
12.48	0.49	0.88	0.51	12.48	0.46	0.89	0.45	12.48	0.56	0.90	0.46
12.29	0.49	0.87	0.51	12.29	0.46	0.88	0.45	12.29	0.54	0.89	0.44
12.10	0.47	0.85	0.49	12.10	0.46	0.86	0.45	12.10	0.55	0.87	0.45
11.90	0.58	0.84	0.60	11.90	0.57	0.85	0.56	11.90	0.69	0.86	0.56
11.71	0.70	0.83	0.72	11.71	0.70	0.84	0.69	11.71	0.89	0.85	0.72
11.52	0.68	0.81	0.70	11.52	0.76	0.82	0.75	11.52	0.97	0.83	0.79
11.33	0.70	0.80	0.73	11.33	0.75	0.81	0.73	11.33	1.01	0.82	0.82
11.14	0.72	0.78	0.75	11.14	0.80	0.80	0.78	11.14	1.03	0.80	0.84

Cont. of Turbidity Current Venting - Location A											
Run V4				Run V6				Run V7			
Measured		Normalized		Measured		Normalized		Measured		Normalized	
h (cm)	u (cm/s)	z/h	u/U	h (cm)	u (cm/s)	z/h	u/U	h (cm)	u (cm/s)	z/h	u/U
10.94	0.71	0.77	0.74	10.94	0.82	0.78	0.80	10.94	1.02	0.79	0.83
10.75	0.74	0.76	0.76	10.75	0.84	0.77	0.82	10.75	0.95	0.78	0.77
10.56	0.75	0.74	0.78	10.56	0.86	0.75	0.85	10.56	0.96	0.76	0.78
10.37	0.99	0.73	1.03	10.37	1.07	0.74	1.05	10.37	1.15	0.75	0.94
10.17	1.11	0.72	1.15	10.17	1.18	0.73	1.15	10.17	1.27	0.74	1.04
9.98	1.21	0.70	1.25	9.98	1.20	0.71	1.17	9.98	1.26	0.72	1.03
9.79	1.21	0.69	1.25	9.79	1.11	0.70	1.09	9.79	1.23	0.71	1.00
9.60	1.20	0.68	1.24	9.60	1.08	0.69	1.06	9.60	1.25	0.69	1.02
9.41	1.13	0.66	1.17	9.41	1.02	0.67	1.00	9.41	1.26	0.68	1.03
9.21	1.10	0.65	1.14	9.21	1.07	0.66	1.05	9.21	1.25	0.67	1.02
9.02	1.15	0.64	1.19	9.02	1.09	0.64	1.07	9.02	1.34	0.65	1.09
8.83	1.38	0.62	1.43	8.83	1.37	0.63	1.34	8.83	1.76	0.64	1.44
8.64	1.27	0.61	1.31	8.64	1.32	0.62	1.29	8.64	1.67	0.62	1.36
8.44	1.31	0.60	1.35	8.44	1.41	0.60	1.38	8.44	1.76	0.61	1.43
8.25	1.32	0.58	1.37	8.25	1.47	0.59	1.44	8.25	1.82	0.60	1.48
8.06	1.27	0.57	1.31	8.06	1.43	0.58	1.40	8.06	1.84	0.58	1.50
7.87	1.35	0.55	1.40	7.87	1.37	0.56	1.34	7.87	1.87	0.57	1.52
7.68	1.24	0.54	1.28	7.68	1.37	0.55	1.35	7.68	1.79	0.55	1.46
7.48	1.26	0.53	1.30	7.48	1.43	0.53	1.40	7.48	1.85	0.54	1.51
7.29	1.30	0.51	1.35	7.29	1.42	0.52	1.39	7.29	1.71	0.53	1.39
7.10	1.24	0.50	1.29	7.10	1.52	0.51	1.49	7.10	1.82	0.51	1.48
6.91	1.25	0.49	1.30	6.91	1.53	0.49	1.50	6.91	1.76	0.50	1.44
6.71	1.25	0.47	1.30	6.71	1.46	0.48	1.43	6.71	1.65	0.48	1.35
6.52	1.24	0.46	1.28	6.52	1.46	0.47	1.43	6.52	1.64	0.47	1.34
6.33	1.37	0.45	1.42	6.33	1.55	0.45	1.52	6.33	1.67	0.46	1.36
6.14	1.40	0.43	1.45	6.14	1.47	0.44	1.44	6.14	1.58	0.44	1.29
5.94	1.40	0.42	1.45	5.94	1.42	0.42	1.40	5.94	1.62	0.43	1.32
5.75	1.35	0.41	1.40	5.75	1.30	0.41	1.28	5.75	1.47	0.42	1.20
5.56	1.24	0.39	1.29	5.56	1.08	0.40	1.06	5.56	1.33	0.40	1.08
5.37	1.17	0.38	1.21	5.37	1.13	0.38	1.11	5.37	1.30	0.39	1.06
5.18	1.13	0.36	1.17	5.18	1.17	0.37	1.15	5.18	1.38	0.37	1.13
4.98	1.13	0.35	1.17	4.98	1.09	0.36	1.07	4.98	1.43	0.36	1.16
4.79	1.09	0.34	1.13	4.79	1.13	0.34	1.11	4.79	1.44	0.35	1.18
4.60	1.03	0.32	1.07	4.60	1.09	0.33	1.07	4.60	1.39	0.33	1.13
4.41	1.11	0.31	1.15	4.41	1.07	0.31	1.05	4.41	1.45	0.32	1.18
4.21	0.98	0.30	1.01	4.21	1.03	0.30	1.01	4.21	1.23	0.30	1.00
4.02	0.91	0.28	0.94	4.02	0.99	0.29	0.97	4.02	1.17	0.29	0.95
3.83	0.90	0.27	0.93	3.83	0.93	0.27	0.91	3.83	1.12	0.28	0.91
3.64	0.91	0.26	0.94	3.64	0.92	0.26	0.90	3.64	1.11	0.26	0.91
3.45	0.89	0.24	0.92	3.45	0.98	0.25	0.96	3.45	1.10	0.25	0.90
3.25	0.85	0.23	0.88	3.25	0.92	0.23	0.90	3.25	1.10	0.24	0.90
3.06	0.87	0.22	0.90	3.06	0.91	0.22	0.89	3.06	1.07	0.22	0.87
2.87	0.91	0.20	0.95	2.87	0.92	0.20	0.90	2.87	1.08	0.21	0.88
2.68	0.81	0.19	0.84	2.68	0.84	0.19	0.82	2.68	0.97	0.19	0.79

Cont. of Turbidity Current Venting - Location A											
Run V4				Run V6				Run V7			
Measured		Normalized		Measured		Normalized		Measured		Normalized	
h (cm)	u (cm/s)	z/h	u/U	h (cm)	u (cm/s)	z/h	u/U	h (cm)	u (cm/s)	z/h	u/U
2.48	0.76	0.18	0.78	2.48	0.78	0.18	0.76	2.48	0.88	0.18	0.72
2.29	0.73	0.16	0.76	2.29	0.78	0.16	0.77	2.29	0.89	0.17	0.73
2.10	0.76	0.15	0.78	2.10	0.75	0.15	0.73	2.10	0.89	0.15	0.72
1.91	0.74	0.13	0.76	1.91	0.80	0.14	0.78	1.91	0.93	0.14	0.76
1.72	0.73	0.12	0.75	1.72	0.78	0.12	0.76	1.72	0.91	0.12	0.74
1.52	0.75	0.11	0.78	1.52	0.74	0.11	0.73	1.52	0.90	0.11	0.73
1.33	0.71	0.09	0.73	1.33	0.80	0.10	0.78	1.33	0.89	0.10	0.73
1.14	0.76	0.08	0.78	1.14	0.74	0.08	0.72	1.14	0.81	0.08	0.66
0.95	0.58	0.07	0.60	0.95	0.60	0.07	0.58	0.95	0.79	0.07	0.64
0.75	0.57	0.05	0.60	0.75	0.61	0.05	0.60	0.75	0.77	0.05	0.63
0.56	0.65	0.04	0.67	0.56	0.67	0.04	0.66	0.56	0.77	0.04	0.63
0.37	0.59	0.03	0.61	0.37	0.63	0.03	0.62	0.37	0.78	0.03	0.63
0.18	0.58	0.01	0.60	0.18	0.62	0.01	0.61	0.18	0.76	0.01	0.62
-0.02	0.57	0.00	0.60	-0.02	0.65	0.00	0.63	-0.02	0.75	0.00	0.61

B5. Turbidity Current Venting - Location B

Turbidity Current Venting - Location B											
Run V4				Run V6				Run V7			
Measured		Normalized		Measured		Normalized		Measured		Normalized	
h (cm)	u (cm/s)	z/h	u/U	h (cm)	u (cm/s)	z/h	u/U	h (cm)	u (cm/s)	z/h	u/U
22.88	0.05	1.26	0.03	22.49	0.06	1.24	0.03	21.53	0.06	1.24	0.03
22.69	0.00	1.25	0.00	22.30	0.00	1.23	0.00	21.34	0.00	1.23	0.00
22.49	0.03	1.24	0.02	22.11	0.02	1.22	0.01	21.15	0.03	1.22	0.02
22.30	0.42	1.23	0.23	21.92	0.32	1.21	0.18	20.96	0.33	1.21	0.17
22.11	0.46	1.22	0.25	21.73	0.62	1.20	0.35	20.76	0.72	1.20	0.37
21.92	0.70	1.21	0.38	21.53	0.66	1.19	0.37	20.57	0.84	1.19	0.44
21.73	0.73	1.20	0.40	21.34	0.64	1.18	0.36	20.38	0.82	1.18	0.43
21.53	0.78	1.19	0.43	21.15	0.63	1.16	0.36	20.19	0.80	1.17	0.42
21.34	0.88	1.18	0.49	20.96	0.60	1.15	0.34	20.00	0.78	1.16	0.41
21.15	0.77	1.17	0.43	20.76	0.60	1.14	0.34	19.80	0.78	1.14	0.41
20.96	0.77	1.15	0.42	20.57	0.63	1.13	0.35	19.61	0.73	1.13	0.38
20.76	0.79	1.14	0.44	20.38	0.59	1.12	0.33	19.42	0.74	1.12	0.39
20.57	0.81	1.13	0.45	20.19	0.62	1.11	0.35	19.23	0.69	1.11	0.36
20.38	0.79	1.12	0.44	20.00	0.63	1.10	0.35	19.03	0.73	1.10	0.38
20.19	0.82	1.11	0.45	19.80	0.61	1.09	0.34	18.84	0.68	1.09	0.36
20.00	0.84	1.10	0.46	19.61	0.63	1.08	0.35	18.65	0.68	1.08	0.35

Cont. of Turbidity Current Venting - Location B												
Run V4				Run V6				Run V7				
Measured		Normalized		Measured		Normalized		Measured		Normalized		
h (cm)	u (cm/s)	z/h	u/U	h (cm)	u (cm/s)	z/h	u/U	h (cm)	u (cm/s)	z/h	u/U	
19.80	0.85	1.09	0.47	19.42	0.64	1.07	0.36	18.46	0.64	1.07	0.33	
19.61	0.86	1.08	0.47	19.23	0.57	1.06	0.32	18.26	0.64	1.06	0.33	
19.42	0.80	1.07	0.44	19.03	0.56	1.05	0.31	18.07	0.63	1.04	0.33	
19.23	0.76	1.06	0.42	18.84	0.53	1.04	0.30	17.88	0.59	1.03	0.31	
19.03	0.75	1.05	0.41	18.65	0.57	1.03	0.32	17.69	0.62	1.02	0.32	
18.84	0.77	1.04	0.43	18.46	0.56	1.02	0.32	17.50	0.64	1.01	0.33	
18.65	0.78	1.03	0.43	18.26	0.63	1.01	0.36	17.30	0.74	1.00	0.38	
18.46	0.75	1.02	0.41	18.07	0.63	1.00	0.35	17.11	0.76	0.99	0.40	
18.26	0.76	1.01	0.42	17.88	0.71	0.98	0.40	16.92	0.75	0.98	0.39	
18.07	0.73	1.00	0.40	17.69	0.74	0.97	0.42	16.73	0.78	0.97	0.41	
17.88	0.68	0.99	0.37	17.50	0.72	0.96	0.41	16.53	0.81	0.96	0.42	
17.69	0.67	0.97	0.37	17.30	0.75	0.95	0.42	16.34	0.84	0.94	0.44	
17.50	0.68	0.96	0.38	17.11	0.74	0.94	0.42	16.15	0.81	0.93	0.42	
17.30	0.65	0.95	0.36	16.92	0.76	0.93	0.43	15.96	0.79	0.92	0.41	
17.11	0.67	0.94	0.37	16.73	0.78	0.92	0.44	15.77	0.79	0.91	0.41	
16.92	0.65	0.93	0.36	16.53	0.78	0.91	0.44	15.57	0.82	0.90	0.43	
16.73	0.66	0.92	0.36	16.34	0.82	0.90	0.46	15.38	0.83	0.89	0.43	
16.53	0.65	0.91	0.36	16.15	0.81	0.89	0.45	15.19	0.83	0.88	0.43	
16.34	0.67	0.90	0.37	15.96	0.82	0.88	0.46	15.00	0.87	0.87	0.46	
16.15	0.71	0.89	0.39	15.77	0.83	0.87	0.46	14.80	0.87	0.86	0.46	
15.96	0.76	0.88	0.42	15.57	0.88	0.86	0.49	14.61	0.92	0.84	0.48	
15.77	0.74	0.87	0.41	15.38	0.94	0.85	0.53	14.42	0.95	0.83	0.50	
15.57	0.77	0.86	0.42	15.19	0.94	0.84	0.53	14.23	0.96	0.82	0.50	
15.38	0.78	0.85	0.43	15.00	0.99	0.83	0.56	14.04	0.98	0.81	0.51	
15.19	0.83	0.84	0.46	14.80	1.03	0.82	0.58	13.84	0.99	0.80	0.52	
15.00	0.83	0.83	0.46	14.61	1.07	0.80	0.60	13.65	1.04	0.79	0.54	
14.80	0.86	0.82	0.47	14.42	1.07	0.79	0.60	13.46	1.04	0.78	0.54	
14.61	0.87	0.80	0.48	14.23	1.13	0.78	0.64	13.27	1.06	0.77	0.56	
14.42	0.95	0.79	0.52	14.04	1.16	0.77	0.65	13.07	1.09	0.76	0.57	
14.23	0.92	0.78	0.51	13.84	1.19	0.76	0.67	12.88	1.15	0.74	0.60	
14.04	0.97	0.77	0.54	13.65	1.21	0.75	0.68	12.69	1.21	0.73	0.63	
13.84	0.99	0.76	0.54	13.46	1.23	0.74	0.69	12.50	1.23	0.72	0.64	
13.65	1.03	0.75	0.57	13.27	1.21	0.73	0.68	12.30	1.25	0.71	0.65	
13.46	1.02	0.74	0.56	13.07	1.24	0.72	0.70	12.11	1.29	0.70	0.68	
13.27	1.04	0.73	0.58	12.88	1.27	0.71	0.72	11.92	1.35	0.69	0.71	
13.07	1.08	0.72	0.60	12.69	1.29	0.70	0.73	11.73	1.38	0.68	0.72	
12.88	1.10	0.71	0.61	12.50	1.27	0.69	0.72	11.54	1.42	0.67	0.74	
12.69	1.16	0.70	0.64	12.30	1.36	0.68	0.77	11.34	1.46	0.66	0.76	
12.50	1.21	0.69	0.67	12.11	1.35	0.67	0.76	11.15	1.50	0.64	0.78	
12.30	1.20	0.68	0.66	11.92	1.40	0.66	0.79	10.96	1.54	0.63	0.80	
12.11	1.28	0.67	0.70	11.73	1.40	0.65	0.79	10.77	1.58	0.62	0.82	

Cont. of Turbidity Current Venting - Location B												
Run V4				Run V6				Run V7				
Measured		Normalized		Measured		Normalized		Measured		Normalized		
h (cm)	u (cm/s)	z/h	u/U	h (cm)	u (cm/s)	z/h	u/U	h (cm)	u (cm/s)	z/h	u/U	
11.92	1.29	0.66	0.71	11.54	1.40	0.64	0.79	10.57	1.63	0.61	0.85	
11.73	1.33	0.65	0.73	11.34	1.45	0.62	0.81	10.38	1.64	0.60	0.86	
11.54	1.35	0.64	0.75	11.15	1.46	0.61	0.82	10.19	1.68	0.59	0.88	
11.34	1.39	0.62	0.77	10.96	1.50	0.60	0.84	10.00	1.73	0.58	0.90	
11.15	1.42	0.61	0.79	10.77	1.53	0.59	0.86	9.81	1.76	0.57	0.92	
10.96	1.44	0.60	0.79	10.57	1.57	0.58	0.88	9.61	1.80	0.56	0.94	
10.77	1.46	0.59	0.80	10.38	1.59	0.57	0.90	9.42	1.87	0.54	0.98	
10.57	1.48	0.58	0.82	10.19	1.62	0.56	0.91	9.23	1.90	0.53	0.99	
10.38	1.52	0.57	0.84	10.00	1.68	0.55	0.95	9.04	1.96	0.52	1.02	
10.19	1.56	0.56	0.86	9.81	1.71	0.54	0.96	8.84	2.01	0.51	1.05	
10.00	1.58	0.55	0.87	9.61	1.75	0.53	0.98	8.65	2.05	0.50	1.07	
9.81	1.62	0.54	0.89	9.42	1.79	0.52	1.01	8.46	2.10	0.49	1.10	
9.61	1.65	0.53	0.91	9.23	1.78	0.51	1.00	8.27	2.13	0.48	1.11	
9.42	1.71	0.52	0.94	9.04	1.81	0.50	1.02	8.08	2.16	0.47	1.13	
9.23	1.76	0.51	0.97	8.84	1.86	0.49	1.05	7.88	2.18	0.46	1.14	
9.04	1.81	0.50	1.00	8.65	1.87	0.48	1.05	7.69	2.24	0.44	1.17	
8.84	1.88	0.49	1.03	8.46	1.93	0.47	1.09	7.50	2.27	0.43	1.19	
8.65	1.92	0.48	1.06	8.27	1.99	0.46	1.12	7.31	2.30	0.42	1.20	
8.46	1.92	0.47	1.06	8.08	2.01	0.44	1.13	7.11	2.33	0.41	1.22	
8.27	1.96	0.46	1.08	7.88	2.03	0.43	1.14	6.92	2.37	0.40	1.24	
8.08	2.01	0.44	1.11	7.69	2.05	0.42	1.15	6.73	2.40	0.39	1.25	
7.88	2.04	0.43	1.13	7.50	2.09	0.41	1.17	6.54	2.42	0.38	1.26	
7.69	2.06	0.42	1.14	7.31	2.10	0.40	1.18	6.34	2.43	0.37	1.27	
7.50	2.14	0.41	1.18	7.11	2.12	0.39	1.19	6.15	2.45	0.36	1.28	
7.31	2.15	0.40	1.19	6.92	2.15	0.38	1.21	5.96	2.48	0.34	1.30	
7.11	2.19	0.39	1.21	6.73	2.20	0.37	1.24	5.77	2.51	0.33	1.31	
6.92	2.22	0.38	1.23	6.54	2.20	0.36	1.24	5.58	2.53	0.32	1.32	
6.73	2.26	0.37	1.24	6.34	2.21	0.35	1.25	5.38	2.54	0.31	1.33	
6.54	2.26	0.36	1.25	6.15	2.24	0.34	1.26	5.19	2.57	0.30	1.34	
6.34	2.32	0.35	1.28	5.96	2.26	0.33	1.27	5.00	2.56	0.29	1.34	
6.15	2.34	0.34	1.29	5.77	2.28	0.32	1.28	4.81	2.58	0.28	1.35	
5.96	2.39	0.33	1.32	5.58	2.30	0.31	1.29	4.61	2.61	0.27	1.36	
5.77	2.42	0.32	1.34	5.38	2.30	0.30	1.29	4.42	2.60	0.26	1.36	
5.58	2.44	0.31	1.34	5.19	2.32	0.29	1.30	4.23	2.60	0.24	1.36	
5.38	2.46	0.30	1.36	5.00	2.34	0.28	1.31	4.04	2.60	0.23	1.35	
5.19	2.49	0.29	1.37	4.81	2.35	0.26	1.32	3.85	2.62	0.22	1.37	
5.00	2.52	0.28	1.39	4.61	2.36	0.25	1.33	3.65	2.60	0.21	1.36	
4.81	2.50	0.26	1.38	4.42	2.39	0.24	1.34	3.46	2.59	0.20	1.35	
4.61	2.56	0.25	1.41	4.23	2.42	0.23	1.36	3.27	2.57	0.19	1.34	
4.42	2.55	0.24	1.41	4.04	2.41	0.22	1.36	3.08	2.56	0.18	1.34	
4.23	2.57	0.23	1.42	3.85	2.43	0.21	1.37	2.88	2.55	0.17	1.33	

Cont. of Turbidity Current Venting - Location B												
Run V4				Run V6				Run V7			
Measured		Normalized		Measured		Normalized		Measured		Normalized	
h (cm)	u (cm/s)	z/h	u/U	h (cm)	u (cm/s)	z/h	u/U	h (cm)	u (cm/s)	z/h	u/U
4.04	2.57	0.22	1.42	3.65	2.44	0.20	1.37	2.69	2.52	0.16	1.32
3.85	2.58	0.21	1.42	3.46	2.45	0.19	1.38	2.50	2.51	0.14	1.31
3.65	2.59	0.20	1.43	3.27	2.46	0.18	1.38	2.31	2.47	0.13	1.29
3.46	2.59	0.19	1.43	3.08	2.45	0.17	1.38	2.12	2.43	0.12	1.27
3.27	2.58	0.18	1.42	2.88	2.46	0.16	1.39	1.92	2.38	0.11	1.24
3.08	2.57	0.17	1.42	2.69	2.45	0.15	1.38	1.73	2.32	0.10	1.21
2.88	2.58	0.16	1.42	2.50	2.44	0.14	1.37	1.54	2.27	0.09	1.19
2.69	2.52	0.15	1.39	2.31	2.36	0.13	1.33	1.35	2.24	0.08	1.17
2.50	2.47	0.14	1.36	2.12	2.30	0.12	1.29	1.15	2.16	0.07	1.13
2.31	2.42	0.13	1.33	1.92	2.29	0.11	1.29	0.96	2.03	0.06	1.06
2.12	2.39	0.12	1.32	1.73	2.25	0.10	1.26	0.77	1.83	0.04	0.96
1.92	2.36	0.11	1.30	1.54	2.16	0.08	1.22	0.58	1.69	0.03	0.88
1.73	2.28	0.10	1.26	1.35	2.11	0.07	1.18	0.38	1.32	0.02	0.69
1.54	2.23	0.08	1.23	1.15	2.02	0.06	1.13	0.19	0.79	0.01	0.41
1.35	2.12	0.07	1.17	0.96	1.84	0.05	1.04	0.00	0.17	0.00	0.09
1.15	2.05	0.06	1.13	0.77	1.69	0.04	0.95				
0.96	2.00	0.05	1.10	0.58	1.62	0.03	0.91				
0.77	1.84	0.04	1.01	0.38	1.30	0.02	0.73				
0.58	1.53	0.03	0.84	0.19	0.46	0.01	0.26				
0.38	0.83	0.02	0.46	0.00	0.16	0.00	0.09				
0.19	0.53	0.01	0.29								
0.00	0.24	0.00	0.14								

B6. Turbidity Current Venting - Location C

Turbidity Current Venting - Location C												
Run V4				Run V6				Run V7				
Measured		Normalized		Measured		Normalized		Measured		Normalized		
h (cm)	u (cm/s)	z/h	u/U	h (cm)	u (cm/s)	z/h	u/U	h (cm)	u (cm/s)	z/h	u/U	
26.31	0.10	1.23	0.07	26.31	0.00	1.22	0.00	26.31	0.06	1.25	0.05	
26.11	0.00	1.22	0.00	26.11	0.01	1.21	0.01	26.11	0.00	1.24	0.00	
25.92	0.03	1.21	0.02	25.92	0.04	1.20	0.03	25.92	0.03	1.23	0.02	
25.73	0.05	1.20	0.04	25.73	0.14	1.19	0.10	25.73	0.05	1.23	0.03	
25.54	0.23	1.19	0.15	25.54	0.38	1.18	0.28	25.54	0.12	1.22	0.09	
25.35	0.53	1.18	0.36	25.35	0.55	1.17	0.41	25.35	0.38	1.21	0.29	
25.15	0.52	1.17	0.35	25.15	0.51	1.16	0.38	25.15	0.47	1.20	0.36	
24.96	0.54	1.16	0.37	24.96	0.49	1.16	0.37	24.96	0.48	1.19	0.37	
24.77	0.55	1.15	0.37	24.77	0.49	1.15	0.36	24.77	0.49	1.18	0.37	
24.58	0.55	1.14	0.38	24.58	0.51	1.14	0.38	24.58	0.51	1.17	0.39	
24.38	0.48	1.14	0.33	24.38	0.46	1.13	0.34	24.38	0.49	1.16	0.38	
24.19	0.53	1.13	0.36	24.19	0.51	1.12	0.38	24.19	0.47	1.15	0.36	
24.00	0.53	1.12	0.36	24.00	0.50	1.11	0.37	24.00	0.51	1.14	0.39	
23.81	0.54	1.11	0.37	23.81	0.53	1.10	0.39	23.81	0.51	1.13	0.39	
23.62	0.54	1.10	0.37	23.62	0.55	1.09	0.41	23.62	0.51	1.12	0.39	
23.42	0.58	1.09	0.39	23.42	0.55	1.08	0.41	23.42	0.56	1.12	0.43	
23.23	0.56	1.08	0.38	23.23	0.54	1.08	0.41	23.23	0.51	1.11	0.39	
23.04	0.58	1.07	0.39	23.04	0.55	1.07	0.41	23.04	0.54	1.10	0.41	
22.85	0.58	1.06	0.39	22.85	0.54	1.06	0.41	22.85	0.56	1.09	0.43	
22.65	0.61	1.05	0.41	22.65	0.57	1.05	0.43	22.65	0.58	1.08	0.44	
22.46	0.64	1.05	0.44	22.46	0.58	1.04	0.43	22.46	0.54	1.07	0.41	
22.27	0.62	1.04	0.43	22.27	0.57	1.03	0.42	22.27	0.54	1.06	0.41	
22.08	0.69	1.03	0.47	22.08	0.60	1.02	0.45	22.08	0.62	1.05	0.47	
21.89	0.66	1.02	0.45	21.89	0.62	1.01	0.46	21.89	0.54	1.04	0.41	
21.69	0.71	1.01	0.48	21.69	0.59	1.00	0.44	21.69	0.59	1.03	0.45	
21.50	0.66	1.00	0.45	21.50	0.55	1.00	0.41	21.50	0.61	1.02	0.46	
21.31	0.70	0.99	0.48	21.31	0.60	0.99	0.45	21.31	0.56	1.01	0.42	
21.12	0.70	0.98	0.47	21.12	0.59	0.98	0.44	21.12	0.59	1.01	0.45	
20.92	0.66	0.97	0.45	20.92	0.63	0.97	0.48	20.92	0.54	1.00	0.41	
20.73	0.67	0.97	0.46	20.73	0.64	0.96	0.48	20.73	0.60	0.99	0.46	
20.54	0.73	0.96	0.49	20.54	0.56	0.95	0.42	20.54	0.64	0.98	0.48	
20.35	0.71	0.95	0.48	20.35	0.64	0.94	0.48	20.35	0.65	0.97	0.49	
20.15	0.71	0.94	0.48	20.15	0.52	0.93	0.39	20.15	0.65	0.96	0.49	
19.96	0.70	0.93	0.48	19.96	0.68	0.92	0.51	19.96	0.63	0.95	0.48	
19.77	0.69	0.92	0.47	19.77	0.61	0.92	0.46	19.77	0.64	0.94	0.49	
19.58	0.69	0.91	0.47	19.58	0.68	0.91	0.51	19.58	0.53	0.93	0.41	
19.39	0.70	0.90	0.48	19.39	0.66	0.90	0.49	19.39	0.68	0.92	0.52	
19.19	0.75	0.89	0.51	19.19	0.68	0.89	0.51	19.19	0.72	0.91	0.55	
19.00	0.76	0.88	0.51	19.00	0.73	0.88	0.55	19.00	0.63	0.90	0.48	
18.81	0.79	0.88	0.54	18.81	0.70	0.87	0.53	18.81	0.71	0.90	0.55	
18.62	0.74	0.87	0.50	18.62	0.69	0.86	0.52	18.62	0.69	0.89	0.52	
18.42	0.76	0.86	0.52	18.42	0.70	0.85	0.52	18.42	0.71	0.88	0.54	

Cont. of Turbidity Current Venting - Location C												
Run V4				Run V6				Run V7			
Measured		Normalized		Measured		Normalized		Measured		Normalized	
h (cm)	u (cm/s)	z/h	u/U	h (cm)	u (cm/s)	z/h	u/U	h (cm)	u (cm/s)	z/h	u/U
18.23	0.77	0.85	0.53	18.23	0.69	0.84	0.52	18.23	0.72	0.87	0.55
18.04	0.75	0.84	0.51	18.04	0.72	0.84	0.54	18.04	0.67	0.86	0.51
17.85	0.76	0.83	0.52	17.85	0.73	0.83	0.55	17.85	0.66	0.85	0.51
17.66	0.77	0.82	0.52	17.66	0.72	0.82	0.54	17.66	0.63	0.84	0.48
17.46	0.77	0.81	0.52	17.46	0.80	0.81	0.60	17.46	0.70	0.83	0.53
17.27	0.81	0.80	0.55	17.27	0.79	0.80	0.59	17.27	0.74	0.82	0.56
17.08	0.80	0.80	0.55	17.08	0.72	0.79	0.54	17.08	0.73	0.81	0.55
16.89	0.76	0.79	0.52	16.89	0.74	0.78	0.55	16.89	0.70	0.80	0.53
16.69	0.76	0.78	0.52	16.69	0.84	0.77	0.63	16.69	0.73	0.79	0.55
16.50	0.82	0.77	0.56	16.50	0.86	0.76	0.65	16.50	0.77	0.79	0.58
16.31	0.81	0.76	0.55	16.31	0.86	0.75	0.65	16.31	0.75	0.78	0.57
16.12	0.83	0.75	0.57	16.12	0.95	0.75	0.71	16.12	0.79	0.77	0.60
15.93	0.92	0.74	0.63	15.93	0.95	0.74	0.71	15.93	0.85	0.76	0.65
15.73	0.93	0.73	0.63	15.73	0.94	0.73	0.71	15.73	0.81	0.75	0.62
15.54	0.91	0.72	0.62	15.54	0.93	0.72	0.69	15.54	0.86	0.74	0.65
15.35	0.89	0.71	0.60	15.35	0.94	0.71	0.70	15.35	0.83	0.73	0.63
15.16	0.89	0.71	0.61	15.16	0.92	0.70	0.69	15.16	0.83	0.72	0.63
14.96	0.91	0.70	0.62	14.96	0.95	0.69	0.71	14.96	0.76	0.71	0.58
14.77	0.93	0.69	0.63	14.77	1.01	0.68	0.76	14.77	0.84	0.70	0.64
14.58	1.01	0.68	0.69	14.58	1.09	0.67	0.82	14.58	0.87	0.69	0.67
14.39	1.06	0.67	0.72	14.39	1.10	0.67	0.83	14.39	0.96	0.69	0.73
14.19	1.08	0.66	0.73	14.19	1.08	0.66	0.81	14.19	0.94	0.68	0.71
14.00	1.10	0.65	0.75	14.00	1.10	0.65	0.83	14.00	0.92	0.67	0.71
13.81	1.09	0.64	0.74	13.81	1.06	0.64	0.79	13.81	0.93	0.66	0.71
13.62	1.11	0.63	0.76	13.62	1.06	0.63	0.79	13.62	0.94	0.65	0.72
13.43	1.13	0.63	0.77	13.43	1.07	0.62	0.80	13.43	0.91	0.64	0.69
13.23	1.07	0.62	0.73	13.23	1.19	0.61	0.90	13.23	0.89	0.63	0.68
13.04	1.26	0.61	0.86	13.04	1.12	0.60	0.84	13.04	1.04	0.62	0.79
12.85	1.22	0.60	0.83	12.85	1.19	0.59	0.89	12.85	1.03	0.61	0.78
12.66	1.26	0.59	0.86	12.66	1.12	0.59	0.84	12.66	1.05	0.60	0.80
12.46	1.25	0.58	0.85	12.46	1.19	0.58	0.89	12.46	1.06	0.59	0.81
12.27	1.26	0.57	0.86	12.27	1.12	0.57	0.84	12.27	1.06	0.58	0.81
12.08	1.25	0.56	0.85	12.08	1.20	0.56	0.90	12.08	1.02	0.58	0.78
11.89	1.30	0.55	0.89	11.89	1.21	0.55	0.91	11.89	1.07	0.57	0.82
11.70	1.33	0.54	0.91	11.70	1.28	0.54	0.96	11.70	1.09	0.56	0.83
11.50	1.35	0.54	0.92	11.50	1.28	0.53	0.96	11.50	1.13	0.55	0.86
11.31	1.38	0.53	0.94	11.31	1.26	0.52	0.94	11.31	1.17	0.54	0.90
11.12	1.38	0.52	0.94	11.12	1.23	0.51	0.92	11.12	1.13	0.53	0.86
10.93	1.33	0.51	0.90	10.93	1.26	0.51	0.95	10.93	1.09	0.52	0.83
10.73	1.41	0.50	0.96	10.73	1.24	0.50	0.93	10.73	1.15	0.51	0.88
10.54	1.38	0.49	0.94	10.54	1.20	0.49	0.90	10.54	1.17	0.50	0.89
10.35	1.34	0.48	0.92	10.35	1.23	0.48	0.92	10.35	1.13	0.49	0.86
10.16	1.40	0.47	0.95	10.16	1.23	0.47	0.93	10.16	1.17	0.48	0.89
9.97	1.37	0.46	0.93	9.97	1.23	0.46	0.92	9.97	1.14	0.47	0.87

Cont. of Turbidity Current Venting - Location C												
Run V4				Run V6				Run V7			
Measured		Normalized		Measured		Normalized		Measured		Normalized	
h (cm)	u (cm/s)	z/h	u/U	h (cm)	u (cm/s)	z/h	u/U	h (cm)	u (cm/s)	z/h	u/U
9.77	1.37	0.46	0.93	9.77	1.27	0.45	0.95	9.77	1.11	0.47	0.85
9.58	1.42	0.45	0.97	9.58	1.26	0.44	0.95	9.58	1.18	0.46	0.90
9.39	1.46	0.44	1.00	9.39	1.25	0.43	0.94	9.39	1.22	0.45	0.93
9.20	1.45	0.43	0.99	9.20	1.28	0.43	0.96	9.20	1.25	0.44	0.95
9.00	1.47	0.42	1.00	9.00	1.35	0.42	1.01	9.00	1.26	0.43	0.96
8.81	1.60	0.41	1.09	8.81	1.36	0.41	1.02	8.81	1.36	0.42	1.04
8.62	1.57	0.40	1.07	8.62	1.40	0.40	1.05	8.62	1.31	0.41	1.00
8.43	1.62	0.39	1.11	8.43	1.38	0.39	1.04	8.43	1.38	0.40	1.05
8.23	1.54	0.38	1.05	8.23	1.35	0.38	1.01	8.23	1.30	0.39	0.99
8.04	1.53	0.37	1.05	8.04	1.32	0.37	0.99	8.04	1.28	0.38	0.97
7.85	1.50	0.37	1.02	7.85	1.49	0.36	1.12	7.85	1.26	0.37	0.96
7.66	1.66	0.36	1.13	7.66	1.48	0.35	1.11	7.66	1.32	0.36	1.01
7.47	1.61	0.35	1.10	7.47	1.49	0.35	1.12	7.47	1.28	0.36	0.98
7.27	1.67	0.34	1.13	7.27	1.50	0.34	1.12	7.27	1.40	0.35	1.07
7.08	1.68	0.33	1.15	7.08	1.59	0.33	1.19	7.08	1.48	0.34	1.13
6.89	1.75	0.32	1.19	6.89	1.46	0.32	1.09	6.89	1.45	0.33	1.11
6.70	1.70	0.31	1.16	6.70	1.55	0.31	1.16	6.70	1.39	0.32	1.06
6.50	1.75	0.30	1.19	6.50	1.55	0.30	1.16	6.50	1.54	0.31	1.17
6.31	1.66	0.29	1.13	6.31	1.66	0.29	1.24	6.31	1.45	0.30	1.11
6.12	1.79	0.29	1.22	6.12	1.64	0.28	1.23	6.12	1.61	0.29	1.23
5.93	1.77	0.28	1.21	5.93	1.68	0.27	1.26	5.93	1.60	0.28	1.22
5.74	1.84	0.27	1.25	5.74	1.70	0.27	1.28	5.74	1.67	0.27	1.27
5.54	1.89	0.26	1.29	5.54	1.73	0.26	1.30	5.54	1.69	0.26	1.29
5.35	1.83	0.25	1.25	5.35	1.68	0.25	1.26	5.35	1.70	0.25	1.29
5.16	1.85	0.24	1.26	5.16	1.72	0.24	1.29	5.16	1.67	0.25	1.27
4.97	1.88	0.23	1.28	4.97	1.81	0.23	1.36	4.97	1.79	0.24	1.36
4.77	1.89	0.22	1.29	4.77	1.88	0.22	1.41	4.77	1.89	0.23	1.44
4.58	1.96	0.21	1.34	4.58	1.89	0.21	1.42	4.58	1.92	0.22	1.46
4.39	1.99	0.20	1.36	4.39	1.87	0.20	1.40	4.39	1.96	0.21	1.49
4.20	2.03	0.20	1.38	4.20	1.90	0.19	1.43	4.20	2.00	0.20	1.52
4.01	2.07	0.19	1.41	4.01	1.88	0.19	1.41	4.01	2.05	0.19	1.56
3.81	2.17	0.18	1.48	3.81	1.92	0.18	1.44	3.81	2.06	0.18	1.57
3.62	2.11	0.17	1.44	3.62	1.93	0.17	1.45	3.62	2.09	0.17	1.59
3.43	2.11	0.16	1.43	3.43	1.94	0.16	1.45	3.43	2.04	0.16	1.55
3.24	2.11	0.15	1.44	3.24	1.95	0.15	1.46	3.24	2.10	0.15	1.60
3.04	2.14	0.14	1.46	3.04	1.98	0.14	1.48	3.04	2.14	0.14	1.63
2.85	2.11	0.13	1.43	2.85	2.03	0.13	1.52	2.85	2.18	0.14	1.66
2.66	2.26	0.12	1.54	2.66	2.09	0.12	1.57	2.66	2.15	0.13	1.64
2.47	2.20	0.11	1.50	2.47	1.91	0.11	1.43	2.47	2.07	0.12	1.58
2.27	2.21	0.11	1.51	2.27	2.03	0.11	1.52	2.27	1.97	0.11	1.50
2.08	2.15	0.10	1.47	2.08	2.12	0.10	1.59	2.08	1.93	0.10	1.47
1.89	2.14	0.09	1.45	1.89	1.96	0.09	1.47	1.89	1.90	0.09	1.45
1.70	2.12	0.08	1.44	1.70	1.80	0.08	1.35	1.70	1.83	0.08	1.39
1.51	2.09	0.07	1.42	1.51	1.77	0.07	1.33	1.51	1.72	0.07	1.31

Cont. of Turbidity Current Venting - Location C												
Run V4				Run V6				Run V7			
Measured		Normalized		Measured		Normalized		Measured		Normalized	
h (cm)	u (cm/s)	z/h	u/U	h (cm)	u (cm/s)	z/h	u/U	h (cm)	u (cm/s)	z/h	u/U
1.31	2.16	0.06	1.47	1.31	1.71	0.06	1.28	1.31	1.70	0.06	1.30
1.12	2.06	0.05	1.40	1.12	1.72	0.05	1.29	1.12	1.67	0.05	1.28
0.93	1.96	0.04	1.34	0.93	1.64	0.04	1.23	0.93	1.60	0.04	1.22
0.74	1.85	0.03	1.26	0.74	1.36	0.03	1.02	0.74	1.31	0.04	1.00
0.54	1.63	0.03	1.11	0.54	1.23	0.03	0.92	0.54	1.09	0.03	0.83
0.35	1.44	0.02	0.98	0.35	0.48	0.02	0.36	0.35	0.85	0.02	0.65
0.16	1.13	0.01	0.77	0.16	0.18	0.01	0.13	0.16	0.18	0.01	0.14

APPENDIX C: SUSPENDED SEDIMENT CONCENTRATION DATA

C1. Normal Reservoir Operation – Location A

Turbidity Currents Venting - Run 1				
Sample Siphon	**Height (inches)**	**Concentration Sample 1 (Initial)**	**Concentration Sample 2 (10 min)**	**Concentration Sample 3 (20 min)**
1A	1.25	0.0057	0.0048	0.0054
2A	3.20	0.0037	0.0038	0.0044
3A	5.70	0.0032	0.0034	0.0040
4A	9.55	0.0018	0.0026	0.0033
5A	13.65	0.0008	0.0023	0.0029
6A	18.40	0.0003	0.0017	0.0027

Turbidity Currents Venting – Run 2				
Sample Siphon	**Height (inches)**	**Concentration Sample 1 (Initial)**	**Concentration Sample 2 (10 min)**	**Concentration Sample 3 (20 min)**
1A	1.25	0.0057	0.0054	0.0058
2A	3.20	0.0041	0.0044	0.0048
3A	5.70	0.0033	0.0035	0.0042
4A	9.55	0.0019	0.0025	0.0035
5A	13.65	0.0008	0.0021	0.0028
6A	18.40	0.0002	0.0015	0.0023

Turbidity Currents Venting - Run 4				
Sample Siphon	**Height (inches)**	**Concentration Sample 1 (Initial)**	**Concentration Sample 2 (10 min)**	**Concentration Sample 3 (20 min)**
1A	1.25	0.0061	0.0055	0.0061
2A	3.20	0.0037	0.0038	0.0046
3A	5.70	0.0027	0.0028	0.0040
4A	9.55	0.0018	0.0021	0.0030
5A	13.65	0.0010	0.0016	0.0026
6A	18.40	0.0002	0.0013	0.0025

Turbidity Currents Venting - Run 6				
Sample Siphon	**Height (inches)**	**Concentration Sample 1 (Initial)**	**Concentration Sample 2 (10 min)**	**Concentration Sample 3 (20 min)**
1A	1.25	0.0057	0.0058	0.0055
2A	3.20	0.0039	0.0042	0.0048
3A	5.70	0.0031	0.0034	0.0044
4A	9.55	0.0018	0.0026	0.0035
5A	13.65	0.0009	0.0020	0.0030
6A	18.40	0.0002	0.0017	0.0027

Turbidity Currents Venting - Average				
Sample Siphon	**Height (inches)**	**Concentration Sample 1 (Initial)**	**Concentration Sample 2 (10 min)**	**Concentration Sample 3 (20 min)**
1A	1.25	0.0058	0.0054	0.0057
2A	3.20	0.0038	0.0040	0.0046
3A	5.70	0.0031	0.0033	0.0041
4A	9.55	0.0018	0.0025	0.0033
5A	13.65	0.0009	0.0020	0.0028
6A	18.40	0.0002	0.0015	0.0026

C2. Normal Reservoir Operation – Location B

Turbidity Currents Venting - Run 1				
Sample Siphon	**Height (inches)**	**Concentration Sample 1 (Initial)**	**Concentration Sample 2 (10 min)**	**Concentration Sample 3 (20 min)**
1B	1.25	0.0042	0.0050	0.0049
2B	3.20	0.0038	0.0045	0.0046
3B	6.00	0.0032	0.0039	0.0042
4B	9.20	0.0026	0.0036	0.0040
5B	13.00	0.0016	0.0034	0.0037
6B	16.85	0.0010	0.0034	0.0036
7B	21.90	0.0002	0.0029	0.0035

Turbidity Currents Venting - Run 2				
Sample Siphon	**Height (inches)**	**Concentration Sample 1 (Initial)**	**Concentration Sample 2 (10 min)**	**Concentration Sample 3 (20 min)**
1B	1.25	0.0046	0.0048	0.0050
2B	3.20	0.0036	0.0043	0.0046
3B	6.00	0.0021	0.0036	0.0042
4B	9.20	0.0017	0.0033	0.0040
5B	13.00	0.0009	0.0030	0.0037
6B	16.85	0.0006	0.0030	0.0036
7B	21.90	0.0002	0.0028	0.0036

Turbidity Currents Venting - Run 4				
Sample Siphon	**Height (inches)**	**Concentration Sample 1 (Initial)**	**Concentration Sample 2 (10 min)**	**Concentration Sample 3 (20 min)**
1B	1.25	0.0040	0.0047	0.0052
2B	3.20	0.0034	0.0043	0.0044
3B	6.00	0.0028	0.0036	0.0042
4B	9.20	0.0024	0.0032	0.0038
5B	13.00	0.0013	0.0028	0.0035
6B	16.85	0.0004	0.0028	0.0035
7B	21.90	0.0001	0.0025	0.0033

Turbidity Currents Venting - Run 6				
Sample Siphon	Height (inches)	Concentration Sample 1 (Initial)	Concentration Sample 2 (10 min)	Concentration Sample 3 (20 min)
1B	1.25	0.0045	0.0048	0.0048
2B	3.20	0.0037	0.0044	0.0045
3B	6.00	0.0029	0.0038	0.0041
4B	9.20	0.0023	0.0034	0.0041
5B	13.00	0.0013	0.0031	0.0036
6B	16.85	0.0006	0.0029	0.0034
7B	21.90	0.0002	0.0027	0.0034

Turbidity Currents Venting - Average				
Sample Siphon	Height (inches)	Concentration Sample 1 (Initial)	Concentration Sample 2 (10 min)	Concentration Sample 3 (20 min)
1B	1.25	0.0043	0.0048	0.0050
2B	3.20	0.0036	0.0044	0.0045
3B	6.00	0.0028	0.0037	0.0042
4B	9.20	0.0022	0.0033	0.0040
5B	13.00	0.0013	0.0031	0.0036
6B	16.85	0.0006	0.0030	0.0035
7B	21.90	0.0002	0.0028	0.0034

C3. Normal Reservoir Operation – Location C

Turbidity Currents Venting - Run 1				
Sample Siphon	Height (inches)	Concentration Sample 1 (Initial)	Concentration Sample 2 (10 min)	Concentration Sample 3 (20 min)
1C	1.25	0.0035	0.0047	0.0047
2C	3.20	0.0033	0.0047	0.0047
3C	5.70	0.0031	0.0046	0.0045
4C	8.90	0.0025	0.0044	0.0046
5C	12.40	0.0019	0.0044	0.0045
6C	16.85	0.0010	0.0042	0.0042
7C	21.60	0.0004	0.0039	0.0040
8C	24.45	0.0002	0.0035	0.0038

Turbidity Currents Venting - Run 2				
Sample Siphon	Height (inches)	Concentration Sample 1 (Initial)	Concentration Sample 2 (10 min)	Concentration Sample 3 (20 min)
1C	1.25	0.0032	0.0043	0.0043
2C	3.20	0.0030	0.0042	0.0045
3C	5.70	0.0025	0.0042	0.0045
4C	8.90	0.0020	0.0042	0.0043
5C	12.40	0.0018	0.0041	0.0042
6C	16.85	0.0011	0.0038	0.0040
7C	21.60	0.0003	0.0036	0.0037
8C	24.45	0.0003	0.0031	0.0035

Turbidity Currents Venting - Run 4				
Sample Siphon	**Height (inches)**	**Concentration Sample 1 (Initial)**	**Concentration Sample 2 (10 min)**	**Concentration Sample 3 (20 min)**
1C	1.25	0.0036	0.0044	0.0048
2C	3.20	0.0033	0.0042	0.0047
3C	5.70	0.0029	0.0042	0.0046
4C	8.90	0.0025	0.0040	0.0047
5C	12.40	0.0021	0.0039	0.0045
6C	16.85	0.0014	0.0038	0.0041
7C	21.60	0.0004	0.0034	0.0038
8C	24.45	0.0003	0.0029	0.0038

Turbidity Currents Venting - Run 6				
Sample Siphon	**Height (inches)**	**Concentration Sample 1 (Initial)**	**Concentration Sample 2 (10 min)**	**Concentration Sample 3 (20 min)**
1C	1.25	0.0033	0.0046	0.0047
2C	3.20	0.0031	0.0045	0.0046
3C	5.70	0.0028	0.0044	0.0045
4C	8.90	0.0023	0.0042	0.0047
5C	12.40	0.0020	0.0041	0.0044
6C	16.85	0.0011	0.0041	0.0040
7C	21.60	0.0004	0.0036	0.0039
8C	24.45	0.0003	0.0033	0.0037

Turbidity Currents Venting - Average				
Sample Siphon	**Height (inches)**	**Concentration Sample 1 (Initial)**	**Concentration Sample 2 (10 min)**	**Concentration Sample 3 (20 min)**
1C	1.25	0.0034	0.0045	0.0046
2C	3.20	0.0032	0.0044	0.0046
3C	5.70	0.0028	0.0044	0.0045
4C	8.90	0.0023	0.0042	0.0046
5C	12.40	0.0020	0.0041	0.0044
6C	16.85	0.0012	0.0040	0.0041
7C	21.60	0.0004	0.0036	0.0039
8C	24.45	0.0003	0.0032	0.0037

C4. Turbidity Current Venting – Location A

Turbidity Currents Venting - Run 1				
Sample Siphon	**Height (inches)**	**Concentration Sample 1 (Initial)**	**Concentration Sample 2 (10 min)**	**Concentration Sample 3 (20 min)**
1A	1.25	0.0047	0.0044	0.0043
2A	3.20	0.0035	0.0040	0.0040
3A	5.70	0.0027	0.0037	0.0037
4A	9.55	0.0017	0.0027	0.0029
5A	13.65	0.0010	0.0024	0.0027
6A	18.40	0.0002	0.0017	0.0024

Turbidity Currents Venting - Run 2				
Sample Siphon	**Height (inches)**	**Concentration Sample 1 (Initial)**	**Concentration Sample 2 (10 min)**	**Concentration Sample 3 (20 min)**
1A	1.25	0.0052	0.0048	0.0044
2A	3.20	0.0030	0.0043	0.0039
3A	5.70	0.0022	0.0039	0.0037
4A	9.55	0.0007	0.0034	0.0033
5A	13.65	0.0003	0.0025	0.0031
6A	18.40	0.0002	0.0014	0.0022

Turbidity Currents Venting - Run 4				
Sample Siphon	**Height (inches)**	**Concentration Sample 1 (Initial)**	**Concentration Sample 2 (10 min)**	**Concentration Sample 3 (20 min)**
1A	1.25	0.0051	0.0049	0.0051
2A	3.20	0.0041	0.0042	0.0044
3A	5.70	0.0026	0.0038	0.0038
4A	9.55	0.0015	0.0033	0.0034
5A	13.65	0.0009	0.0025	0.0029
6A	18.40	0.0004	0.0018	0.0022

Turbidity Currents Venting - Run 6				
Sample Siphon	**Height (inches)**	**Concentration Sample 1 (Initial)**	**Concentration Sample 2 (10 min)**	**Concentration Sample 3 (20 min)**
1A	1.25	0.0052	0.0051	0.0053
2A	3.20	0.0040	0.0044	0.0047
3A	5.70	0.0032	0.0042	0.0044
4A	9.55	0.0022	0.0039	0.0041
5A	13.65	0.0009	0.0031	0.0034
6A	18.40	0.0004	0.0017	0.0023

Turbidity Currents Venting - Average				
Sample Siphon	**Height (inches)**	**Concentration Sample 1 (Initial)**	**Concentration Sample 2 (10 min)**	**Concentration Sample 3 (20 min)**
1A	1.25	0.0051	0.0048	0.0048
2A	3.20	0.0037	0.0042	0.0043
3A	5.70	0.0027	0.0039	0.0039
4A	9.55	0.0015	0.0033	0.0034
5A	13.65	0.0008	0.0026	0.0030
6A	18.40	0.0003	0.0016	0.0023

C5. Turbidity Current Venting – Location B

Turbidity Currents Venting - Run 1				
Sample Siphon	**Height (inches)**	**Concentration Sample 1 (Initial)**	**Concentration Sample 2 (10 min)**	**Concentration Sample 3 (20 min)**
1B	1.25	0.0038	0.0037	0.0036
2B	3.20	0.0033	0.0036	0.0036
3B	6.00	0.0026	0.0034	0.0033
4B	9.20	0.0022	0.0030	0.0029
5B	13.00	0.0015	0.0025	0.0025
6B	16.85	0.0008	0.0022	0.0024
7B	21.90	0.0002	0.0017	0.0021

Turbidity Currents Venting - Run 2				
Sample Siphon	**Height (inches)**	**Concentration Sample 1 (Initial)**	**Concentration Sample 2 (10 min)**	**Concentration Sample 3 (20 min)**
1B	1.25	0.0039	0.0042	0.0039
2B	3.20	0.0035	0.0040	0.0037
3B	6.00	0.0025	0.0038	0.0035
4B	9.20	0.0020	0.0036	0.0033
5B	13.00	0.0015	0.0031	0.0031
6B	16.85	0.0008	0.0023	0.0027
7B	21.90	0.0002	0.0018	0.0023

Turbidity Currents Venting - Run 4				
Sample Siphon	**Height (inches)**	**Concentration Sample 1 (Initial)**	**Concentration Sample 2 (10 min)**	**Concentration Sample 3 (20 min)**
1B	1.25	0.0039	0.0039	0.0041
2B	3.20	0.0033	0.0035	0.0036
3B	6.00	0.0026	0.0031	0.0032
4B	9.20	0.0023	0.0027	0.0029
5B	13.00	0.0015	0.0026	0.0024
6B	16.85	0.0004	0.0019	0.0020
7B	21.90	0.0001	0.0017	0.0019

Turbidity Currents Venting - Run 6				
Sample Siphon	**Height (inches)**	**Concentration Sample 1 (Initial)**	**Concentration Sample 2 (10 min)**	**Concentration Sample 3 (20 min)**
1B	1.25	0.0042	0.0043	0.0046
2B	3.20	0.0037	0.0041	0.0044
3B	6.00	0.0028	0.0038	0.0041
4B	9.20	0.0023	0.0036	0.0036
5B	13.00	0.0018	0.0031	0.0032
6B	16.85	0.0010	0.0025	0.0028
7B	21.90	0.0001	0.0019	0.0024

Turbidity Currents Venting - Average				
Sample Siphon	**Height (inches)**	**Concentration Sample 1 (Initial)**	**Concentration Sample 2 (10 min)**	**Concentration Sample 3 (20 min)**
1B	1.25	0.0040	0.0040	0.0040
2B	3.20	0.0034	0.0038	0.0038
3B	6.00	0.0026	0.0035	0.0035
4B	9.20	0.0022	0.0032	0.0032
5B	13.00	0.0016	0.0028	0.0028
6B	16.85	0.0008	0.0022	0.0025
7B	21.90	0.0002	0.0018	0.0022

C6. Turbidity Current Venting – Location C

Turbidity Currents Venting - Run 1				
Sample Siphon	**Height (inches)**	**Concentration Sample 1 (Initial)**	**Concentration Sample 2 (10 min)**	**Concentration Sample 3 (20 min)**
1C	1.25	0.0035	0.0033	0.0036
2C	3.20	0.0033	0.0033	0.0035
3C	5.70	0.0030	0.0028	0.0032
4C	8.90	0.0022	0.0025	0.0028
5C	12.40	0.0017	0.0024	0.0026
6C	16.85	0.0009	0.0022	0.0025
7C	21.60	0.0004	0.0021	0.0024
8C	24.45	0.0002	0.0011	0.0014

Turbidity Currents Venting - Run 2				
Sample Siphon	**Height (inches)**	**Concentration Sample 1 (Initial)**	**Concentration Sample 2 (10 min)**	**Concentration Sample 3 (20 min)**
1C	1.25	0.0036	0.0039	0.0036
2C	3.20	0.0033	0.0036	0.0035
3C	5.70	0.0027	0.0035	0.0034
4C	8.90	0.0021	0.0031	0.0031
5C	12.40	0.0016	0.0026	0.0027
6C	16.85	0.0011	0.0025	0.0027
7C	21.60	0.0006	0.0024	0.0025
8C	24.45	0.0002	0.0011	0.0013

Turbidity Currents Venting - Run 4				
Sample Siphon	**Height (inches)**	**Concentration Sample 1 (Initial)**	**Concentration Sample 2 (10 min)**	**Concentration Sample 3 (20 min)**
1C	1.25	0.0036	0.0036	0.0037
2C	3.20	0.0029	0.0034	0.0034
3C	5.70	0.0023	0.0029	0.0031
4C	8.90	0.0017	0.0023	0.0025
5C	12.40	0.0010	0.0019	0.0022
6C	16.85	0.0004	0.0018	0.0020
7C	21.60	0.0000	0.0018	0.0020
8C	24.45	0.0000	0.0006	0.0009

Turbidity Currents Venting - Run 6				
Sample Siphon	**Height (inches)**	**Concentration Sample 1 (Initial)**	**Concentration Sample 2 (10 min)**	**Concentration Sample 3 (20 min)**
1C	1.25	0.0038	0.0039	0.0040
2C	3.20	0.0035	0.0037	0.0038
3C	5.70	0.0031	0.0035	0.0038
4C	8.90	0.0024	0.0030	0.0033
5C	12.40	0.0020	0.0027	0.0030
6C	16.85	0.0011	0.0026	0.0029
7C	21.60	0.0004	0.0024	0.0026
8C	24.45	0.0002	0.0010	0.0012

Turbidity Currents Venting - Average				
Sample Siphon	**Height (inches)**	**Concentration Sample 1 (Initial)**	**Concentration Sample 2 (10 min)**	**Concentration Sample 3 (20 min)**
1C	1.25	0.0036	0.0037	0.0037
2C	3.20	0.0033	0.0035	0.0036
3C	5.70	0.0028	0.0032	0.0034
4C	8.90	0.0021	0.0027	0.0029
5C	12.40	0.0016	0.0024	0.0026
6C	16.85	0.0009	0.0023	0.0025
7C	21.60	0.0004	0.0022	0.0024
8C	24.45	0.0002	0.0010	0.0012

APPENDIX D: SEDIMENT DEPOSITION & DEPOSITION RATES DATA

D1. Sediment Deposition Data – Normal Operation

N4 - Time Interval 1		N6 - Time Interval 2		N7 - Time Interval 3	
Distance from Dam (cm)	Deposition (cm)	Distance from Dam (cm)	Deposition (cm)	Distance from Dam (cm)	Deposition (cm)
0.00	1.20	0.00	2.30	0.00	3.30
30.48	1.54	30.48	2.44	30.48	3.24
76.20	1.94	76.20	2.84	76.20	3.64
121.92	2.49	121.92	3.44	121.92	4.34
167.64	3.14	167.64	4.19	167.64	5.24
213.36	3.75	213.36	4.80	213.36	5.95
261.62	4.38	261.62	5.68	261.62	6.98
307.34	5.03	307.34	6.48	307.34	7.98
353.06	5.68	353.06	7.23	353.06	9.18
374.00	6.59	369.00	8.29	362.00	10.39
403.86	21.77	403.86	23.37	403.86	24.07
472.44	23.51	472.44	26.31	472.44	27.61
518.16	24.81	518.16	28.01	518.16	28.01
594.36	27.14	594.36	29.04	594.36	29.24

D2. Sediment Deposition Data – Turbidity Currents Venting

V4 - Time Int 1		V6 - Time Int 2		V7 - Time Int 3	
Distance from Dam (cm)	Deposition (cm)	Distance from Dam (cm)	Deposition (cm)	Distance from Dam (cm)	Deposition (cm)
0.00	0.70	0.00	1.20	0.00	1.65
30.48	1.14	30.48	1.79	30.48	2.34
76.20	1.59	76.20	2.44	76.20	3.14
121.92	2.14	121.92	2.99	121.92	3.84
167.64	2.74	167.64	3.54	167.64	4.44
213.36	3.35	213.36	4.25	213.36	5.25
261.62	3.78	261.62	4.88	261.62	5.98
307.34	4.43	307.34	5.53	307.34	6.88
353.06	5.03	353.06	6.38	353.06	8.08
376.00	5.89	373.00	7.69	369.00	9.99
403.86	20.97	403.86	21.52	403.86	21.77
472.44	23.21	472.44	24.31	472.44	25.31
518.16	24.41	518.16	26.41	518.16	26.91
594.36	26.14	594.36	27.74	594.36	27.74

D3. Accumulated Deposition Rate Data – Normal Operation

Time Interval	80 mins	160 mins	240 mins
Distance from Dam (cm)	N4 Deposition Rate (cm/min)	N6 Deposition Rate (cm/min)	N7 Deposition Rate (cm/min)
0.00	0.015	0.014	0.014
30.48	0.015	0.013	0.012
76.20	0.014	0.013	0.012
121.92	0.014	0.013	0.013
167.64	0.016	0.015	0.014
213.36	0.018	0.015	0.015
261.62	0.019	0.018	0.017
307.34	0.021	0.019	0.019
353.06	0.023	0.021	0.022
381.00	0.030	0.026	0.026
403.86	0.026	0.023	0.018
472.44	0.028	0.031	0.026
518.16	0.030	0.035	0.023
594.36	0.036	0.030	0.021

D4. Accumulated Deposition Rate Data – Turbidity Currents Venting

Time Interval	80 mins	160 mins	240 mins
Distance from Dam (cm)	V4 Deposition Rate (cm/min)	V6 Deposition Rate (cm/min)	V7 Deposition Rate (cm/min)
0.00	0.009	0.008	0.007
30.48	0.010	0.009	0.008
76.20	0.009	0.010	0.010
121.92	0.010	0.010	0.010
167.64	0.011	0.011	0.011
213.36	0.013	0.012	0.012
261.62	0.011	0.013	0.013
307.34	0.013	0.013	0.015
353.06	0.014	0.016	0.018
381.00	0.021	0.022	0.024
403.86	0.016	0.012	0.009
472.44	0.024	0.019	0.017
518.16	0.025	0.025	0.019
594.36	0.024	0.022	0.015

D5. Deposition Rate Data for 80 Minutes Intervals – Normal Operation

Time Interval	80 mins	80 mins	80 mins
Distance from Dam (cm)	N4 Deposition Rate (cm/min)	N6 Deposition Rate (cm/min)	N7 Deposition Rate (cm/min)
0.00	0.015	0.014	0.013
30.48	0.015	0.011	0.010
76.20	0.014	0.011	0.010
121.92	0.014	0.012	0.011
167.64	0.016	0.013	0.013
213.36	0.018	0.013	0.014
261.62	0.019	0.016	0.016
307.34	0.021	0.018	0.019
353.06	0.023	0.019	0.024
381.00	0.030	0.021	0.026
403.86	0.026	0.020	0.009
472.44	0.028	0.035	0.016
518.16	0.030	0.040	0.000
594.36	0.036	0.024	0.003

D6. Deposition Rate Data for 80 Minutes Intervals – Turbidity Currents Venting

Time Interval	80 mins	80 mins	80 mins
Distance from Dam (cm)	V4 Deposition Rate (cm/min)	V6 Deposition Rate (cm/min)	V7 Deposition Rate (cm/min)
0.00	0.009	0.006	0.006
30.48	0.010	0.008	0.007
76.20	0.009	0.011	0.009
121.92	0.010	0.011	0.011
167.64	0.011	0.010	0.011
213.36	0.013	0.011	0.013
261.62	0.011	0.014	0.014
307.34	0.013	0.014	0.017
353.06	0.014	0.017	0.021
381.00	0.021	0.023	0.029
403.86	0.016	0.007	0.003
472.44	0.024	0.014	0.013
518.16	0.025	0.025	0.006
594.36	0.024	0.020	0.000